Development of Triplet-Triplet Annihilation Based Photon Upconversion in Condensed Systems

間瀬, 一馬

https://doi.org/10.15017/1931875

出版情報：Kyushu University, 2017, 博士（工学）, 課程博士
バージョン：
権利関係：

Development of Triplet-Triplet Annihilation Based Photon Upconversion in Condensed Systems

Kazuma Mase

Department of Chemistry and Biochemistry

Graduate School of Engineering

KYUSHU UNIVERSITY

2018

Index

Chapter 1 General introduction

1-1 Photon upconversion (UC)

Light is one of the most important energy sources because of its intriguing applications in photoreactions, including photocatalysis, photovoltaic power generation, and biotechnology. However, photoreactions occur only at a specific range of wavelengths and are difficult to utilize the light energy effectively. For example, photocatalytic reactions are induced by sunlight limited to the ultraviolet-visible (UV-Vis) region, suggesting 44% of the light source was wasted for nothing. In addition, the near-infrared (NIR) light has attracted much attention from the biological field because it shows good tissue penetration. However, the photon energy in this region is too weak for important biotechnologies such as bioimaging, photodynamic therapy, and drug release.

In recent years, there has been a rapid growth of interest in photon upconversion (UC) being a solution to the aforementioned problems. UC is a process that converts lower energy (longer wavelength) photons to higher energy (shorter wavelength) photons. Although there are several UC mechanisms, such as two-photon absorption (TPA), and energy transfer upconversion (ETU) of lanthanide nano-particles, most of them have limited applications because they require high excitation light intensity.

TPA is an UC mechanism that utilizes a virtual excited state (Figure 1-1).[1] One disadvantage is that the lifetime of the virtual state is extremely short (1–10 fs),[2] leading to high excitation light intensity (10^6–10^9 W cm-2) required for an electron at the virtual state to absorb the energy of the excited photon within the lifetime.

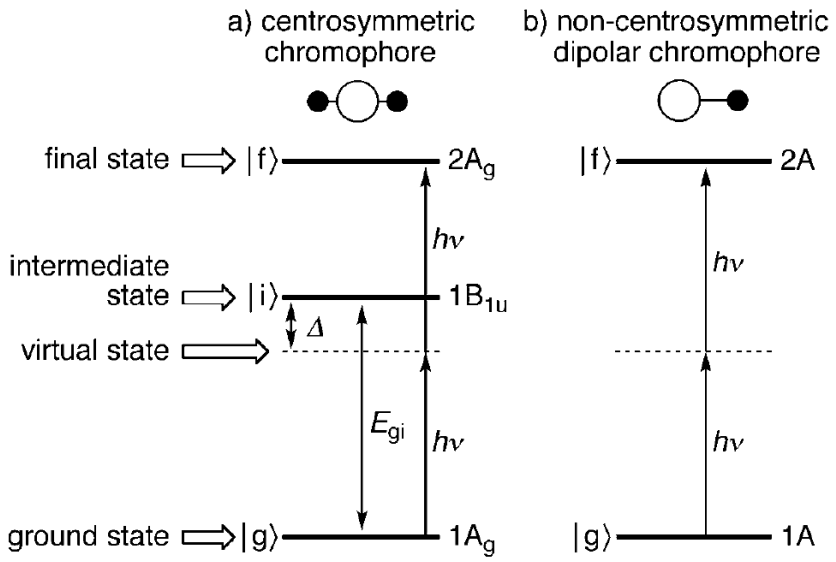

Figure 1-1. Energy level diagrams of the essential states in two-photon absorption (TPA).[1]

On the other hand, ETU can work with relatively low excitation intensity (W cm^{-2}–kW cm^{-2}), because the energy transfer process uses physically existing intermediate energy states of lanthanide ions (Figure 1-2).[3-6] However, considering the excitation light intensity necessary for UC applications such as solar energy conversion (0.1 W cm^{-2} for solar irradiance) and biotechnology (0.726 W cm^{-2} for maximum permissible exposure of skin),[6] the intensity is still too strong.

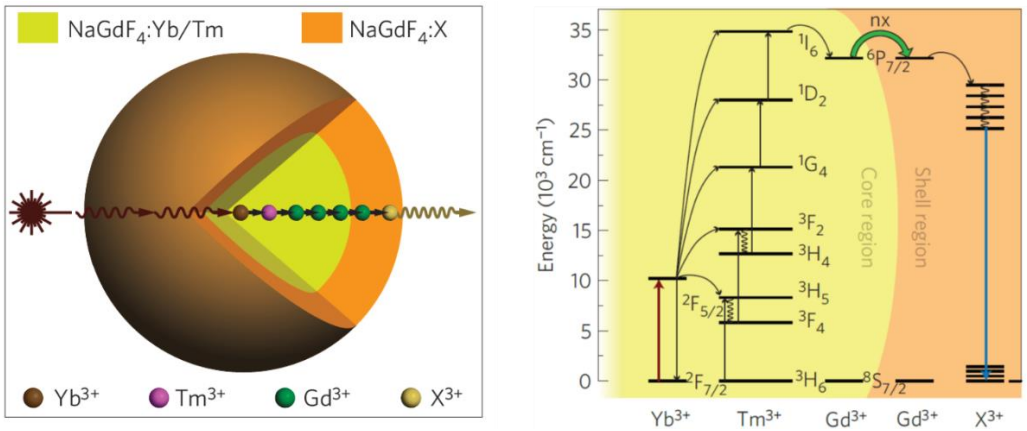

Figure 1-2. Schematic design of a lanthanide-doped $NaGdF_4$@$NaGdF_4$ core–shell nanoparticle for energy transfer upconversion (ETU) (left). Proposed energy transfer mechanisms in the core-shell nanoparticle (right).[4]

To solve the problem of the excitation light intensity, triplet-triplet annihilation-based UC (TTA-UC) has been attracting much attention. In this mechanism, a long-lived triplet state as the intermediate state allows UC to occur under low excitation power density (mW cm^{-2}–W cm^{-2}).[7-18] A common TTA-UC energy diagram is shown in Figure 1-3. The TTA-UC involves a donor (sensitizer) with high intersystem crossing (ISC) efficiency and an acceptor (emitter) with high fluorescence quantum yield. The sensitizer first absorbs the low-energy light to produce the excited singlet state (S_1), and subsequently, the triplet state (T_1) is populated through ISC. The acceptor's T_1 is generated by the triplet-triplet energy transfer (TTET) from donor's T_1 via the Dexter mechanism. At last, the collision and annihilation (TTA) between two acceptor triplets produce a high-energy singlet excited state S_1 that radiates upconverted emission.

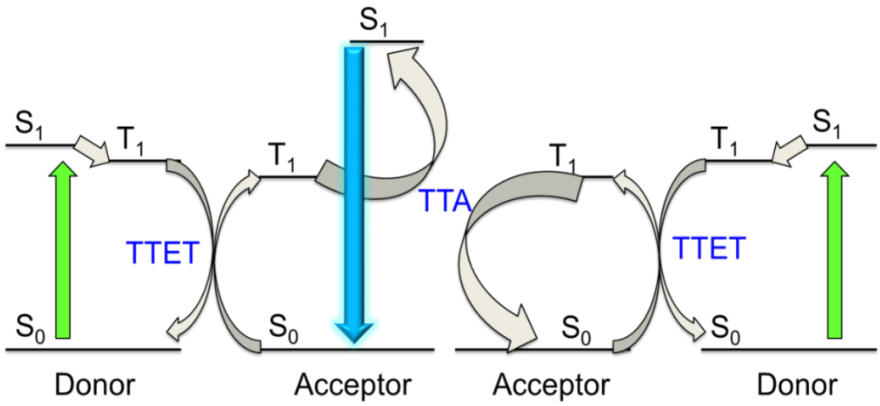

Figure 1-3. Outline of the TTA-UC process, showing the energy levels involved in the TTA-UC (S = singlet, T = triplet)

In this chapter, the trend of recent researches on TTA-UC will be described. Moreover, the expansion of TTA-UC to condensed systems for device applications and its problems will be outlined.

1-2 Molecular diffusion based TTA-UC

In TTET and TTA processes, the excited molecules at the triplet state need to collide with one another in order to efficiently exchange electrons (Dexter energy transfer). Therefore, to achieve highly efficient TTA-UC with low-intensity excitation light, it is necessary that the donor and the acceptor are uniformly mixed, and the two acceptor triplets collide effectively. Most of the previous studies on TTA-UC obtained good TTET and TTA by exploiting the translational diffusion of excited molecules in solutions and soft polymers.

A threshold excitation light intensity, I_{th}, has been used as a parameter to evaluate the excitation light intensity required for TTA-UC.[19-22] In general, the TTA-UC emission intensity shows quadratic and linear dependences on the incident light intensity at low and high excitation intensities, respectively. The quadratic-to-linear transition takes place at threshold excitation intensity I_{th}. Above I_{th}, TTA becomes the main deactivation channel for the acceptor triplets, and the UC quantum yield (Φ_{UC}) in the system is maximized (Figure 1-4). Therefore, the system shows lower I_{th}, and weak excitation light can be utilized more efficiently.

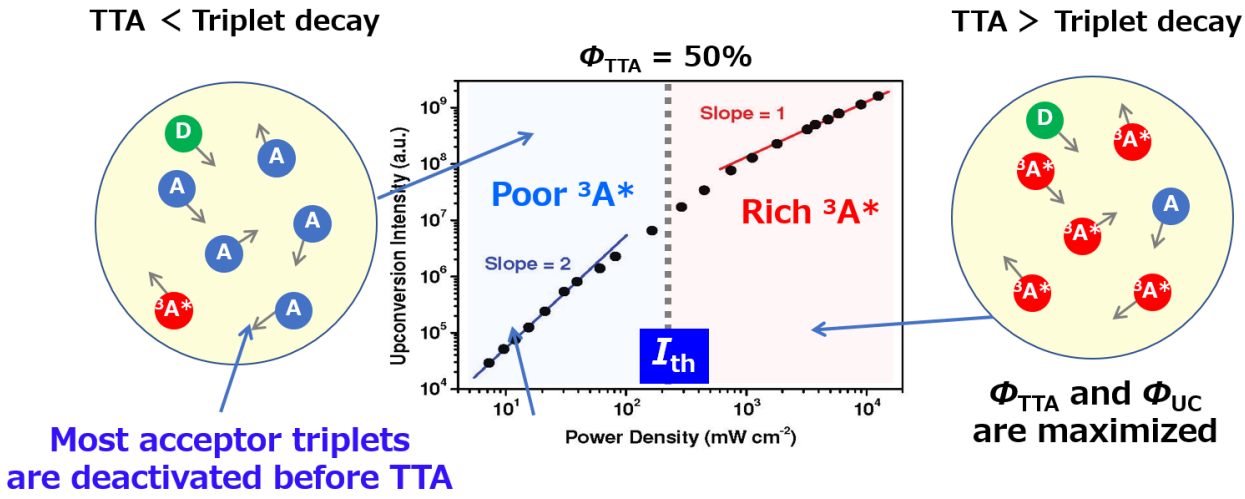

Figure 1-4. Excitation power intensity dependence of TTA-UC emission (A = acceptor, D = donor, and $^3A^*$ = excited triplet state of the acceptor). In the slope = 2 region, acceptor triplets are deactivated by the natural decay before TTA. On the other hand, in the slope = 1 region, most acceptor triplets are consumed by TTA.

It was reported that I_{th} obeys Equation 1-1:

$$I_{th} = \frac{\left(k_{A,T}\right)^2}{\Phi_{TTET}\alpha\gamma_{TT}}$$

(Equation 1-1)

where $k_{A,T}$ is the triplet decay rate constant of acceptor, α is the sensitizer absorption coefficient, Φ_{TTET} is the donor-to-acceptor TTET efficiency, and γ_{TT} is the bimolecular reaction (TTA) rate constant. In a three-dimensional (3D) diffusion-limited system, such as solution systems, γ_{TT} follows Equation 1-2:

$$\gamma_{TT} = 8\pi D_T a_0$$

(Equation 1-2)

where D_T is the diffusion constant of acceptor triplet, and a_0 is the interaction distance of an acceptor triplet pair. Therefore, I_{th} decreases as D_T becomes larger, and TTA occurs with high efficiency even under low acceptor triplet density conditions. In solution systems, D_T value obeys the Stokes-Einstein equation (Equation 1-3):

$$D_T = \frac{k_B T}{6\pi\eta r}$$

(Equation 1-3)

where k_B is Boltzmann constant, T is the temperature, η is the viscosity of solvents, and r is the molecular radius of acceptors. Therefore, I_{th} in solution systems depends on the viscosity of solvents. Mongizzi *et al* achieved significantly low I_{th} (0.8 mW cm^{-2}), which is less than the magnitude of sunlight intensity by dispersing donor (Pt(II)octaethylporphyrin, PtOEP) and acceptor (9,10-diphenylanthracene, DPA) in a low viscousity solvent (Fig, 1-5).[19]

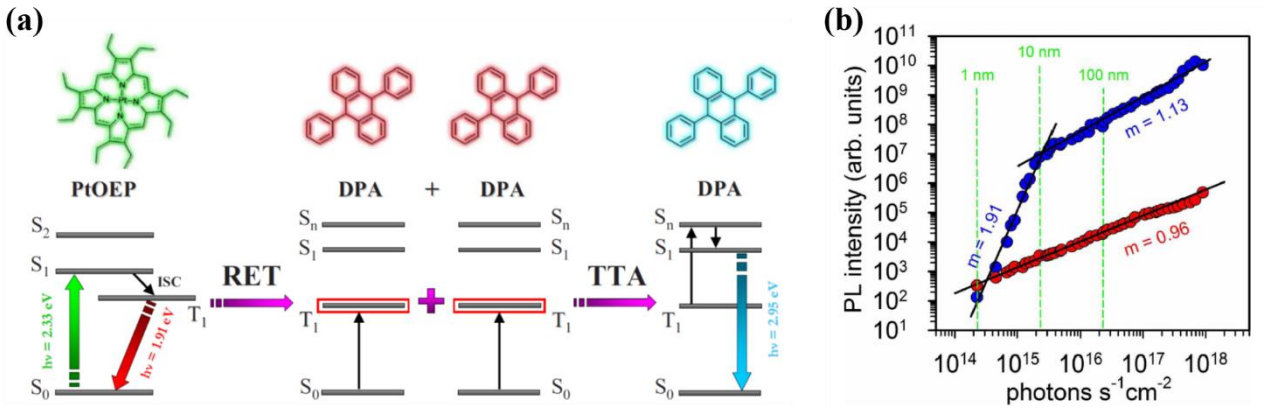

Figure 1-5. (a) Molecular structures of PtOEP and DPA, and their corresponding energy diagram. (b) Upconverted DPA emission (blue dots) and PtOEP phosphorescence (red dots) intensity vs the excitation power intensity for a 1,1,2-trichloroethane solution of PtOEP/DPA (PtOEP and DPA concentrations: 1.5×10^{-4} and 1.0×10^{-1} M, respectively).[19]

As aforementioned, fast molecular diffusion in organic solvents gives highly efficient TTA-UC with low I_{th}. However, the use of volatile organic solvents is not suitable for device applications. Moreover, for the donor to efficiently absorb the excitation light, it is necessary to accumulate the donor molecules at high density. Therefore, development of TTA-UC in condensed systems is required.

1-3 TTA-UC in condensed systems

There are three major problems needed to be solved for TTA-UC in condensed systems.

The first problem is that molecular diffusion is significantly inhibited in the condensed system. Singh-Rachford *et al*. reported the temperature dependence of TTA-UC emission intensity on a sample with the donor-acceptor pair dispersing in a polymer matrix.[23] The results showed that TTA-UC luminescence is completely quenched below the glass transition temperature (236 K) of the polymer matrix (Figure 1-6). It is noteworthy that even at room temperature above the glass transition temperature, TTA-UC emission intensity was weak because of the largely inhibited molecular diffusion. This suggests that alternate triplet transportation is required to achieve highly efficient TTA-UC in condensed systems.

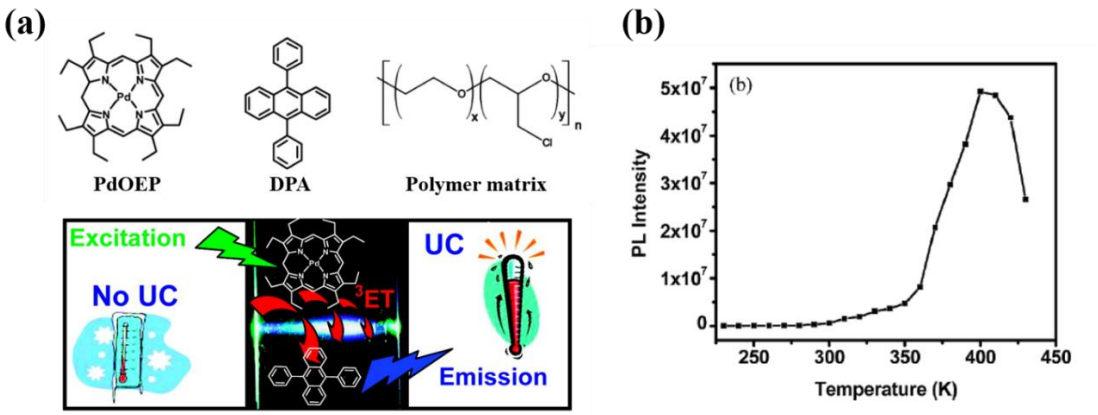

Figure 1-6. Temperature dependence of TTA-UC emission intensity. (a) Molecular structures of the donor (PdOEP), the acceptor (DPA), and the polymer matrix. (b) Integrated upconverted emission intensity as a function of temperature.[23]

The second problem is the phase separation of donor and acceptor. Monguzzi *et al*. have synthesized a PtOEP-doped DPA single crystal, and the TTA-UC property was reported (Figure 1-7).[24] This sample showed only weak TTA-UC emission while a strong donor phosphorescence was observed (Figure 1-7a). Investigation of the crystalline sample under a confocal microscope revealed that the donor and the acceptor were phase separated (Figure 1-7b), resulting in a significant decrease in TTET efficiency.

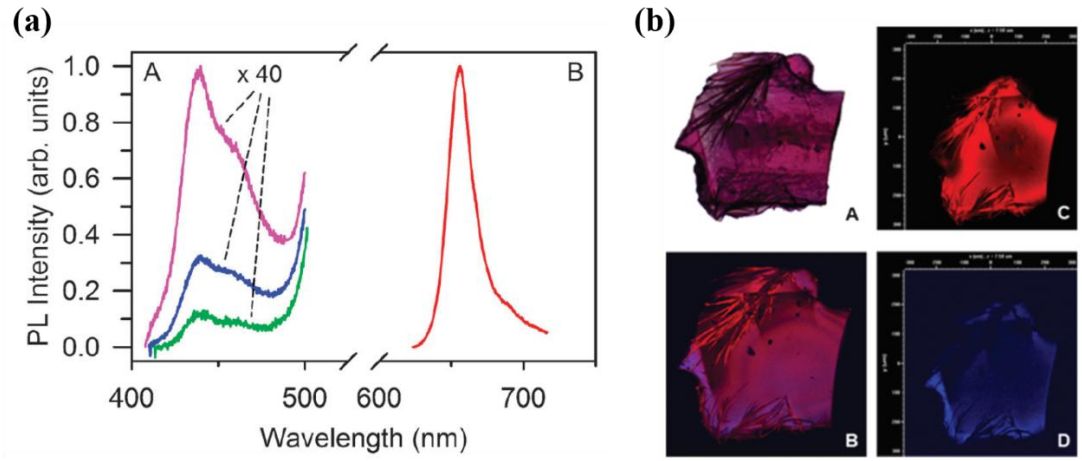

Figure 1-7. (a) Blue photoluminescence (PL) spectrum of the crystalline sample under continuous wave excitation at 532 nm as a function of incident power at 1 mW (green), 2 mW (blue) and 3 mW (pink), and a donor phosphorescence under 2 mW excitation (red). (b) (A) White light transmission image of the crystalline sample, (B) RGB PL image under 532 nm excitation, (C) red filtered PL (donor phosphorescence) spectrum, and (D) blue filtered PL (upconverted emission) spectrum.[24]

The third problem is the red-shifts of the acceptor emission due to the intermolecular interactions and the accompanying reduction of the anti-Stokes shift which is the difference between wavelengths of the excitation light and the UC emission. In general, luminescent acceptor molecules have aromatic rings and are likely to π-stack to one another. The π-π interaction works strongly in condensed systems and stabilizes the singlet excitation state of the luminescent acceptor molecules (Figure 1-8). The decrease in the anti-Stokes shift in condensed TTA-UC systems reduces the efficacy of converting lower-energy photons to higher-energy photons.

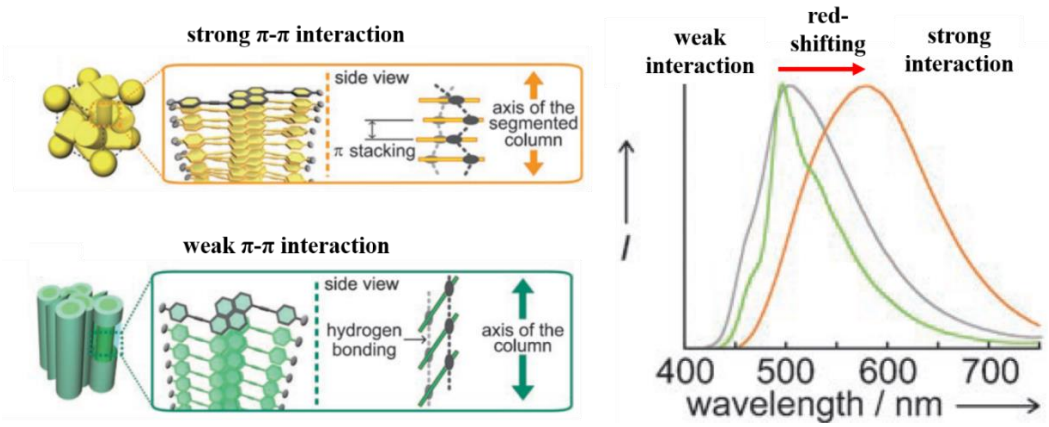

Figure 1-8. Fluorescence red-shifting of the pyrene-contained liquid crystal by π-π interactions.[25]

In order to effectively promote TTA-UC in condensed systems, it is necessary to solve the major three problems, (1) the low triplet diffusion, (2) the phase separation of the donor and the acceptor, and (3) the red-shifting of the acceptor emission. Strategies to solve those problems will be described in the later section.

1-4 Triplet energy-migration based TTA-UC

As a solution to the low triplet diffusion coefficient in condensed systems, I demonstrated an alternative strategy based on the triplet energy-migration based TTA-UC which is independent of the molecular diffusion (Figure 1-9).[16,26-28] In our previous reports, acceptor molecules are designed to give ordered molecular assemblies in which acceptor chromophores are regularly aligned. To achieve efficient donor-to-acceptor energy transfer, donor molecules are preorganized in the vicinity (<1 nm) of the acceptor arrays. In these donor–acceptor self-assembled systems, the excited triplets are locally accumulated and the rapid migration of excited triplet states leads to efficient TTA-UC emission (Figure 1-9a).[16] It is noteworthy that the self-assembled structures of donor and acceptor showed not only efficient triplet energy migration but also novel functions that cannot be obtained in molecular dispersion systems, such as oxygen blocking ability (Figure 1-9b).[27]

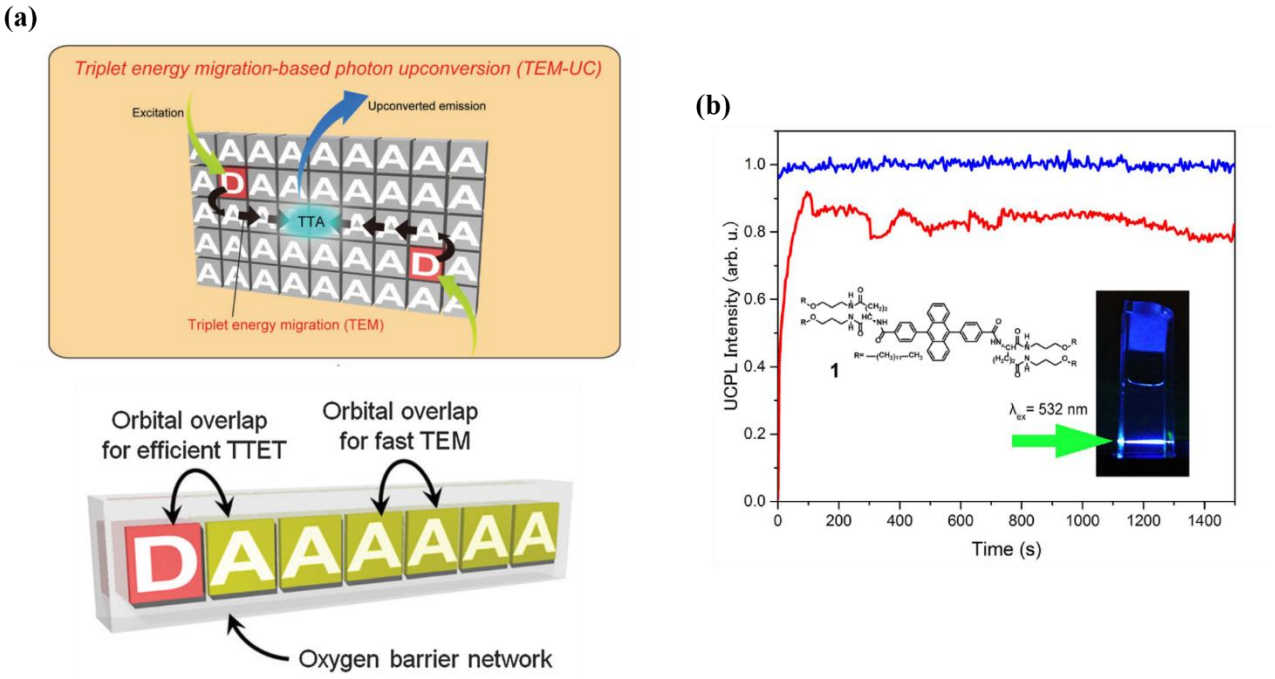

Figure 1-9. Triplet energy-migration based TTA-UC. (a) Scheme of the concept of triplet energy migration-based photon upconversion in the self-assembled system. (b) In-air UC emission of the supramolecular assembly. Chloroform solutions of acceptor **1** and PtOEP in deaerated (blue line) and air-saturated (red line) condition. TTA-UC emission is maintained even in the air-saturated solution.[16,27]

Meanwhile, there remain some essential issues awaited to be solved for the development of this new strategy. Although the effective triplet exciton migration via electron-exchange Dexter mechanism has been demonstrated by controlling the acceptor arrangement, it is still difficult to obtain quantitative TTET in the solvent-free highly-ordered state. In addition, it is not clear how the structural order and range of chromophore alignment contribute to the triplet energy migration that plays a crucial role in maximizing the TTA yield at low excitation power.

1-5 TTA-UC utilized inorganic triplet sensitizers

As described above, one of the problems in the TTA-UC in condensed systems is the decrease in anti-Stokes shifts. This problem can be solved by introducing triplet donor that has an ability to sensitize acceptor triplets without large energy loss. Although phosphorescent molecules have been mainly used as triplet sensitizers for TTA-UC, most of them have intrinsic issues such as relatively large energy loss during S_1-to-T_1 intersystem crossing (ISC). Recently, to solve this matter, inorganic triplet sensitizers such as CdSe/ZnS and PbS quantum dots (QDs) have attracted much attention.[29-34] The literature show that the inorganic triplet donor can sensitize the organic acceptor triplet without energy loss during ISC, and TTA-UC with large anti-Stokes shift can be achieved (Figure 1-10).[33] However, the choice of inorganic materials for TTA-UC is still limited.

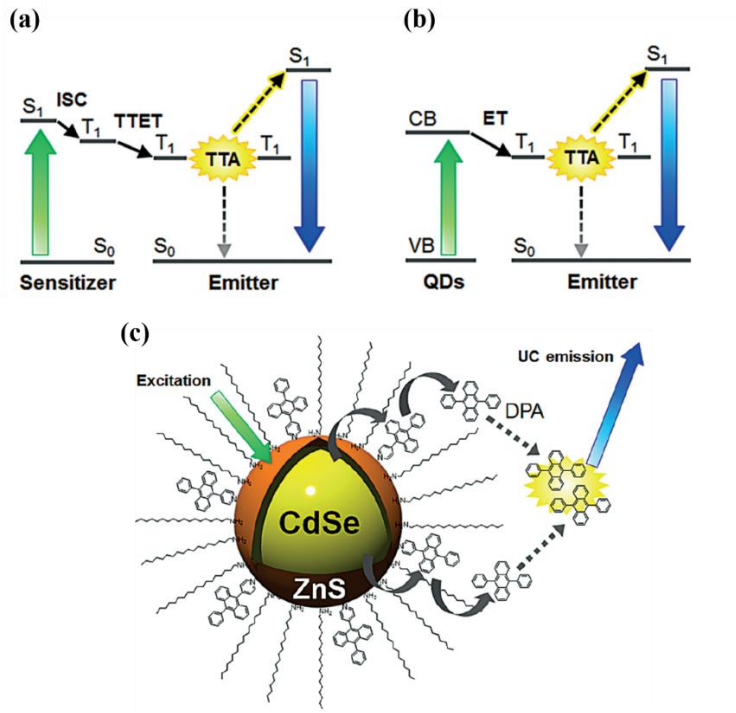

Figure 1-10. Outlines of TTA-UC using (a) phosphorescent organic molecules and (b) inorganic QDs sensitizers, showing the involved energy levels (S = singlet, T = triplet, VB = valence band, CB = conduction band, ISC = intersystem crossing, TTET = triplet-triplet energy transfer, TTA = triplet-triplet annihilation, ET = energy transfer). (c) Schematic illustration of TTA-UC system using acceptor-modified CdSe/ZnS core-shell QDs.[33]

1-6 Motivation and Outline

For the development of TTA-UC in condensed systems, it is necessary to solve three fundamental problems: (1) low triplet diffusion, (2) phase separation of donor and acceptor, and (3) red-shifting of acceptor emission. The triplet energy-migration based TTA-UC and the inorganic sensitizer can be implemented to solve these matters. However, these techniques are still under development. It is necessary to find solutions to avoid phase separation between donors and acceptors, to further improve the triplet-energy-migration efficiency, and to gain a deeper understanding of the inorganic sensitizers. In this dissertation, I describe TTA-UC in condensed systems with the aim to solve the issues above.

In **Chapter 2**, the strategy to solve the problems of phase separation of donors and acceptors and triplet energy migration efficiency is described. This issue was solved by utilizing liquid crystalline acceptor for energy migration in the TTA-UC system. I expected that the structural flexibility and the orientation of the liquid crystal would allow homogeneous doping with the donor and fast energy-migration for efficient TTA. Furthermore, critical effect of the structural order upon the performance of TTA-UC was unveiled by systematic control over the domain size of the liquid crystal.

Chapter 3 focuses on the solution to the decrease in anti-Stokes shift. I employed 3D perovskite nanocrystals as a new inorganic triplet sensitizer. The optical properties of perovskite nanocrystals were tuned by facile halide exchange reactions, which made triplet sensitization possible with various excitation wavelengths. Moreover, studies of triplet states in 3D perovskite promoted a variety of fundamental advances and optical/optoelectronic applications to the perovskite research field.

New function of TTA-UC is discussed in **Chapter 4**. By solving the intrinsic problems of condensed systems, I successfully obtained a stimuli-responsive dual-color TTA-UC. This function is specific to condensed systems, and the result clearly exhibited the availability of TTA-UC in condensed systems.

Chapter 5 summarizes this dissertation.

1-7 Reference

1 M. Pawlicki, H. A. Collins, R. G. Denning and H. L. Anderson, *Angew. Chem. Int. Ed.*, 2009, **48**, 3244-3266.

2 R. R. Birge and B. M. Pierce, *Int. J. Quantum Chem*, 1986, **29**, 639-656.

3 F. Wang, D. Banerjee, Y. Liu, X. Chen and X. Liu, *Analyst*, 2010, **135**, 1839-1854.

4 F. Wang, R. Deng, J. Wang, Q. Wang, Y. Han, H. Zhu, X. Chen and X. Liu, *Nat. Mater.*, 2011, **10**, 968-973.

5 W. Zou, C. Visser, J. A. Maduro, M. S. Pshenichnikov and J. C. Hummelen, *Nat. Photon.*, 2012, **6**, 560-564.

6 S. He, K. Krippes, S. Ritz, Z. Chen, A. Best, H. J. Butt, V. Mailander and S. Wu, *Chem. Commun.*, 2015, **51**, 431-434.

7 S. Baluschev, T. Miteva, V. Yakutkin, G. Nelles, A. Yasuda and G. Wegner, *Phys. Rev. Lett.*, 2006, **97**, 143903.

8 T. N. Singh-Rachford and F. N. Castellano, *Coord. Chem. Rev.*, 2010, **254**, 2560-2573.

9 J. Zhao, S. Ji and H. Guo, *Rsc Adv.*, 2011, **1**, 937-950.

10 J.-H. Kim and J.-H. Kim, *J. Am. Chem. Soc.*, 2012, **134**, 17478-17481.

11 Y. C. Simon and C. Weder, *J. Mater. Chem.*, 2012, **22**, 20817-20830.

12 K. Börjesson, D. Dzebo, B. Albinsson and K. Moth-Poulsen, *J. Mater. Chem. A*, 2013, **1**, 8521-8524.

13 S. H. C. Askes, A. Bahreman and S. Bonnet, *Angew. Chem. Int. Ed.*, 2014, **53**, 1029-1033.

14 M. Häring, R. Pérez-Ruiz, A. Jacobi von Wangelin and D. D. Díaz, *Chem. Commun.*, 2015, **51**, 16848-16851.

15 T. F. Schulze and T. W. Schmidt, *Energy Environ. Sci.*, 2015, **8**, 103-125.

16 N. Yanai and N. Kimizuka, *Chem. Commun.*, 2016, **52**, 5354-5370.

17 S. P. Hill and K. Hanson, *J. Am. Chem. Soc.*, 2017, **139**, 10988-10991.

18 Z. Huang and M. L. Tang, *J. Am. Chem. Soc.*, 2017, **139**, 9412-9418.

19 A. Monguzzi, R. Tubino and F. Meinardi, *Phys. Rev. B*, 2008, **77**, 155122.

20 Y. Y. Cheng, T. Khoury, R. G. C. R. Clady, M. J. Y. Tayebjee, N. J. Ekins-Daukes, M. J. Crossley and T. W. Schmidt, *Phys. Chem. Chem. Phys.*, 2010, **12**, 66-71.

21 A. Monguzzi, F. Bianchi, A. Bianchi, M. Mauri, R. Simonutti, R. Ruffo, R. Tubino and F. Meinardi, *Adv. Energy Mater.*, 2013, **3**, 680-686.

22 A. Haefele, J. Blumhoff, R. S. Khnayzer and F. N. Castellano, *The Journal of Physical Chemistry Letters*, 2012, **3**, 299-303.

23 T. N. Singh-Rachford, J. Lott, C. Weder and F. N. Castellano, *J. Am. Chem. Soc.*, 2009, **131**, 12007-12014.

24 A. Monguzzi, R. Tubino, S. Hoseinkhani, M. Campione and F. Meinardi, *Phys. Chem. Chem. Phys.*, 2012, **14**, 4322-4332.

25 Y. Sagara and T. Kato, *Angew. Chem. Int. Ed.*, 2008, **47**, 5175-5178.

26 P. Duan, N. Yanai and N. Kimizuka, *J. Am. Chem. Soc.*, 2013, **135**, 19056-19059.

27 T. Ogawa, N. Yanai, A. Monguzzi and N. Kimizuka, *Sci. Rep.*, 2015, **5**, 10882.

28 T. Ogawa, N. Yanai, H. Kouno and N. Kimizuka, *J. Photon. Energy*, 2017, **8**, 022003.

29 Z. Y. Huang, X. Li, M. Mahboub, K. M. Hanson, V. M. Nichols, H. Le, M. L. Tang and C. J. Bardeen, *Nano Lett.*, 2015, **15**, 5552-5557.

30 Z. Y. Huang, X. Li, B. D. Yip, J. M. Rubalcava, C. J. Bardeen and M. L. Tang, *Chem. Mater.*, 2015, **27**, 7503-7507.

31 M. Mahboub, Z. Y. Huang and M. L. Tang, *Nano Lett.*, 2016, **16**, 8037-8037.

32 C. Mongin, S. Garakyaraghi, N. Razgoniaeva, M. Zamkov and F. N. Castellano, *Science*, 2016, **351**, 369-372.

33 K. Okumura, K. Mase, N. Yanai and N. Kimizuka, *Chem. -Eur. J.*, 2016, **22**, 7721-7726.

34 M. F. Wu, D. N. Congreve, M. W. B. Wilson, J. Jean, N. Geva, M. Welborn, T. Van Voorhis, V. Bulovic, M. G. Bawendi and M. A. Baldo, *Nat. Photon.*, 2016, **10**, 31-34.

Chapter 2 Controlling One-Dimensional Triplet Exciton Diffusion in Columnar Liquid Crystals for Low-Power Photon Upconversion

2-1 Introduction

ABSTRACT: The critical effect of structural order upon performances of triplet-triplet annihilation-based photon upconversion (TTA-UC) was unveiled by experimental and theoretical analysis of triplet exciton diffusion in columnar liquid crystals (LCs). A triplet sensitizer was homogeneously doped in flexible columnar LCs composed of π-stacked acceptor perylene arrays, leading to a sequence of quantitative donor-to-acceptor triplet-triplet energy transfer (TTET), triplet energy migration, and consequent TTA-UC in LCs. Co-assembly with acceptors having shorter alkyl chains enhanced the triplet exciton diffusion constant, resulting in the significant reduction of threshold excitation intensity I_{th} of TTA-UC. This work provides important guidelines for designing energy-migration-based TTA-UC in soft materials workable at low excitation intensity.

Photon upconversion (UC), the phenomenon converting lower energy photons to higher energy photons, has been attracting considerable attention for its potential to improve the efficiency of sunlight-powered energy production devises including photocatalysis and photovoltaics.[1-15] The UC mechanism based on triplet−triplet annihilation (TTA-UC) is particularly useful since it works under low excitation power densities (<100 mW cm^{-2}).[1-12] The TTA-UC involves a series of photo-relaxation processes as depicted in Figure 1-1. Two acceptor (emitter) triplets populated by triplet-triplet energy transfer (TTET) from donors (sensitizer) collide to undergo TTA within their lifetimes. A higher energy excited singlet the of emitter is generated, which emits upconverted fluorescence.

Most of the previous studies on TTA-UC utilized the translational diffusion of excited molecules in solutions or soft polymers. However, the use of volatile organic solvents is not suitable for practical applications, whereas the diffusion of dye molecules embedded in solid polymers is inevitably low. As a solution to these problems, several research groups including ours demonstrated an alternative

strategy based on energy-migration-based TTA-UC, which exploits the triplet exciton diffusion and annihilation in densely preorganized chromophore arrays.[10,16-23] Meanwhile, the detailed understanding of triplet diffusion dynamics in these complex condensed materials is still lacking. Moreover, more systematic and detailed studies are required to unveil the relationship between structural order/defects and UC performances.

In this chapter, I describe a combined experimental and theoretical study for understanding and controlling triplet exciton diffusion in columnar liquid crystals (LCs) for low-power TTA-UC (Figure 2-1a). A triplet donor Pt(II) tetraphenyltetra-benzoporphyrin (PtTPBP) was doped in a columnar LC of 3,4,9,10-tetra(2-ethylhexyloxy-carbonyl)-perylene (**1**)[24,25] that consist of the stacked array of acceptor perylene units (Figure 2-1b). Structural flexibility of the LC allowed homogeneous doping of the donor and consequent quantitative donor-to-acceptor TTET. Interestingly, the threshold excitation intensity I_{th} of TTA-UC was significantly reduced by being co-assembled with tetra(ethyloxy-carbonyl)-perylene (**2**) containing shorter alkyl chains.[26,27] Transient absorption spectroscopies revealed that the triplet exciton diffusion in these columnar LCs is purely one-dimensional. In addition, the diffusion constant of triplet excitons is improved by the addition of **2**. The unveiled relationship between structural order and UC properties provides a basis for designing solvent- and matrix-free low-power TTA-UC soft materials

.

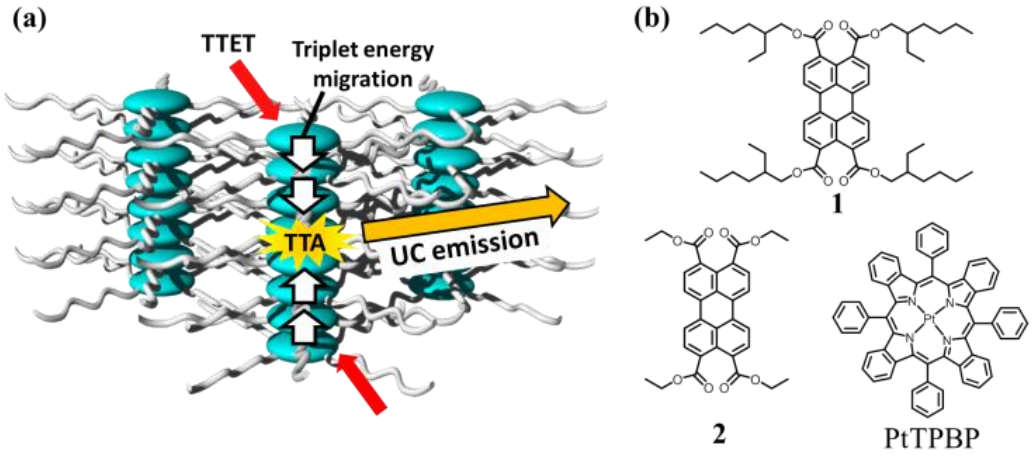

Figure 2-1. (a) Schematic representations of TTA-UC in columnar LCs. Excited triplet state of acceptor moieties (cyan) of a columnar LC are sensitized by homogeneously-doped donor molecules (TTET). This is followed by a sequence of triplet energy migration among the acceptors, TTA, and delayed fluorescence from the upconverted acceptor singlet. (b) Chemical structures of acceptor **1** and **2**, and donor PtTPBP.

2-2 Results and Discussion

As a fluorescent columnar LC, **1** having typical acceptor unit (perylene) was prepared according to the reported procedure.[24,25] Differential scanning calorimetry (DSC) measurements of **1** showed a glass transition temperature at −73 °C and a melting temperature at 249 °C, which confirms the presence of stable columnar LC phase over a wide temperature range including room temperature (Figure 2-2).

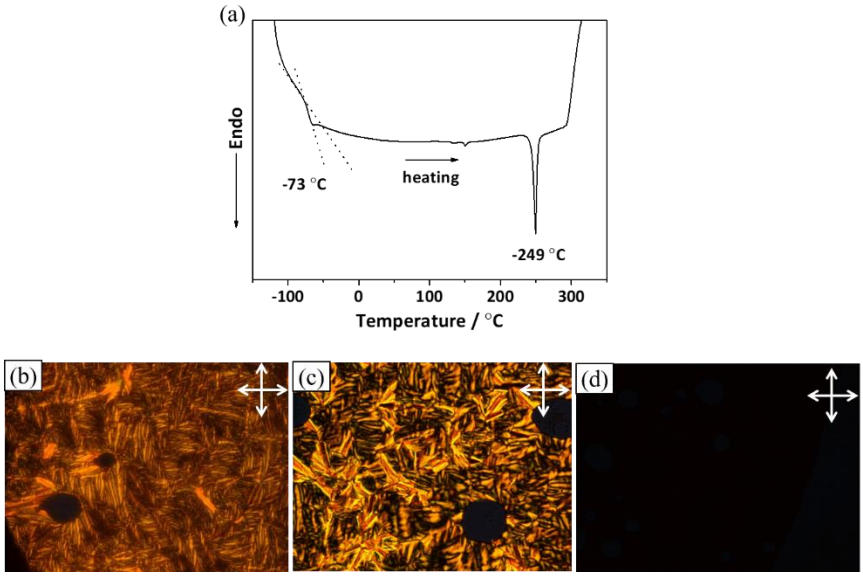

Figure 2-2. (a) DSC thermogram of **1** (10 °C/min) under N_2 atmosphere. Polarized optical microscope images at (b) −130°C (glass phase), (c) at the room temperature (liquid crystal phase), and (d) at 280°C (isotropic phase).

As previously characterized,[28] the X-ray powder diffraction (XRPD) pattern of **1** showed a typical hexagonal columnar LC structure with an inter-column separation of 2.05 nm and an intra-column π-π stacking distance of 0.35 nm (Figure 2-3).

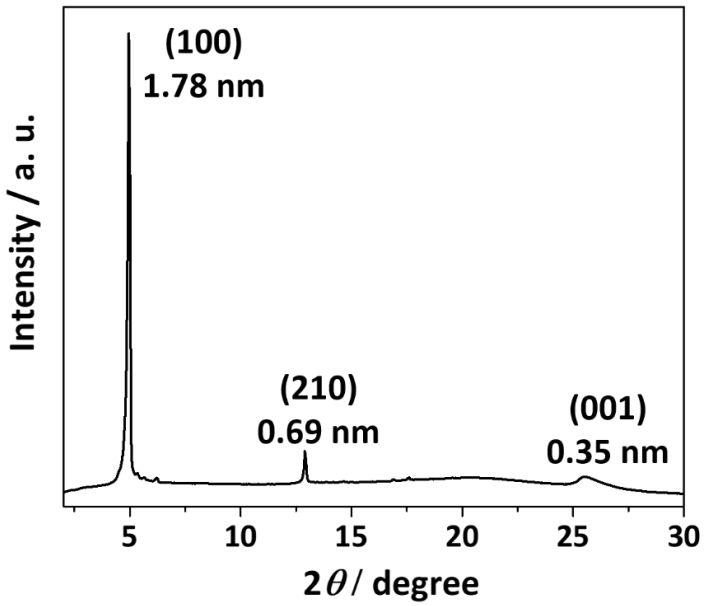

Figure 2-3. X-ray powder diffraction (XRPD) patterns of **1** as typical peak positions of hexagonal columnar LCs.

To investigate the molecular arrangements of **1** more in detail, I measured absorption and fluorescence spectra, fluorescence lifetime, and absolute fluorescence quantum yields in $CHCl_3$ ([**1**] = 5 μM) and in the solvent-free columnar LC state. The absorption spectrum of **1** in $CHCl_3$ showed structured bands and an S_0-S_1 absorption maximum at 472 nm (Figure 2-4a). On the other hand, the absorption spectrum of the columnar LC **1** showed broadened bands with a much less resolved vibronic structure, in which a band splitting into the blue-shifted (454 nm) and red-shifted (488 nm) peaks was observed. The observed splitting pattern is indicative of the excitonic interactions between rotationally displaced long molecular axis of perylene chromophores (Figure 2-4b).[29-31] The fluorescence spectrum of **1** in the LC phase showed a large red shift (110 nm) with spectral broadening as compared with that in solution, which is ascribed to the excimer-like delocalized excitons in the stacked perylene chromophores. This is further supported by a longer fluorescence lifetime in columnar LC **1** (27.2 ns) than that observed in $CHCl_3$ solution (3.8 ns, Figure 2-5). The absolute fluorescence quantum yield of **1** in the LC phase was determined as 33%, not high as a $CHCl_3$ solution (89%).

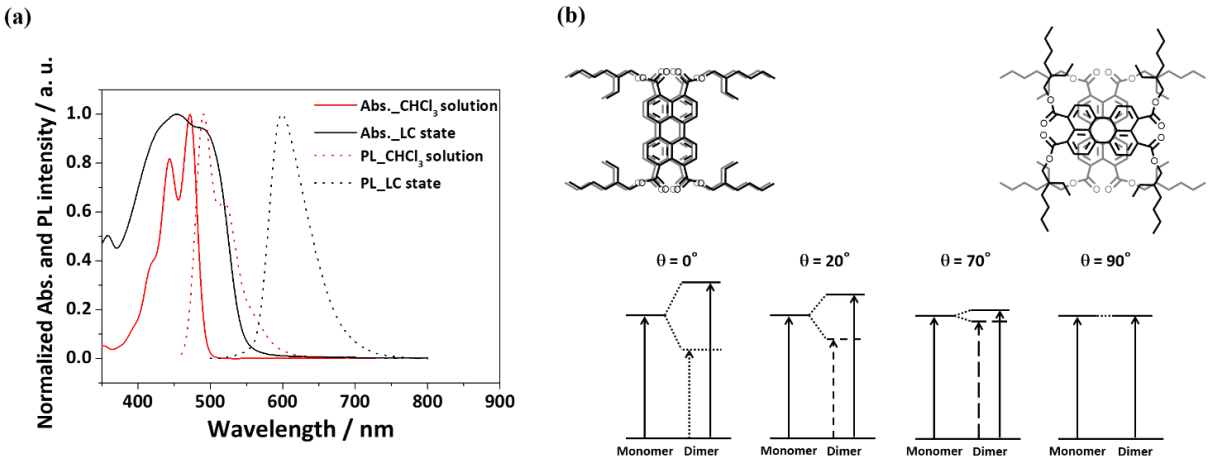

Figure 2-4. (a) Normalized absorption (Abs.) spectra of **1** in $CHCl_3$ solution (100 μM, red solid line) and in the solvent-free LC state (black solid line). Normalized photoluminescence (PL) spectra of **1** in $CHCl_3$ solution (5 μM, red dotted line) and in the solvent-free LC state (black dotted line). (b) Exciton band structures in dimers of various rotational displacement θ between two neighboring chromophores.[29-31] When the θ value is around 90° (but not precisely 90°), the absorption band splits into two.

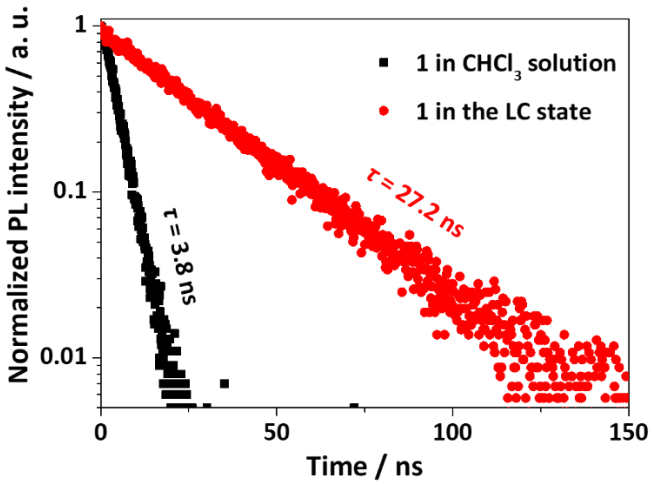

Figure 2-5. Fluorescence lifetimes of **1** in $CHCl_3$ solution (black, 5 μM, $\tau = 3.8$ ns) and in the solvent-free LC state (red, $\tau = 27.2$ ns).

The acceptor columnar LC **1** was doped with a donor PtTPBP by drop-casting a mixed toluene solution of **1** and PtTPBP ([PtTPBP]/[**1**] = 0.05 mol%) on substrates and subsequent annealing at 290 °C. The donor PtTPBP and acceptor **1** have appropriate singlet/triplet energy levels for TTA-UC, as confirmed by the appearance of TTA-UC emission in deaerated solution (Figure 2-6 and 2-7).

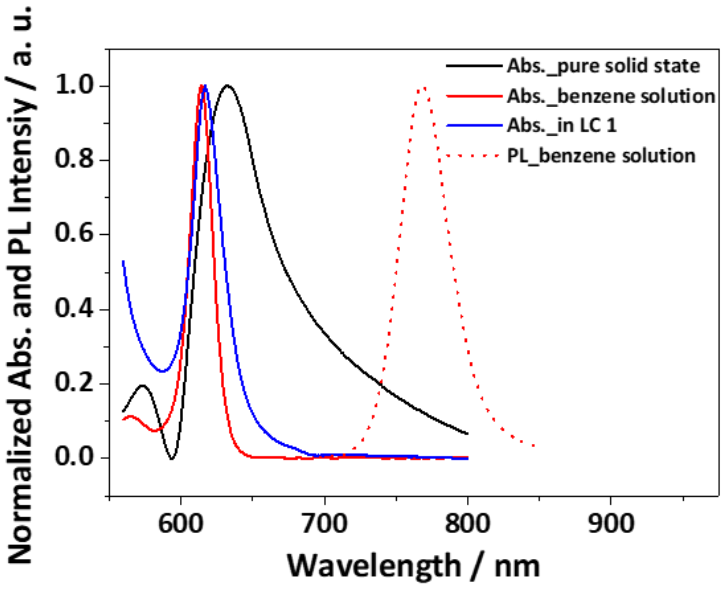

Figure 2-6. Normalized absorption (Abs) spectra of PtTPBP in pure solid state (black solid line), benzene solution (0.1 μM, red solid line) and LC **1** (blue solid line), and the normalized photoluminescence (PL) spectrum of PtTPBP in deaerated benzene solution (red dotted line, 100 μM).

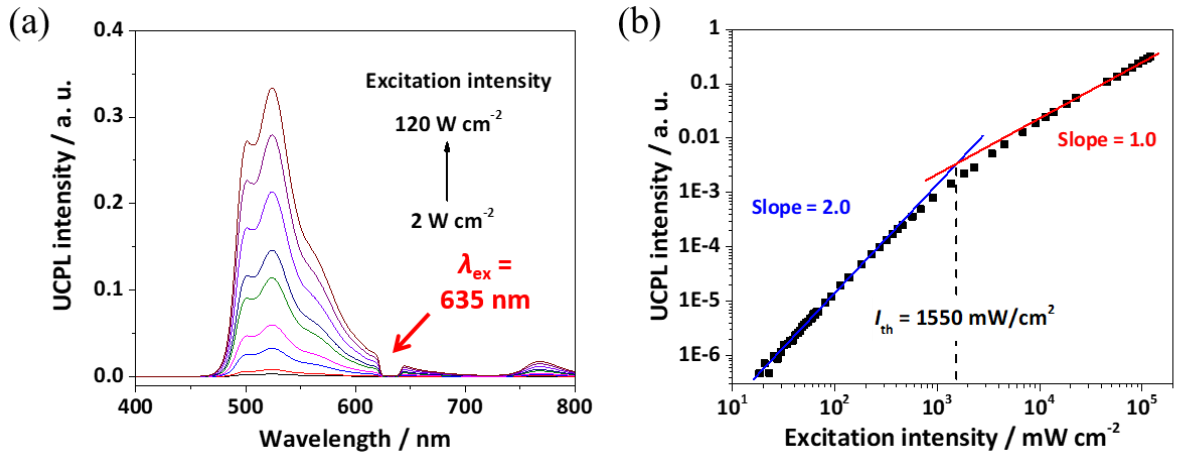

Figure 2-7. (a) Upconversion photoluminescence (UCPL) spectra of the mixture of PtTPBP and **1** in toluene ([PtTPBP]/[**1**] = 1mol %, [**1**] = 1 mM) with different incident power density of 635 nm laser. A notch filter (λ = 635 nm) was used to remove the scattered incident light. (b) Dependence of TTA-assisted emission intensity at 530 nm on the incident power density. Blue and red lines are fitting results with slopes of 2.0 (blue) and 1.0 (red) in the low- and high-power regimes. The high I_{th} value comes from low absorption coefficient α (0.15 cm^{-1}).

Optical microscopy images of PtTPBP-doped **1** showed the retention of LC phase without macroscopic segregation of PtTPBP (Figure 2-8a). The absorption band of PtTPBP in LC **1** was close to that in solution rather than the neat solid PtTPBP, indicating the donor is molecularly dispersed in the regular LC structure without segregation (Figure 2-6). The PtTPBP-doped **1** was filled in a 0.05 mm-thick quarts cell and sealed in an Ar-filled grove box ([O_2] < 0.1 ppm). Interestingly, the solvent-free PtTPBP-doped **1** showed a clear yellow upconverted emission upon excitation by a 635 nm red laser (Figure 2-8b). It is noteworthy that the donor phosphorescence at 760 nm was quenched regardless of the excitation power, demonstrating the quantitative donor-to-acceptor TTET process.

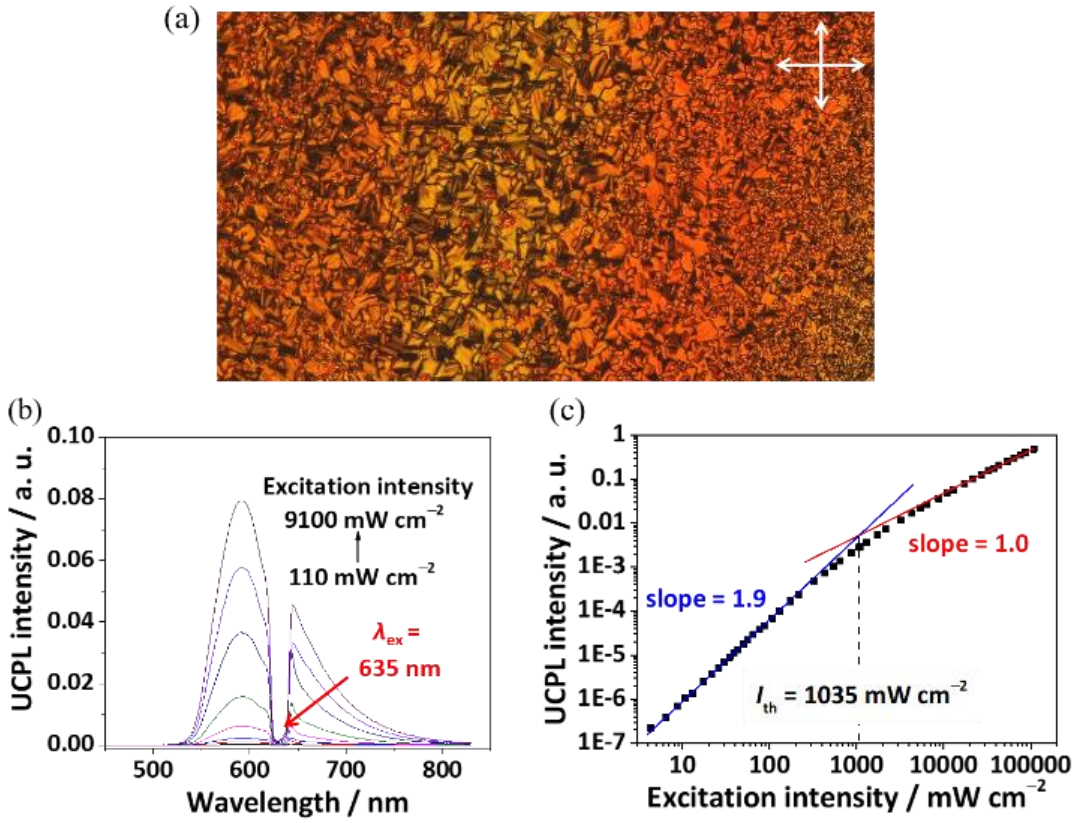

Figure 2-8. (a) Polarized optical microscope image of PtTPBP-doped **1** ([PtTPBP]/[**1**] = 0.05 mol %). (b) UC photoluminescence (UCPL) spectra of the PtTPBP-doped LC **1** ([PtTPBP]/[**1**] = 0.05 mol%) with different incident power density of 635 nm laser. A notch filter (λ = 635 nm) was used to remove the scattered incident light. (c) Dependence of UC emission intensity at 580 nm on the incident power density. Blue and red lines are fitting results with slopes of 1.9 (blue) and 1.0 (red) in the low and high-power regimes.

To further characterize the UC emission, I measured an excitation power dependence of the UC emission intensity. In general, TTA-UC emission intensity shows a quadratic and linear incident light intensity dependence in weak and strong excitation regimes.[32-35] Figure 2-8c presents a double logarithm plot of the TTA-UC emission intensity of the PtTPBP-doped columnar LC **1** as a function of the incident light power density. A change of slope from ca. 2 to 1 was observed. The threshold excitation intensity at which the two fitting lines cross, I_{th}, is the key parameter characterizing TTA-UC emission processes, which defines the useful irradiance working range. The I_{th} value around 1000

mW/cm^2 was observed for the current LC system, which is relatively high compared to previous TTA-UC systems.[10,16-21]

In order to reduce the I_{th} value, I attempted to enhance the triplet diffusivity. The diffusion of triplet excitons occurs via electron-exchange Dexter mechanism, which is severely affected by the orbital overlap between neighboring aromatic moieties.[36] I hypothesized that the bulky 2-ethylhexyloxy groups of LC **1** reduce the effective overlap of molecular orbitals in the columnar assembly, thus limiting the Dexter transfer rate. To overcome this issue, the perylene derivative **2** having shorter alkyl chains was mixed with LC **1** to alleviate the steric hindrance between the bulky side groups (Figure 2-1b). The acceptor **2** was prepared by following the reported method.[26,27] I mixed **1** and **2** in different mixing ratio and annealed them above isotropic phase temperatures (270-290°C). This annealing process was necessary to homogeneously mix **1** and **2**. DSC measurements showed that the LC-to-isotropic phase transition temperature gradually decreased with increasing the mixing ratio up to **2**/(**1**+**2**) = 30 mol%, where the transition peaks of neat **2** were not observed (Figure 2-9).

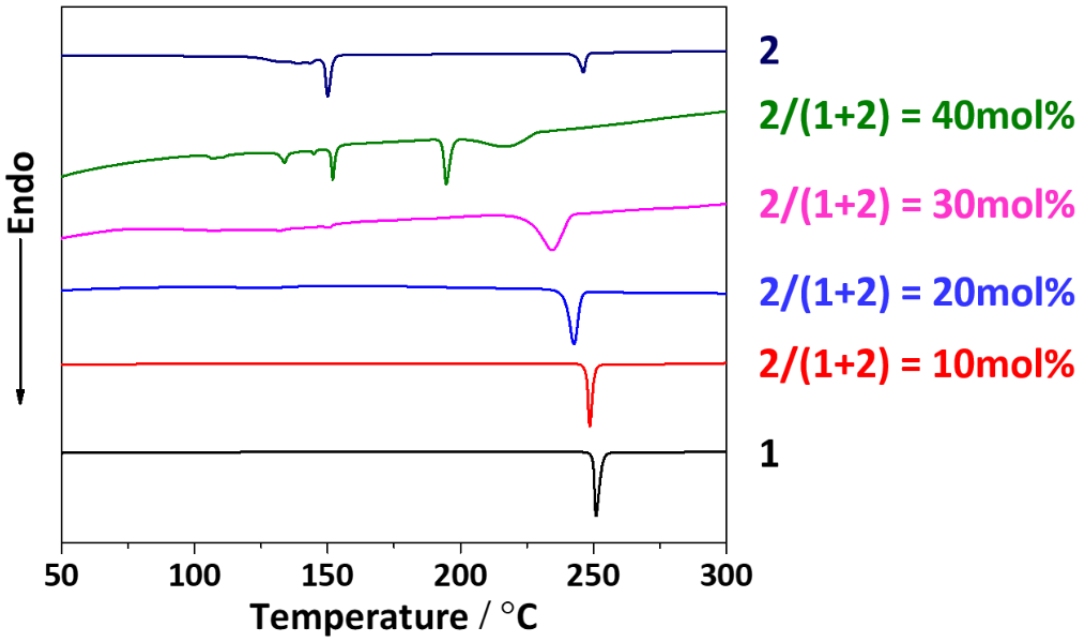

Figure 2-9. DSC thermograms of **1**, **2** and binary LC **1**-**2** in mixing ratio of 10-40mol% under N_2 atmosphere (heating, 10 °C/min).

This result indicates the mixing of **1** and **2** without macroscopic phase separation. In this range of mixing ratio, the hexagonal columnar LC structure was maintained, as confirmed by XRPD and optical microscopy measurements (Figure 2-10 and 2-11). On the other hand, when the mixing ratio was increased to **2**/(**1**+**2**) = 40 mol%, the DSC thermogram and XRPD pattern showed unassignable peaks, suggesting the inhomogenous mixing (Figure 2-9 and 2-10). The absorption band around 450 nm becomes narrower by the addition of **2**, indicating the improved arrangement of perylene cores (Figure 2-12). On the other hand, the pristine **1** and the **1**-**2** binary LCs showed no fluorescence shifts. (Figure 2-13).

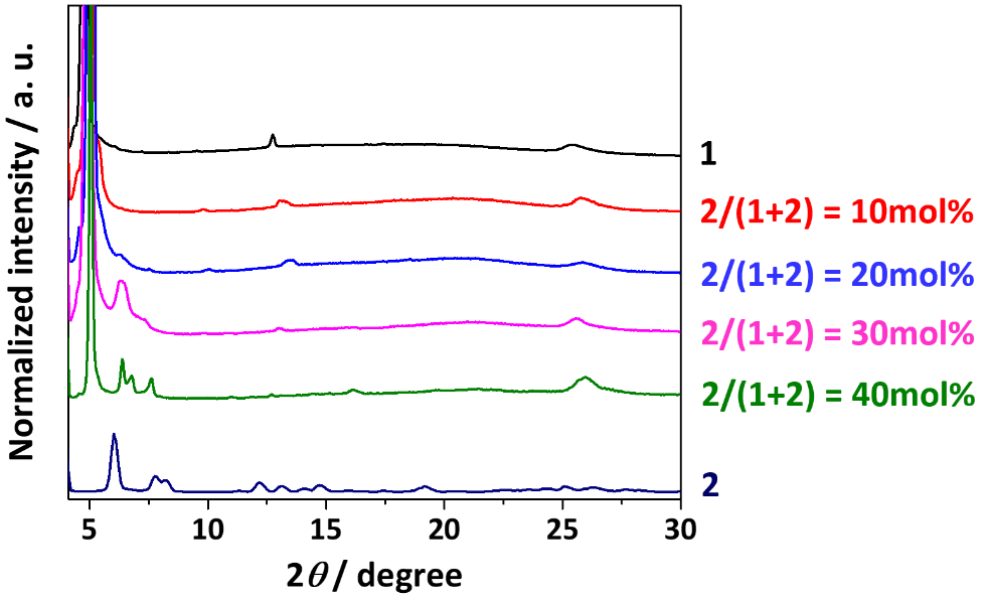

Figure 2-10. XRPD patterns of **1**, **2** and binary LC **1**-**2** with mixing ratio of 10-40mol%. All samples were prepared by heating the materials to the isotropic phase (270-290 °C) on Si wafer, followed by cooling to room temperature. There are additional peaks in the binary LC **1**-**2** (**2**/(**1**+**2**) = 40 mol%) at 6.8 and 7.6° compared with the pristine **1** due to the inhomogeneous mixing between **1** and **2**. The peak at 6.4° was observed for both of the pristine LC **1** and binary LC **1**-**2**. The position and intensity of this peak is sensitive to the preparation method (ex. substrate, sample thickness, mechanical shearling), and thus this peak is probably related to different orientation or partial crystal formation at surfaces. Nevertheless, almost all part of **1** and binary LC **1**-**2** (**2**/(**1**+**2**) ≤ 30 mol%) has the hexagonal columnar LC structure. This conclusion is consistent with the optical microscopy results (Figure 2-11).

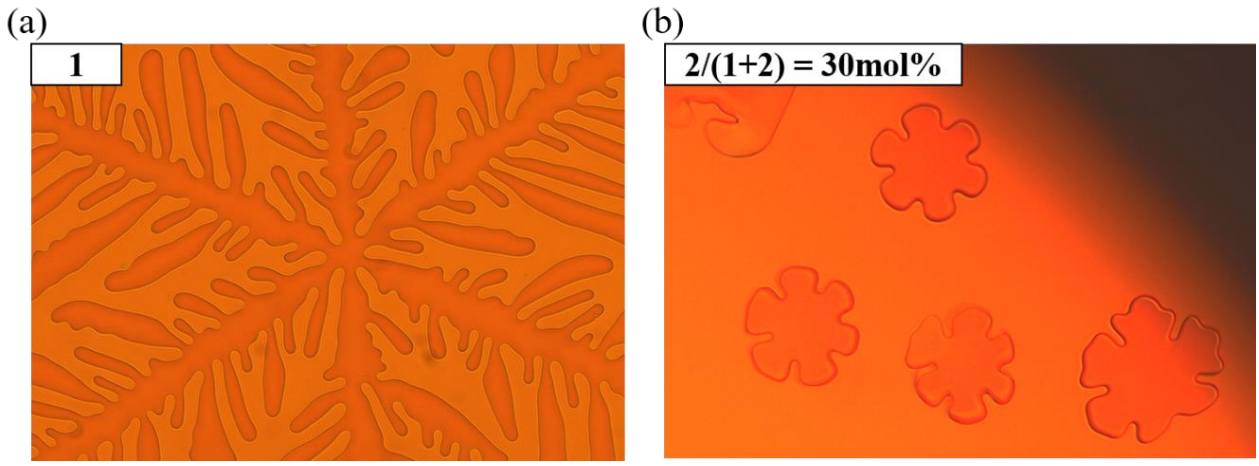

Figure 2-11. Optical microscope images of (a) **1** at 250 °C and (b) **2**/(**1**+**2**) = 30mol% at 245 °C. The samples were sandwiched by polyimide-modified glass substrates for homeotropic alignment. Both samples showed typical hexagonal growing textures of hexagonal columnar LC.

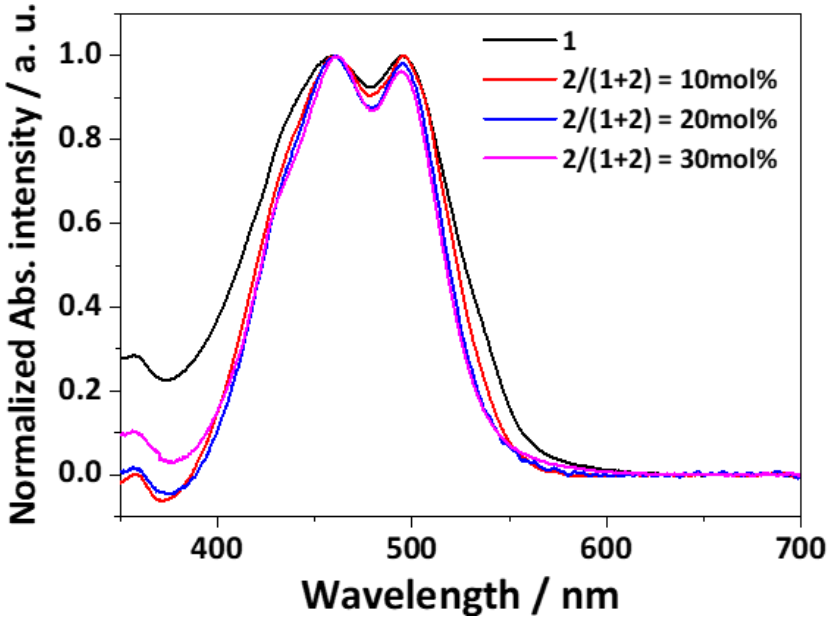

Figure 2-12. Normalized a absorption spectra of the LC **1** (black), the binary LCs **1**-**2** with mixing ratio of **2**/(**1**+**2**) = 10mol% (red), 20mol% (blue), 30mol% (purple). The absorption band becomes narrower as the portion of **2** increases, indicating that improved arrangements (homogeneous environment) of perylene cores.

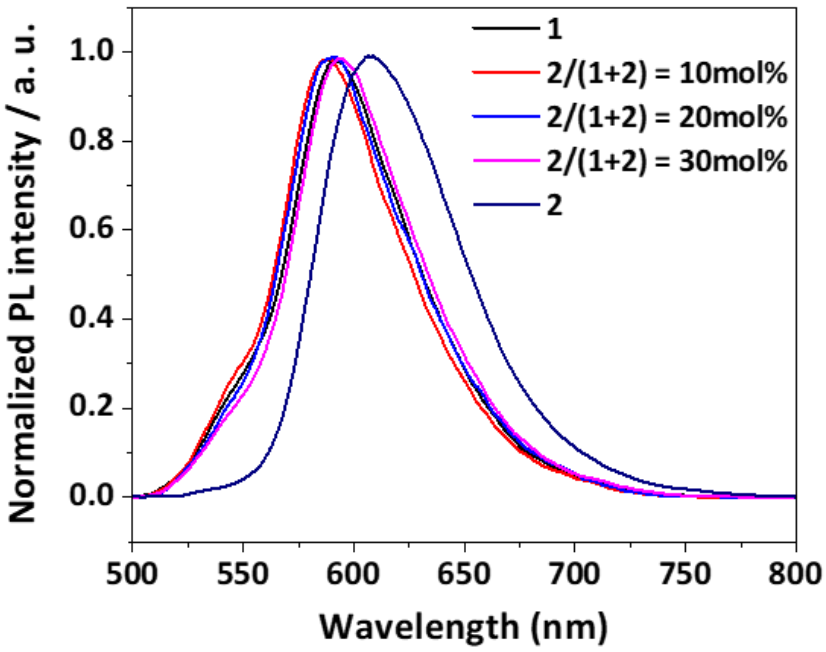

Figure 2-13. Normalized PL spectra of the LC **1** (black), the binary LCs **1**-**2** with mixing ratio of **2**/(**1**+**2**) = 10mol% (red), 20mol% (blue), 30mol% (purple), and **2** (navy).

The **1**-**2** binary columnar LCs were then doped with PdTPBP and their TTA-UC properties were investigated ((PtTPBP)/(**1**+**2**) = 0.05 mol%, **2**/(**1**+**2**) = 0~30 mol%). Under excitation by 635 nm laser, TTA-UC emission was observed in **1**-**2** binary columnar LCs (Figure 2-14). There was no difference in UC quantum yield between PtTPBP-doped LC **1** and binary LC **1**-**2** (**2**/(**1**+**2**) = 30mol%) showed the similar UC efficiency Φ_{UC}' of 1.7% at 4.1 W/cm^2, which is reasonably high values. Note that the donor phosphorescence at 760 nm was completely quenched in all the samples, indicating the quantitative TTET also in the mixed LC systems. Significantly, as the mixing ratio (**2**/(**1**+**2**)) increased from 0 to 30 mol%, the I_{th} value dramatically decreased from 1035 to 51 mW/cm^2 (Figure 2-15). Since there was no large difference in triplet lifetime and PtTPBP absorbance between LC **1** and binary LC **1**-**2**, these results suggest that triplet diffusivity is the main factor affecting I_{th} (Figure 2-16 and 2-17).

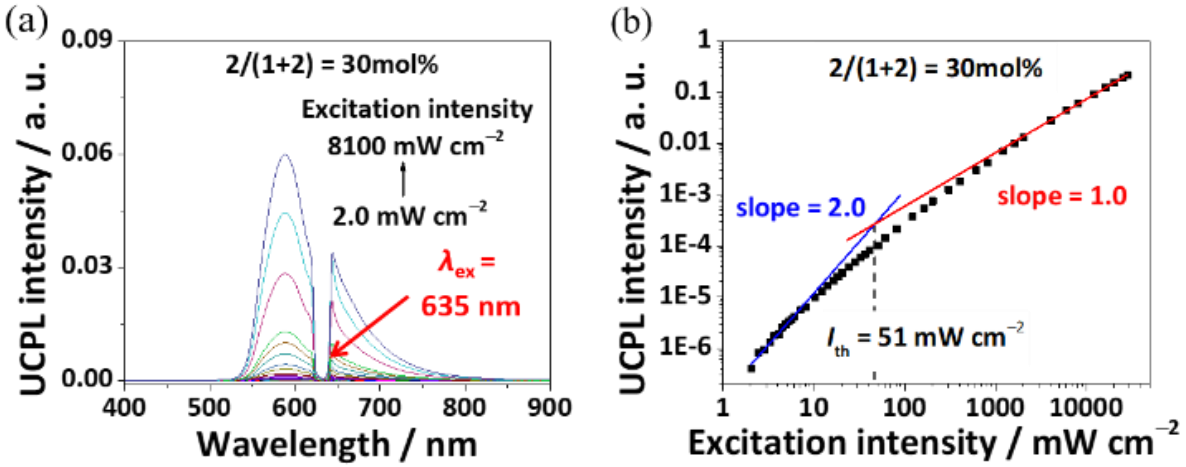

Figure 2-14. (a) UCPL spectra of the PtTPBP-doped binary LC **1-2** (PtTPBP/(**1**+**2**) = 0.05 mol%, **2**/(**1**+**2**) = 30mol%) with different incident power densities of 635 nm laser. A notch filter (λ = 635 nm) was used to remove the scattered incident light. (b) Dependence of UC emission intensity at 580 nm on the incident power density. Blue and red lines are fitting results with slopes of 2.0 (blue) and 1.0 (red) in the low and high-power regimes.

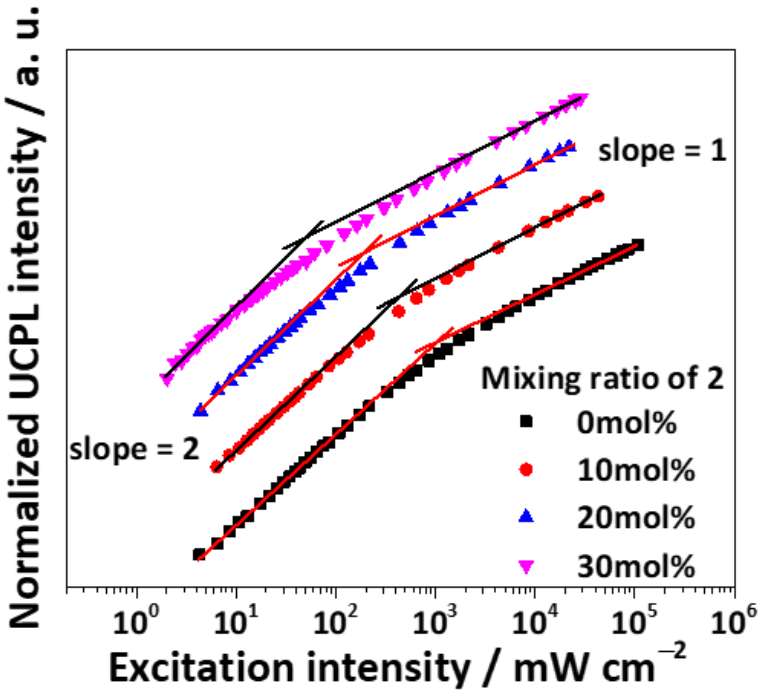

Figure 2-15. Mixing ratio of **2** dependences of threshold excitation intensity I_{th} (LC **1**: black square, the binary LCs **1-2** with mixing ratio of **2**/(**1**+**2**) = 10mol%: red circle, 20mol%: blue triangle, 30mol%: purple triangle).

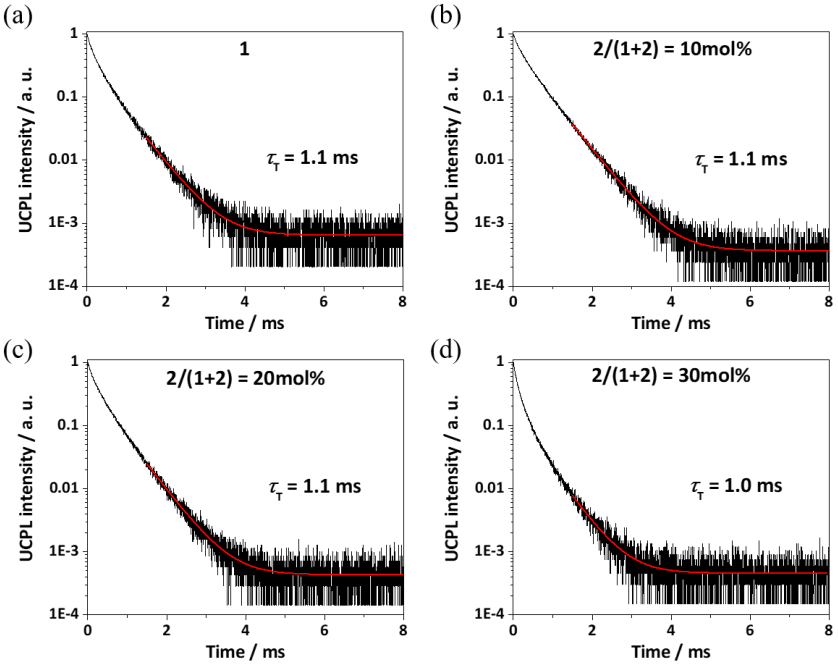

Figure 2-16. TTA-UC emission decay of the PtTPBP-doped LC **1** (a) and binary LC **1**-**2** with mixing ratio of **2**/(**1**+**2**) = 10mol% (b), 20mol% (c), 30mol% (d) ([PtTPBP]/[**1**+**2**] = 0.05mol%, λ_{ex} = 630 nm, λ_{em} = 590 nm). The red line is fitting result with the function $I_{UC}(t) = I_{UC}(0)\exp(-2t/\tau_T)$.

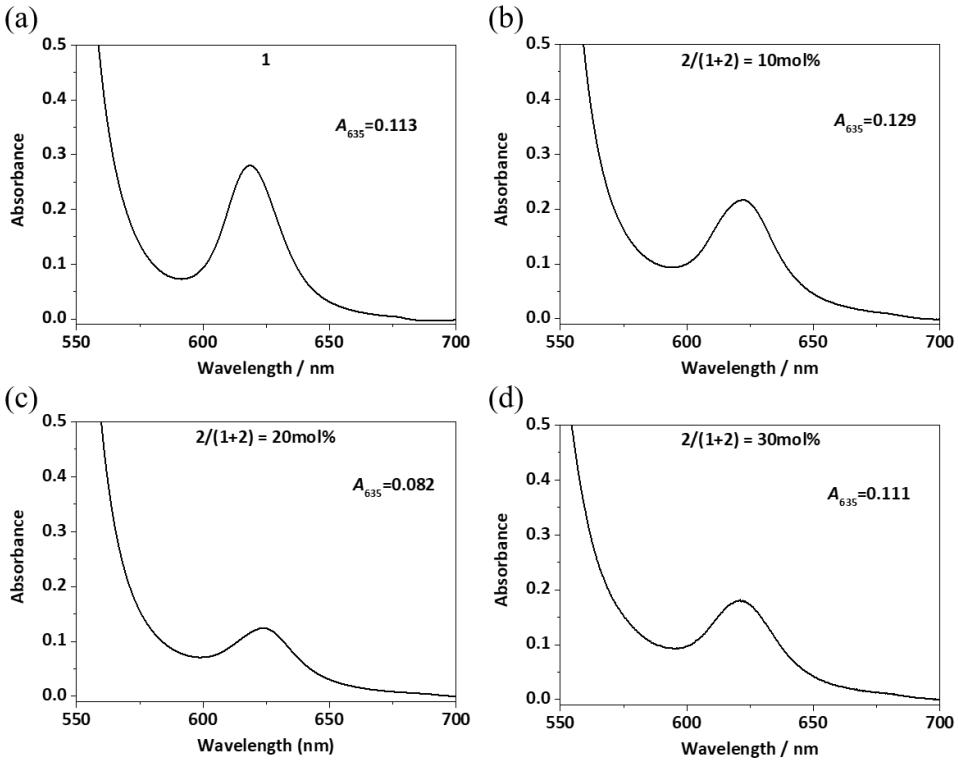

Figure 2-17. Absorption spectra of PtTPBP in the LC **1**, and in the binary LCs **1**-**2** with mixing ratio of **2**/(**1**+**2**) = 10mol%, 20mol%, 30mol%.

To get insights into the origin of I_{th} reduction, I investigated the triplet diffusion dynamics in the LC **1** and the binary LCs **1**-**2** by transient absorption spectroscopy. The LC **1** was introduced into a 9 μm-thick LC cell at 290°C and sealed by using thermoplastic resin in an Ar-filled glove box ([O_2] < 0.1 ppm). Due to the large overlap of signals from **1** and PtTPBP, I directly excited the singlet state of LC **1** by a 355 nm pulse laser and populated triplet states of **1** through S_1-to-T_1 ISC. The transient absorption spectrum of the LC **1** showed an absorption maximum at 540 nm (Figure 2-18a). The decay lifetime of this transient absorption was 1.0 ms (Figure 2-18b), which is consistent with the triplet lifetime obtained from the UC emission lifetime (1.1 ms, Figure 2-16a). This absorption band is therefore assignable to a T_1-T_n absorption of **1**.

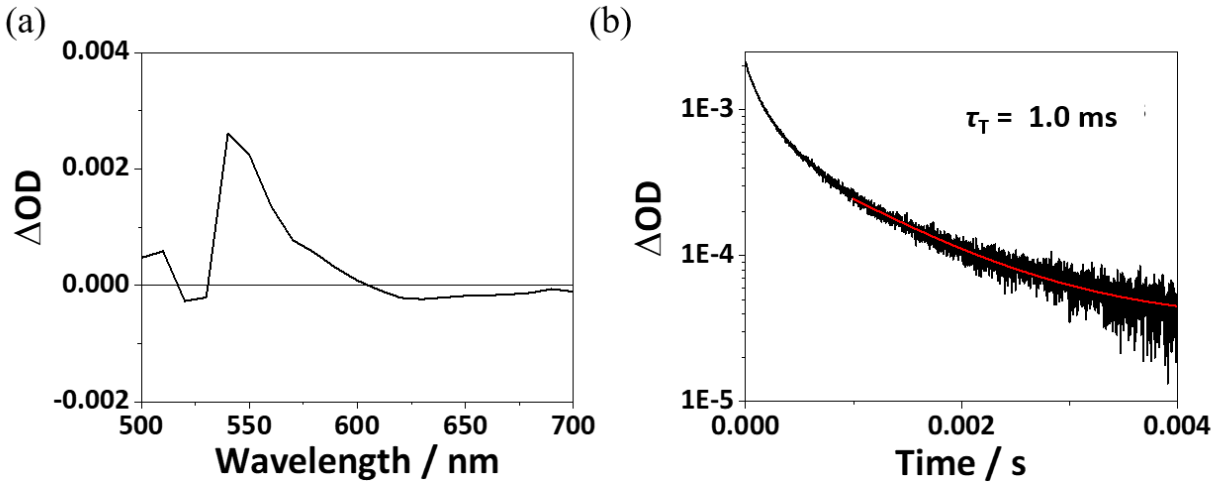

Figure 2-18. (a) The transient absorption spectrum of LC **1** measured at 20 μs after the laser excitation. The excitation wavelength and power were 355 nm and 5.9 mJ/cm^2, respectively. (b) The decay trace of ΔOD of LC **1** at 540 nm. The red line is a fitting result with the function $\Delta OD(t) = \Delta OD(0)\exp(-t/\tau_T)$.

It has been reported that the diffusion-limited bimolecular TTA rate constant γ_{TT} largely depend on the dimensionality of the system.[37-41] The γ_{TT} value becomes time-independent for the 3D system and $t^{-\alpha}$ dependent ($\alpha < 1/2$) for the 2D system at larger delay time t and is consistently $t^{-1/2}$ dependent for the 1D system over the entire time domain.[37-41] According to the previous reports, I extracted the γ_{TT}

from the triplet decay dynamics.[41-43] The rate equation for the triplet exciton decay can be described by the following equation,

$$\frac{dn(t)}{dt} = -\frac{n(t)}{\tau} - \gamma_{TT}(t)n^2(t)$$

(Equation 2-1)

where $n(t)$ is the triplet exciton density at a delay time t after the laser excitation, τ is the natural triplet lifetime (in the absence of the TTA), and $\gamma_{TT}(t)$ is the bimolecular decay (TTA) rate constant. The calculation of the time dependence of the γ_{TT} is made by renormalizing the data with a new variable $Y(t)$: [41-43]

$$Y(t) = \frac{\exp\left(-{}^{t}/_{\tau}\right)}{n(t)}$$

(Equation 2-2)

By substituting Equation 2-1 into Equation 2-2, a linearized differential equation is obtained (Equation 2-3).

$$\gamma_{TT}(t) = \exp({}^{t}/_{\tau})\frac{dY(t)}{dt}$$

(Equation 2-3)

Therefore, the time evolution of γ_{TT} can be obtained from experimental values of the $n(t)$ and the τ.

The diffusion-limited bimolecular reaction rates significantly depend on the dimensionality of the system. The γ_{TT} for 1D and 3D diffusion systems are given by Equation 2-4 and Equation 2-5, respectively. [37,38,40,41]

$$\gamma_{TT,1D}(t) = \frac{1}{aN_0}\sqrt{\frac{8D}{\pi t}}$$

(Equation 2-4)

$$\gamma_{TT,3D}(t) = 8\pi DR\left(1 + \frac{R}{\sqrt{2\pi Dt}}\right)$$

(Equation 2-5)

where, a is the 1D-lattice constant, N_0 is the three-dimensional molecular density, and R is the effective interaction radius of triplet excitons.

The $n(t)$ can be obtained from the ΔOD and the Beer-Lambert law: [39]

$$n(t) = 6.02\times10^{23}\frac{\Delta\mathrm{OD}}{10^3\Delta\varepsilon l_e}$$

(Equation 2-6)

where $\Delta\varepsilon$ is the differential molar extinction coefficient (M^{-1} cm^{-1}) at the laser excitation wavelength, and l_e is the effective optical path length (cm). The $\Delta\varepsilon$ can be estimated from an absorbed laser pulse intensity dependence of ΔOD at $t = 0$ and Equation 2-7.

$$\Delta\mathrm{OD}_{(t=0)} = \frac{\Delta\varepsilon\Phi_T}{6\times10^{20}}I_a$$

(Equation 2-7)

where Φ_T is the triplet quantum yield, and I_a is the absorbed light intensity (photons cm^{-2}).

The Φ_T value of the **1** was determined from the laser intensity dependence of the $\Delta OD_{(t=0)}$ of the **1** in deoxygenated toluene (10 μM, Figure 2-19), and Equation 2-8 and Equation 2-9.[44-47]

$$\Delta\mathrm{OD}_{(t=0)} = a\{1-\exp(-bE)\}$$

(Equation 2-8)

$$\mathrm{b} = 2303\varepsilon^0_{exc}\Phi_T$$

(Equation 2-9)

where E is the laser intensity (Einstein cm^{-2}), and ε^0_{exc} is the molar absorption coefficient of the ground state at the laser excitation wavelength.

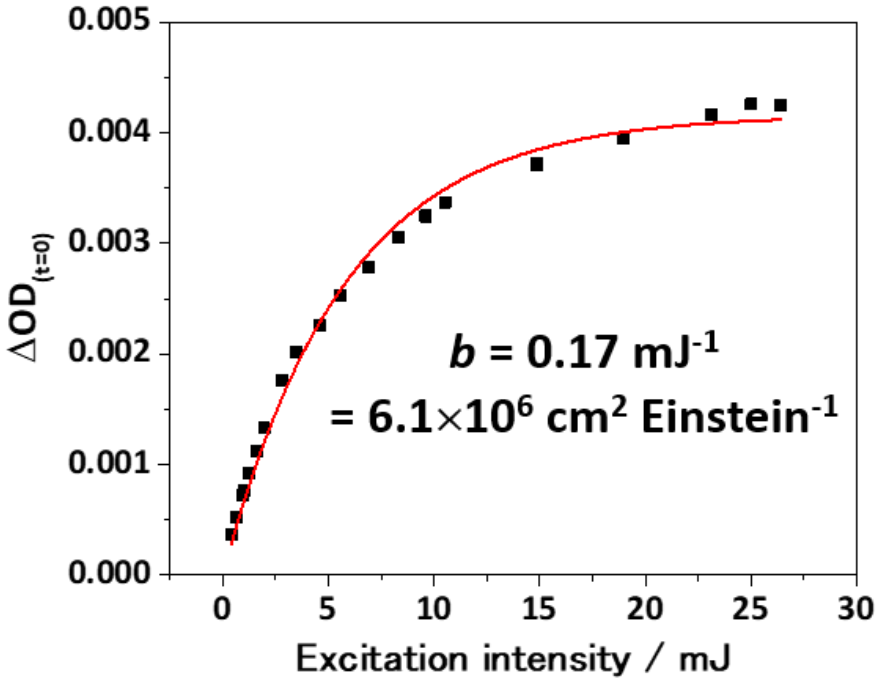

Figure 2-19. Laser intensity dependence of the $\Delta OD_{(t=0)}$ of the **1** in deoxygenated toluene (10 μM). The laser excitation wavelength was 475 nm. The ΔOD detected wavelength was 550 nm. The red line is the fitting result with the Equation 2-8.

From the steady-state absorption spectrum, the ε_{exc}^{0} of **1** in deoxygenated toluene (10 μM) was estimated as 4.0×10^4 M^{-1} cm^{-1}. As a result, the Φ_T of **1** was estimated as 0.066 from the Equation 2-9.

For the estimation of the D_T value by the transient absorption measurement, the LC **1** was introduced into an LC cell (9 μm thickness). In the transient absorption measurement, the S_0-S_1 absorption band of LC **1** was directly excited by 355 nm pulse laser, and triplet states were generated by the S_1-T_1 inter-system crossing. The absorbed laser intensity dependence of ΔOD at $t = 0$ in the LC **1** was shown in Figure 2-20.

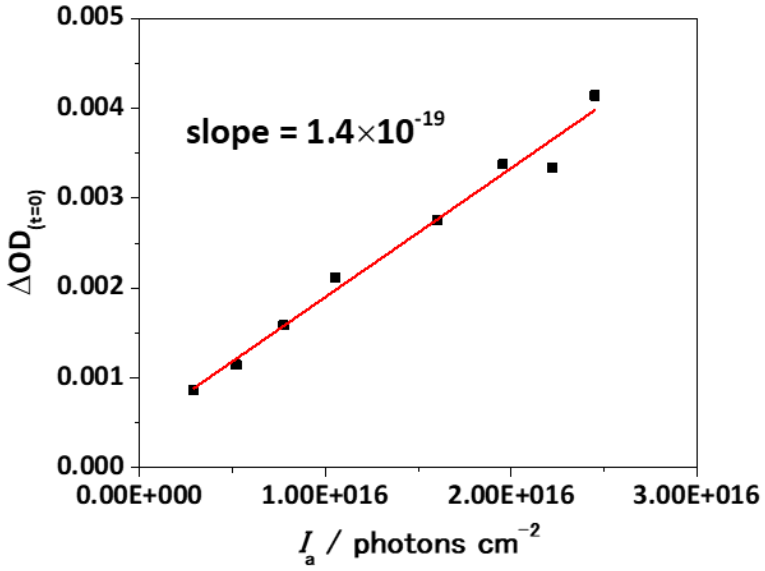

Figure 2-20. The absorbed laser intensity dependence of ΔOD at t = 0 in the LC **1** in the LC cell (9 μm thickness). The laser excitation wavelength was 355 nm. The ΔOD detected wavelength was 540 nm.

From Equation 2-7, the $\Delta\varepsilon$ value of the LC **1** was calculated as 1300 M^{-1} cm^{-1}. The l_e of the LC **1** in the LC cell at 355 nm was estimated from the steady-state absorption spectrum (Figure 2-21) and the sample thickness (9 μm).

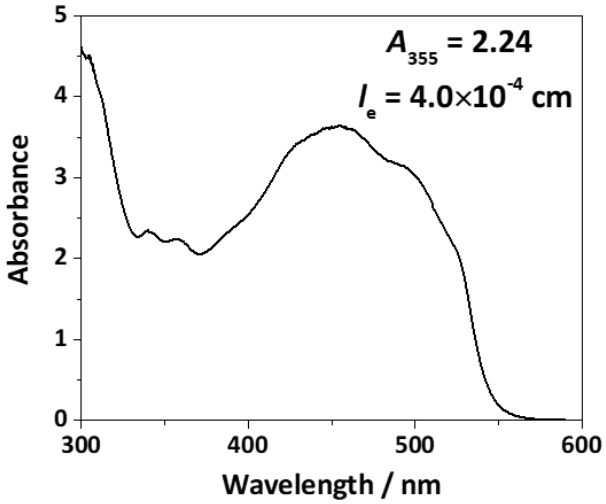

Figure 2-21. The steady-state absorption spectrum of the LC **1** in the LC cell (9 μm thickness).

These values were substituted for Equation 2-6, and the ΔOD in the LC **1** was rewritten to the triplet exciton density $n(t)$ (Figure 2-22).

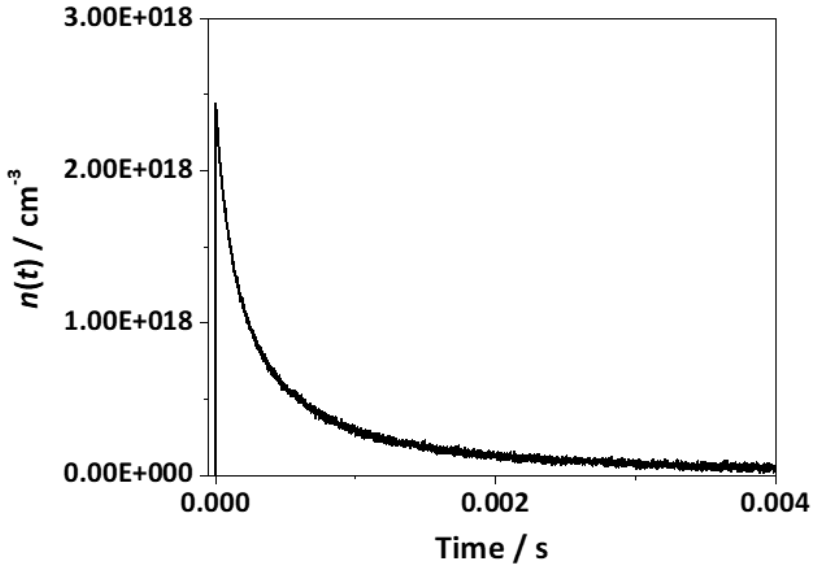

Figure 2-22. Triplet exciton decay of the LC **1** in the LC cell (9 μm thickness) measured at 540 nm. The laser excitation wavelength was 355 nm (5.9 mJ cm^{-2}).

The obtained $n(t)$ was rewritten to the $Y(t)$ by Equation 2-2. For the triplet lifetime τ in Equation 2-2, the value obtained from the UC lifetime measurement (Figure 2-16) was substituted. In order to the $\gamma_{TT}(t)$ extraction, a temporal differentiation of the variable $Y(t)$ fitted with simple equations so that it can accurately reproduce the time evolution of Equation 2-2. The temporal differentiation of the variable $Y(t)$ in the 1D and the 3D is represented by Equation 2-10 and Equation 2-11, respectively.

$$\frac{dY}{dt} = at^{-0.5}e^{-bt} \qquad \text{(1D)}$$

(Equation 2-10)

$$\frac{dY}{dt} = a'e^{-bt} \qquad \text{(3D)}$$

(Equation 2-11)

Therefore, the variable $Y(t)$ is represented by Equation 2-12 and Equation 2-13.

$$Y(t) = 2at^{0.5}e^{-bt} + 2\frac{2}{3}abt^{1.5}e^{-bt} + 2\frac{2}{3}\frac{2}{5}ab^2t^{2.5}e^{-bt} \ldots \qquad \text{(1D)}$$

(Equation 2-12)

$$Y(t) = ae^{-bt} + c \qquad \text{(3D)}$$

(Equation 2-13)

The obtained $Y(t)$ in the LC **1** was fitted by Equation 2-12 and Equation 2-13 (Figure 2-23). Clearly the 1D diffusion model gave the best fitting result.

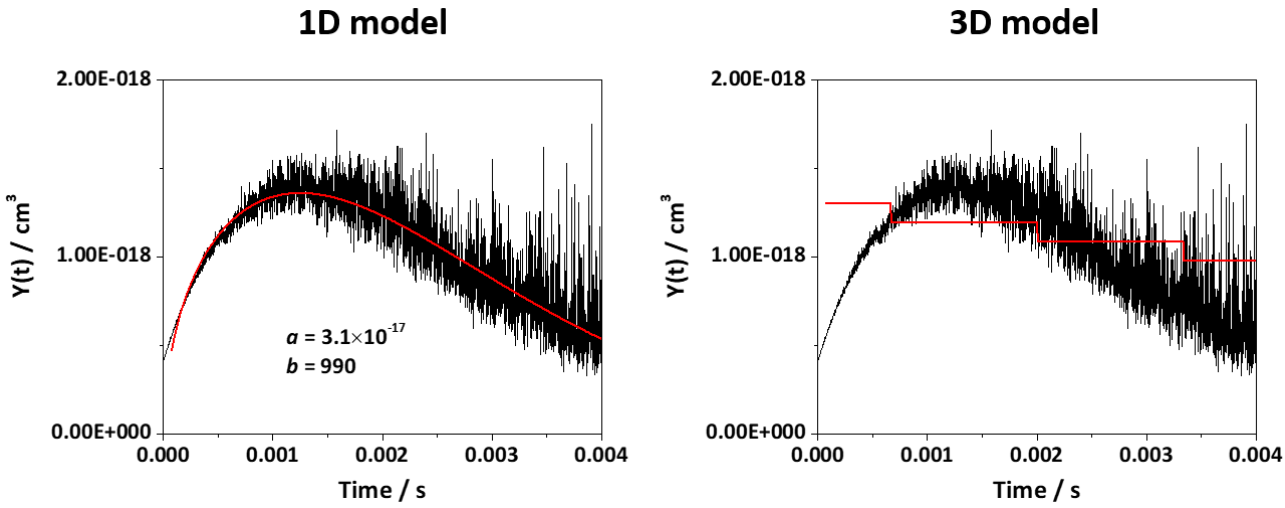

Figure 2-23. Time evolution of the variable $Y(t)$ of the LC **1** in the LC cell (9 μm thickness) measured at 540 nm. The laser excitation wavelength was 355 nm (5.9 mJ cm^{-2}). (left) The red line is the fitting result with the Equation 2-12. (right) The red line is the fitting result with the Equation 2-13.

These results clearly indicate that triplet excitons diffuse predominantly along the one-dimensional column,[39] which is consistent with the much larger inter-columnar distance (2.05 nm) than Dexter energy transfer distance (< 1 nm).

From the fitting result (a = 3.1×10^{-17}, b = 990) and Equation 2-10, the temporal differentiation of the variable $Y(t)$ was obtained, and it was substituted into Equation 2-3 for $\gamma_{TT}(t)$ estimation. The $\gamma_{TT}(t)$ was fitted with Equation 2-4. For the 1D-lattice constant a and the three-dimensional molecular density N_0 in Equation 2-2, the values obtained from the XRPD measurement (a = 0.35 nm) and the density measurement (ρ = 1.048 g cm^{-3}, N_0 = 7.2×10^{20} molecules cm^{-3}) were plugged. The calculation result provides the D_T value in LC **1** as 2.3×10^{-7} cm^2 s^{-1} (Figure 2-24b).

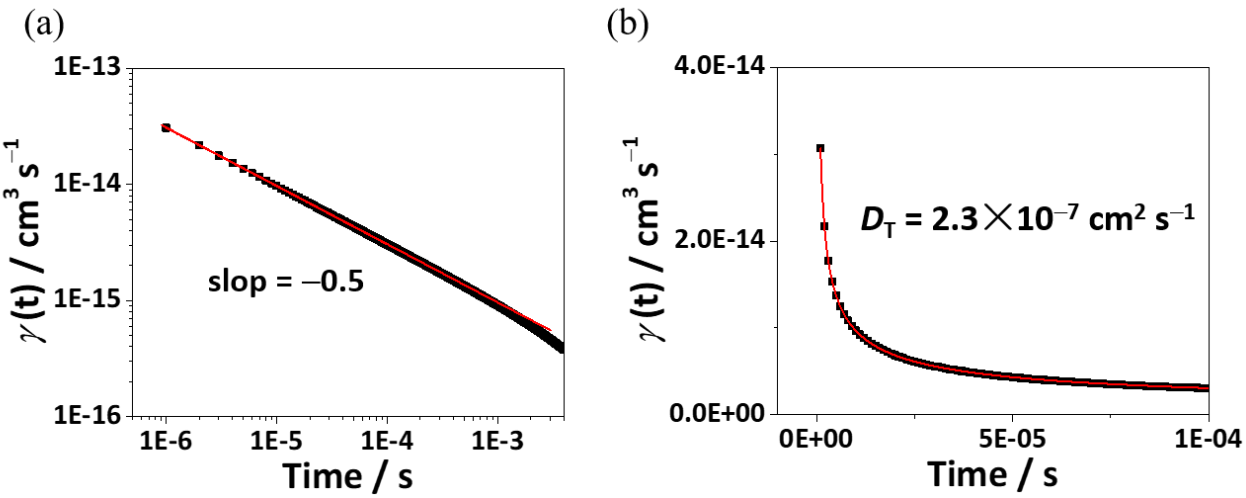

Figure 2-24. (a) Double logarithmic plots of γ_{TT} of LC **1** against *t*. (b) triplet diffusion constant D_T at different mixing ratios of **2** (**2**/(**1**+**2**) = 0-30mol%) in the binary LC **1**-**2**.

The D_T in the binary LCs **1**-**2** were also evaluated by the same procedure. In all the samples, the triplet decay curves could be fitted by the 1D diffusion model (Figure 2-25).

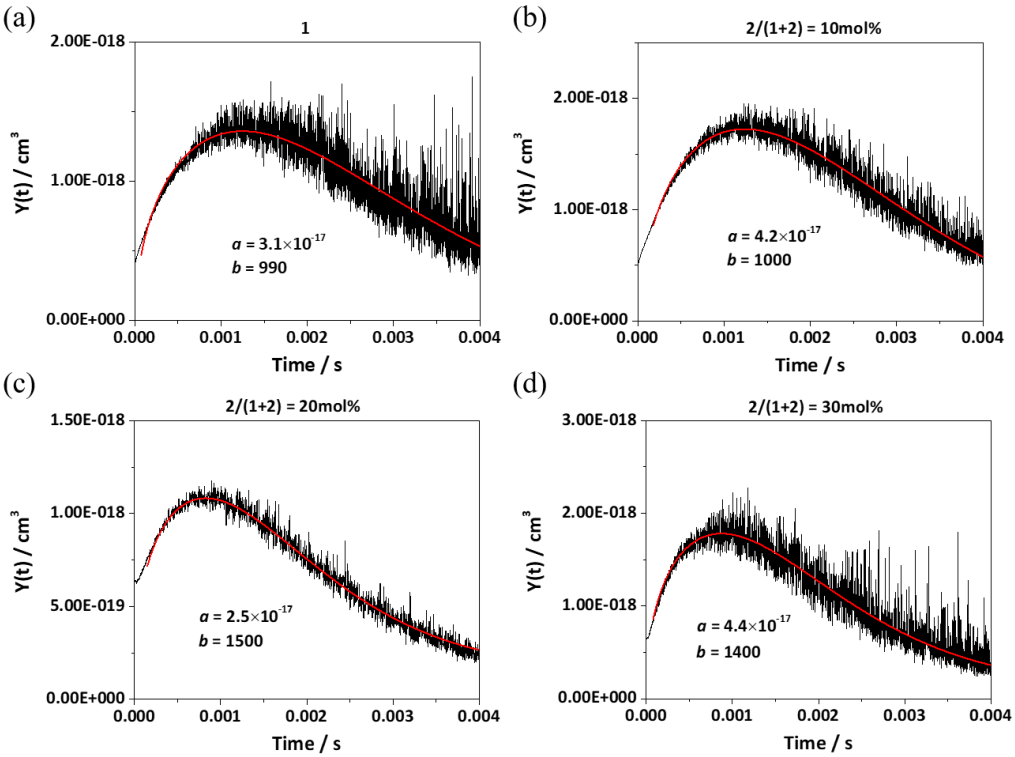

Figure 2-25. Time evolution of the variable $Y(t)$ of the pristine LC **1** and binary LC **1**-**2** in the LC cell (9 μm thickness). All red lines are fitting result with the Equation 2-12. (a) The LC **1**. The laser excitation wavelength was 355 nm (5.9 mJ cm^{-2}). The ΔOD detected wavelength was 540 nm. (b) The binary LC **1**-**2** (**2**/(**1**+**2**) = 10mol%). The laser excitation wavelength was 355 nm (6.3 mJ cm^{-2}). The ΔOD detected wavelength was 540 nm. (c) The binary LC **1**-**2** (**2**/(**1**+**2**) = 20mol%). The laser excitation wavelength was 355 nm (6.2 mJ cm^{-2}). The ΔOD detected wavelength was 550 nm. (d) The binary LC **1**-**2** (**2**/(**1**+**2**) = 30mol%). The laser excitation wavelength was 355 nm (6.3 mJ cm^{-2}). The ΔOD detected wavelength was 530 nm.

The D_T values were plotted as a function of the mixing ratio of **2** (Figure 2-26). Interestingly, as the content of **2** increased, the D_T value increased from 2.3×10^{-7} cm^3 s^{-1} to 7.4×10^{-7} cm^3 s^{-1}. The result strongly suggests that it is possible to increase the triplet diffusion constant by improving the structural order of columnar LCs. However, the observed 3.1 times increment of D_T value is not enough to explain the large reduction of I_{th} (20 times from 1035 to 51 mW cm^{-2}). The I_{th} appears to be affected by factors other than D_T.

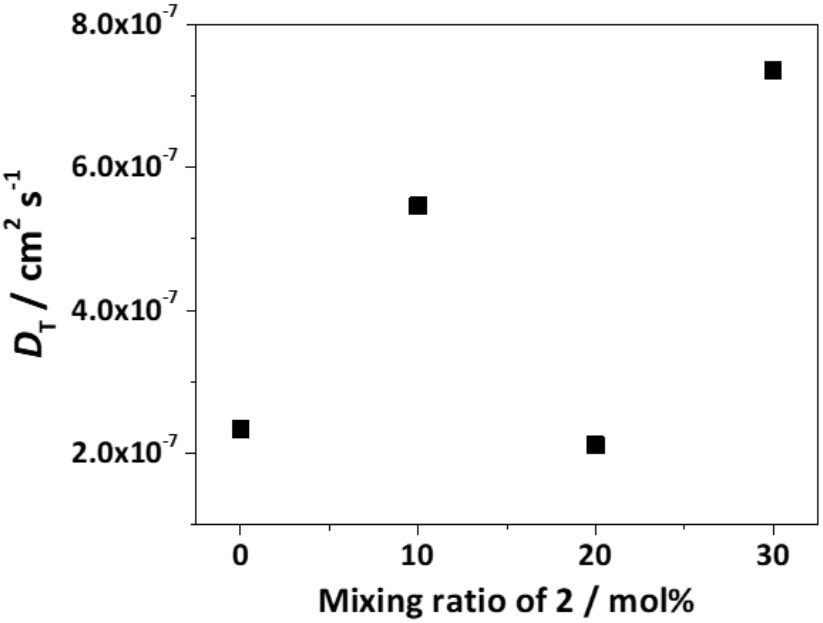

Figure 2-26. Mixing ratio of **2** (**2**/(**1**+**2**) = 0-30mol%) dependences of triplet diffusion constant D_T.

In conclusion, I successfully correlate the structural order of columnar LCs with the TTA-UC performances based on the detailed understanding of triplet exciton dynamics. The homogeneous mixing of donors in ordered acceptor arrays enables quantitative TTET efficiency. I devised a molecular co-assembling approach between LC **1** and shorter-chain compound **2** that rendered low threshold excitation intensity I_{th}. The transient absorption studies revealed the predominant one-dimensional triplet exciton diffusion in the LCs, and the increase in the triplet diffusion constant D_T by the mixing with **2**, which partly explains the reduction of I_{th}. This work clearly demonstrated the relationship between the structural order in molecular assemblies and triplet exciton diffusivity, providing an important guideline for designing soft materials that show energy-migration-based, low-power photon upconversion.

2-3 Synthesis

All reagents and solvents for synthesis were used as received without further purification. Platinum(II) tetraphenyltetrabenzoporphyrin (PtTPBP) was purchased from Frontier Scientific and used as received.

tetrakis(2-ethylhexyl) perylene-3,4,9,10-tetracarboxylate (1)

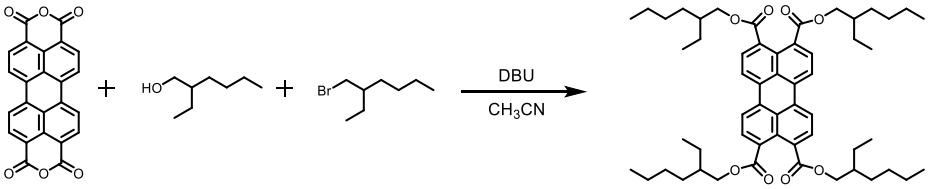

1

The title compound was prepared based on the literature method.[24,25] A mixture of 3,4,9,10-perylenetetracarboxylic dianhydride (3.1 g, 7.9 mmol), 1,8-diazabicyclo[5.4.0]undec-7-ene (DBU, 9.6 g, 21.1 mmol), 2-ethylhexanol (6.2 g, 47.6 mmol), and 1-bromo-2-ethylhexane (9.1 g, 47.1 mmol) in 125 mL acetonitrile was heated under reflux for 24 h. After the removal of acetonitrile under reduced pressure, the residual was dispersed in methanol. Then the precipitate was collected by filtration. The crude product was further purified using silica gel column chromatography (chloroform). Orange solid, Yield : 4.3 g, 62 %. ^{1}H NMR (300 MHz, $CDCl_3$) : δ = 0.89-0.99 (m, 24H), 1.33-1.54 (m, 32H), 1.74-1.82 (m, 4H), 4.21-4.31 (m, 8H), 8.02 (d, 4H), 8.30 (d, 4H). Elemental analysis, calculated for $C_{56}H_{76}O_8$: C, 76.68; H, 8.73; N, 0.00; found : C, 76.62 ; H, 8.71; N, 0.05

tetraethyl perylene-3,4,9,10-tetracarboxylate (2)

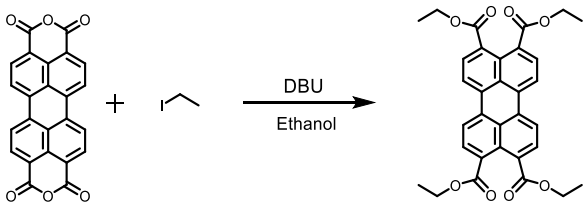

2

The title compound was prepared based on the literature method.[26,27] A mixture of 3,4,9,10-perylenetetracarboxylic dianhydride (2.0 g, 5.1 mmol), DBU (6.3 g, 41 mmol) and ethyl iodide (4.8 g, 43 mmol) in 80 mL ethanol was heated under reflux for 4 h. After the reaction, the mixture was poured into 100 mL hexane and the precipitate was collected by filtration. The crude product was purified by

silica gel column chromatography (ethyl acetate : chloroform = 1 : 40) and recrystallization from ethanol. Yield : 2.2 g, 79%. ^{1}H NMR (300 MHz, Toluene-d_8) : δ = 1.24 (t, 12H), 4.29 (q, 8H), 7.51 (d, 4H), 7.88 (d, 4H). Elemental analysis, calculated for $C_{32}H_{28}O_8$: C, 71.10; H, 5.22; N, 0.00; found : C, 71.11; H, 5.20; N, 0.02.

2-4 Characterizations

^{1}H NMR spectra were measured on a JEOL JNM-ECX 400 spectrometer. Elemental analysis was conducted at the Elemental Analysis Center, Kyushu University. Differential scanning calorimetry was conducted on a Hitachi High-Tech Science Corporation DSC6100 (for the measurement of the glass transition temperature of LC **1**), and a METTLER TOLEDO Excellence DSC 1. X-ray powder diffraction was conducted on a Bruker D2 PHASER with a copper Cu Kα source (λ= 1.5418 Å). UV/Vis absorption spectra were recorded on a JASCO V-670 spectrophotometer. Fluorescence spectra were measured by using a PerkinElmer LS 55 fluorescence spectrometer. The absolute quantum yields were measured in an integrating sphere using a Hamamatsu Photonics absolute quantum yield measurement system. Time-resolved photoluminescence lifetime measurements were carried out by using a time-correlated single photon counting lifetime spectroscopy system, HAMAMATSU Quantaurus-Tau C11567–01 (for delayed luminescence lifetime)/C11567–02 (for fluorescence lifetime). For TTA-UC emission measurements, a diode laser (635 nm, 75 mW, RGB Photonics) was used as excitation source. The laser power was controlled by combining a software (Ltune) and a variable neutral density filter, and measured using a PD300-UV photodiode sensor (OPHIR Photonics). The laser beam was focused on a sample using a lens. The diameter the of laser beam ($1/e^2$) was measured at the sample position using a CCD beam profiler SP620 (OPHIR Photonics). Typical laser size was 4.5×10^{-4} cm^2. The emitted light was collimated by an achromatic lens, the excitation light was removed using a 633 nm notch filter (Thorlabs), and the emitted light was again focused by an achromatic lens to an optical fiber connected to a multichannel detector MCPD-9800 (Otsuka Electronics). The TTA-UC quantum yield was measured by using an absolute quantum yield measurement

system. The sample was held in an integration sphere and excited by the laser excitation source (635 nm, 75 mW, RGB Photonics). The scattered excitation light was removed using a 633 nm notch filter and emitted light was monitored with a multichannel detector C10027-01 (Hamamatsu Photonics). The spectrometer was calibrated including the integration sphere and notch filter by Hamamatsu Photonics. The upconverted emission was integrated over the 512-616 nm to calculate the TTA-UC quantum yield. In general, the quantum yield is defined as the ratio of absorbed photons to emitted photons, and thus the maximum yield (Φ_{UC}) of the bimolecular TTA-UC process is 50%. However, many reports multiply this value by 2 to set the maximum quantum yield at 100%. To avoid the confusion between these different definitions, the UC quantum yield is written as Φ_{UC}' (= $2\Phi_{UC}$) when the maximum efficiency is normalized to be 100%. Transient absorption spectra were measured using a UNISOKU TSP-2000 laser flash photolysis system. The LC cell (KSSZ-09/B207P1NTS05, cell gap: 9 ± 0.5 μm) was purchased from EHC.

2-5 Reference

1 S. Baluschev, T. Miteva, V. Yakutkin, G. Nelles, A. Yasuda and G. Wegner, *Phys. Rev. Lett.*, 2006, **97**, 143903.

2 T. N. Singh-Rachford and F. N. Castellano, *Coord. Chem. Rev.*, 2010, **254**, 2560-2573.

3 J. Zhao, S. Ji and H. Guo, *Rsc Adv.*, 2011, **1**, 937-950.

4 J.-H. Kim and J.-H. Kim, *J. Am. Chem. Soc.*, 2012, **134**, 17478-17481.

5 Y. C. Simon and C. Weder, *J. Mater. Chem.*, 2012, **22**, 20817-20830.

6 K. Börjesson, D. Dzebo, B. Albinsson and K. Moth-Poulsen, *J. Mater. Chem. A*, 2013, **1**, 8521-8524.

7 S. H. C. Askes, A. Bahreman and S. Bonnet, *Angew. Chem. Int. Ed.*, 2014, **53**, 1029-1033.

8 M. Häring, R. Pérez-Ruiz, A. Jacobi von Wangelin and D. D. Díaz, *Chem. Commun.*, 2015, **51**, 16848-16851.

9 T. F. Schulze and T. W. Schmidt, *Energy Environ. Sci.*, 2015, **8**, 103-125.

10 N. Yanai and N. Kimizuka, *Chem. Commun.*, 2016, **52**, 5354-5370.

11 S. P. Hill and K. Hanson, *J. Am. Chem. Soc.*, 2017, **139**, 10988-10991.

12 Z. Huang and M. L. Tang, *J. Am. Chem. Soc.*, 2017, **139**, 9412-9418.

13 A. Monguzzi, R. Tubino, S. Hoseinkhani, M. Campione and F. Meinardi, *Phys. Chem. Chem. Phys.*, 2012, **14**, 4322-4332.

14 N. Yanai and N. Kimizuka, *Acc. Chem. Res.*, 2017, **50**, 2487-2495.

15 J. Han, Y. Jiang, A. Obolda, P. Duan, F. Li and M. Liu, *J. Phys. Chem. Lett.*, 2017, **8**, 5865-5870.
16 S. Baluschev, V. Yakutkin, G. Wegner, B. Minch, T. Miteva, G. Nelles and A. Yasuda, *J. Appl. Phys.*, 2007, **101**, 023101.
17 P. Duan, N. Yanai and N. Kimizuka, *J. Am. Chem. Soc.*, 2013, **135**, 19056-19059.
18 J. S. Lissau, D. Nauroozi, M.-P. Santoni, S. Ott, J. M. Gardner and A. Morandeira, *J. Phys. Chem. C*, 2013, **117**, 14493-14501.
19 R. Vadrucci, C. Weder and Y. C. Simon, *J. Mater. Chem. C*, 2014, **2**, 2837-2841.
20 T. Ogawa, N. Yanai, A. Monguzzi and N. Kimizuka, *Sci. Rep.*, 2015, **5**, 10882.
21 T. Ogawa, N. Yanai, H. Kouno and N. Kimizuka, *J. Photon. Energy*, 2017, **8**, 022003.
22 R. Andemach, H. Utzat, S. D. Dimitrov, I. McCulloch, M. Heeney, J. R. Durrant and H. Bronstein, *J. Am. Chem. Soc.*, 2015, **137**, 10383-10390.
23 T. Dilbeck, J. C. Wang, Y. Zhou, A. Olsson, M. Sykora and K. Hanson, *J. Phys. Chem. C*, 2017, **121**, 19690-19698.
24 T. Hassheider, S. A. Benning, H.-S. Kitzerow, M.-F. Achard and H. Bock, *Angew. Chem. Int. Ed.*, 2001, **40**, 2060-2063.
25 W. Chen, X. Yang, G. Long, X. Wan, Y. Chen and Q. Zhang, *J. Mater. Chem. C*, 2015, **3**, 4698-4705.
26 I. Seguy, P. Jolinat, P. Destruel, R. Mamy, H. Allouchi, C. Courseille, M. Cotrait and H. Bock, *ChemPhysChem*, 2001, **2**, 448-452.
27 H. Zhang, Y. Shao, H. Chen, K. Miao and L.-J. Fan, *J. Polym. Sci., Part A: Polym. Chem.*, 2017, **55**, 1880-1886.
28 E. Grelet, S. Dardel, H. Bock, M. Goldmann, E. Lacaze and F. Nallet, *Eur. Phys. J. E*, 2010, **31**, 343-349.
29 M. Kasha. *Spectroscopy of the Excited State*; Plenum Press: New York, 1976.
30 A. Hayer, V. de Halleux, A. Köhler, A. El-Garoughy, E. W. Meijer, J. Barberá, J. Tant, J. Levin, M. Lehmann, J. Gierschner, J. Cornil and Y. H. Geerts, *J. Phys. Chem. B*, 2006, **110**, 7653-7659.
31 J. Seibt, P. Marquetand, V. Engel, Z. Chen, V. Dehm and F. Würthner, *Chem. Phys.*, 2006, **328**, 354-362.
32 A. Monguzzi, R. Tubino and F. Meinardi, *Phys. Rev. B*, 2008, **77**, 155122.
33 Y. Y. Cheng, T. Khoury, R. G. C. R. Clady, M. J. Y. Tayebjee, N. J. Ekins-Daukes, M. J. Crossley and T. W. Schmidt, *Phys. Chem. Chem. Phys.*, 2010, **12**, 66-71.
34 A. Haefele, J. Blumhoff, R. S. Khnayzer and F. N. Castellano, *The Journal of Physical Chemistry Letters*, 2012, **3**, 299-303.
35 A. Monguzzi, F. Bianchi, A. Bianchi, M. Mauri, R. Simonutti, R. Ruffo, R. Tubino and F. Meinardi, *Adv. Energy Mater.*, 2013, **3**, 680-686.
36 G. D. Scholes, *Annu. Rev. Phys. Chem.*, 2003, **54**, 57-87.
37 K. Razinaqvi, *Chem. Phys. Lett.*, 1974, **28**, 280-284.
38 D. C. Torney and H. M. Mcconnell, *J. Phys. Chem.*, 1983, **87**, 1941-1951.
39 D. Markovitsi, I. Lécuyer and J. Simon, *J. Phys. Chem.*, 1991, **95**, 3620-3626.
40 E. Engel, K. Leo and M. Hoffmann, *Chem. Phys.*, 2006, **325**, 170-177.
41 Y. Tamai, Y. Matsuura, H. Ohkita, H. Benten and S. Ito, *J. Phys. Chem. Lett.*, 2014, **5**, 399-403.

42 A. Dogariu, D. Vacar and A. J. Heeger, *Phys. Rev. B*, 1998, **58**, 10218-10224.
43 S. M. King, D. Dai, C. Rothe and A. P. Monkman, *Phys. Rev. B*, 2007, **76**, 085204.
44 G. L. Hug and I. Carmichael, *J. Photochem.*, 1985, **31**, 179-192.
45 P. Murasecco-Suardi, E. Gassmann, A. M. Braun and E. Oliveros, *Helv. Chim. Acta*, 1987, **70**, 1760-1773.
46 S. Amemori, N. Yanai and N. Kimizuka, *Phys. Chem. Chem. Phys.*, 2015, **17**, 22557-22560.
47 G. Orellana and A. M. Braun, *J. Photochem. Photobiol. A*, 1989, **48**, 277-289.

Chapter 3 Triplet Sensitization by Perovskite Nanocrystals for Photon Upconversion

3-1 Introduction

ABSTRACT: The potential of three-dimensional (3D) metal-halide perovskites to sensitize organic triplets is unveiled. Nanocrystals of surface-modified inorganic cesium lead halide perovskite ($CsPbX_3$, X = Br/I) are found to work as efficient triplet sensitizers for photon upconversion based on triplet-triplet annihilation (TTA-UC) at low excitation intensity.

The organic-inorganic metal-halide perovskites have attracted many interests because of their structural diversity and the consequent unique magnetic, electric and exciton-related optical properties.[1-4] Among them, 3D perovskites have recently received renewed interest as light harvesters in solid-sate sensitized solar cells by their tunable bandgaps and small exciton biding energy which is suitable for the photoinduced carrier generation.[5-8] These perovskites are also promising as photoluminescent materials in light-emitting diodes and lasers.[9-11] Although the small exciton binding energy in 3D perovskites results in small electron-hole capture rates, the radiative recombination can be promoted by spatial confinement of the electrons and holes in nanoscale geometries.[7,10,11] Recent magneto-optical studies of perovskites showed that singlet and triplet excitons are populated by relaxation from the spin-antiparallel and spin-parallel electron-hole pairs, respectively.[9,12,13] The formation of triplet excited states opens the way for the new photophysics area of perovskites. However, their potential to sensitize useful organic triplets have remained unexplored.

In this chapter, I discuss the generation of organic triplet excited states sensitized by 3D metal halide perovskites, which lead to triplet-triplet annihilation-based photon upconversion (TTA-UC). The TTA-UC has been a topic of active research since it functions under low excitation intensity.[14-27] Although phosphorescent molecules have been mainly used as triplet sensitizers for TTA-UC, the most of them have intrinsic problems such as relatively large energy loss during S_1-to-T_1 intersystem

crossing (ISC) and narrow absorption bands. Despite efforts to solve these problems using inorganic triplet sensitizers,[28-33] the successful examples have been still limited. To fulfill the potential of 3D perovskites as triplet sensitizers in TTA-UC, it is indispensable to control their size, chemical composition, and surface modification to facilitate the triplet energy transfer processes.

In this study, I employed nanocrystals of cesium lead halide perovskite ($CsPbX_3$) as a novel class of inorganic triplet sensitizers. The surface of $CsPbX_3$ nanocrystals is modified with triplet acceptor (emitter) **3** having an amino group (Figure 3-1). The bandgap of $CsPbX_3$ nanocrystals is finely tunable by exchanging halide ions,[34-36] which allows matching of the sensitizer energy level with that of the acceptor triplet. The photo-excited energy is transferred from the $CsPbX_3$ nanocrystals to triplets of surface-bound **3**, which relay the triplet energy to free DPA molecules in solution where subsequent bimolecular TTA occurs to give an UC emission.

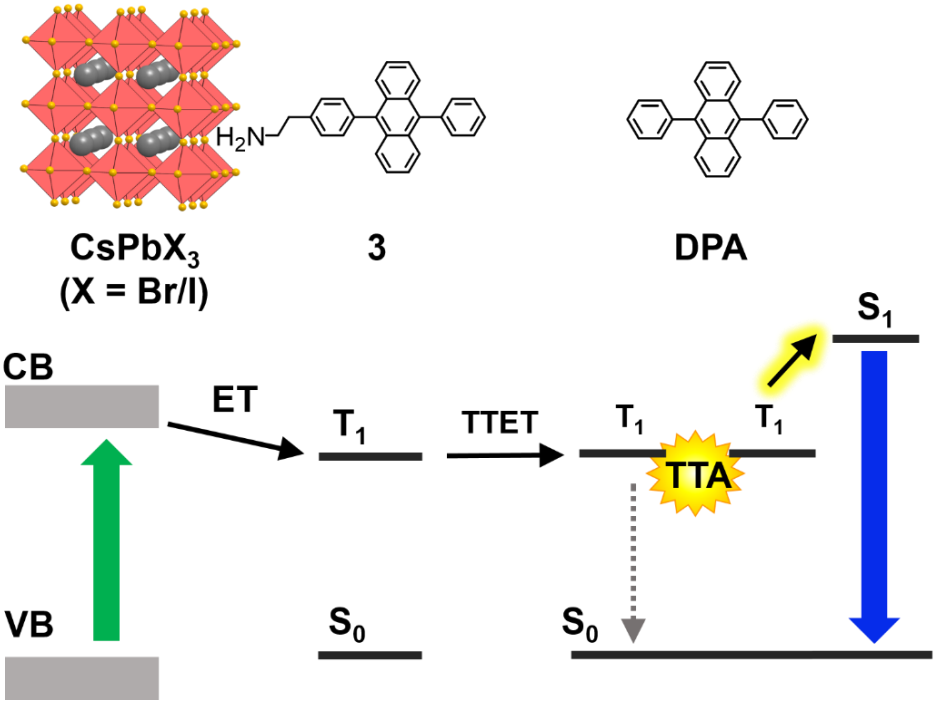

Figure 3-1. Scheme for TTA-UC sensitized by inorganic perovskite nanocrystals. Photoexcitation (green arrow) of CsPbX3 (X = Br/I) nanocrystals is followed by a sequence of energy transfer (ET) to the surface-bound **3**, triplet-triplet energy transfer (TTET) to the free DPA molecules in solution, TTA between the excited DPA molecules, and finally higher-energy UC emission (blue arrow).

3-2 Results and Discussion

Inorganic $CsPbBr_3$ nanocrystals were synthesized according to the previous report.[36] The surface of as-synthesized nanocrystals is capped with oleic acid and oleylamine to secure their solubility in organic media. The triplet energy transfer usually occurs based on the electron-exchange Dexter mechanism which requires short distances around 1 nm, and the presence of such a thick surface passivation layer is expected to interrupt the energy transfer from $CsPbBr_3$ nanocrystals to acceptors in solution. I solved this issue by replacing some of the surface ligands with acceptor molecules which facilely relayed the triplet energy to the emitter molecules in solution. This surface modification was done by simply adding amine-containing acceptor **3** to the toluene dispersion of $CsPbBr_3$ nanocrystals. After the addition of **3**, no changes were observed in absorption spectra nor X-ray powder diffraction (XRPD) patterns of $CsPbBr_3$ nanocrystals, indicating that the cubic perovskite structure was retained (Figure 3-2). This was also supported by transmission electron microscopy (TEM) measurements. The size and morphology of $CsPbBr_3$ nanocrystals were retained after the treatment with **3** (Figure 3-3). The modification of nanocrystal surface with **3** is supported by the effective energy transfer as discussed later.

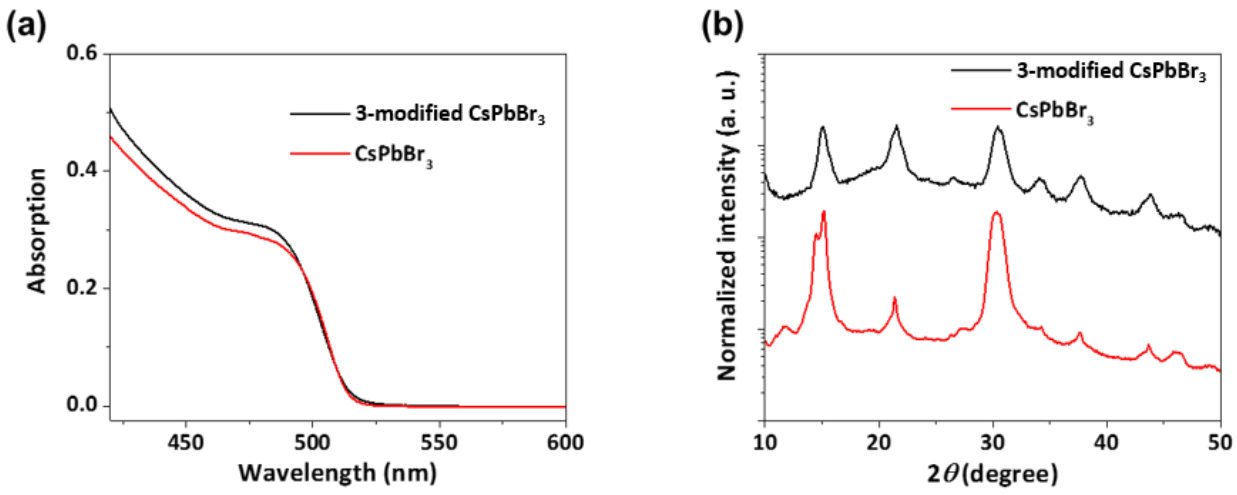

Figure 3-2. (a) Absorption spectra and (b) XRPD patterns of $CsPbBr_3$ nanocrystals (red) and **3**-modified $CsPbBr_3$ nanocrystals (black)

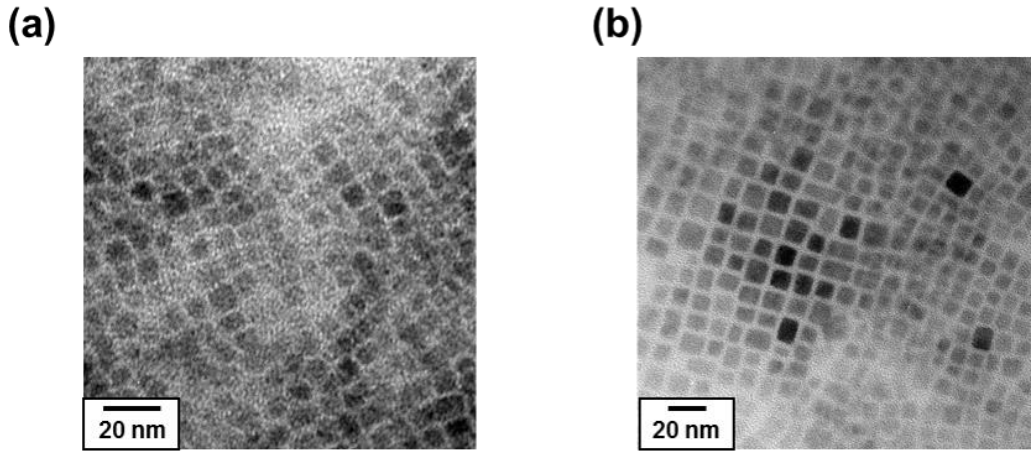

Figure 3-3. TEM images of (a) $CsPbBr_3$ nanocrystals (average size = 8.1 ± 1.5 nm) and (b) **3**-modified $CsPbBr_3$ nanocrystals (average size = 8.8 ± 1.9 nm).

To achieve optimum energy level matching between the perovskite nanocrystals and acceptor molecules, the halide exchange reactions of $CsPbBr_3$ were applied to the **3**-modified $CsPbBr_3$ nanocrystals. It has been reported that the nanocrystal bandgap can be finely tuned by adding specific concentrations of LiI to $CsPbBr_3$.[36] Accordingly, the absorption and photoluminescence bands were facilely tuned depending on the LiI concentration (Figure 3-4a). The original **3**-$CsPbBr_3$ showed an emission peak at 508 nm. By increasing the LiI concentration from 0.25 M to 0.95 M, the emission peak showed a gradual shift to 644 nm. These spectral shifts are consistent with those reported for $CsPbBr_3$ nanocrystals,[36] indicating that the halide exchange reaction well proceeded in the presence of surface-bound **3**. The maintenance of basic cubic structure after the halide exchange reaction was confirmed by XRPD measurements (Figure 3-4b). Similary to the previous report,[36] the (200) peak gradually shifted from 30.2° to 29.0° by increasing the LiI concentration from 0.25 M to 0.95 M. Elemental analysis by energy dispersive X-ray (EDX) spectroscopy of **3**-$CsPbX_3$ having an emission wavelength of 618 nm showed an atomic ratio (Cs : Pb : Br : I) of 18.7±1.3%: 21.4±0.18%: 34.9±0.89%: 25.1±0.62%. This confirms an atomic ratio of 1 : 1 : 3 for the $CsPbX_3$ nanocrystals. These results indicate that the halogen exchange reaction occurred homogeneously in **3**-modified perovskite nanocrystals.

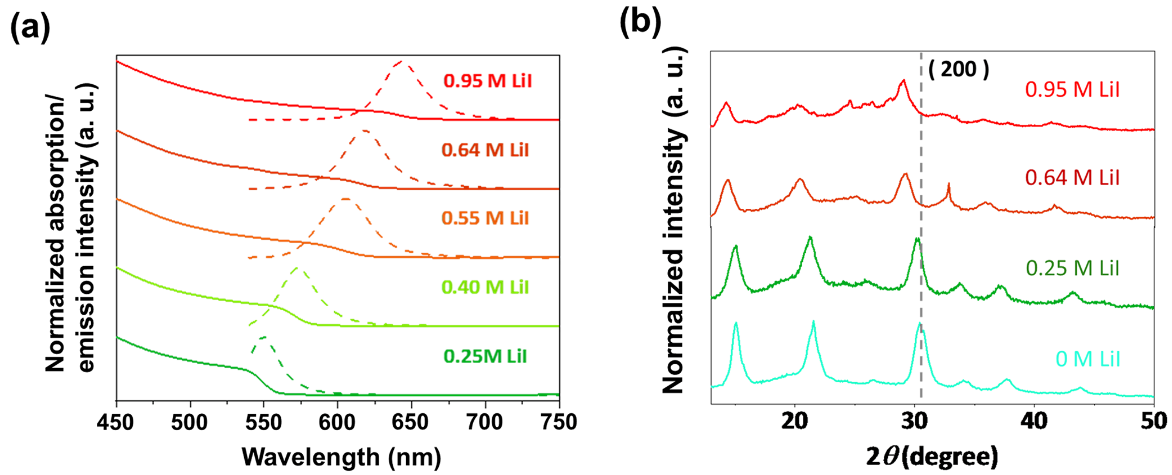

Figure 3-4. (a) Absorption (solid line) and emission (dash line) spectra of **3**-$CsPbBr_3$ exchanged with different concentrations of LiI. (b) XRPD patterns of **3**-$CsPbBr_3$ exchanged with different concentrations of LiI.

To gain an insight into the energy transfer from perovskite nanocrystals to **3**, I measured decays of perovskite photoluminescence (Figure 3-5). Upon the addition of **3,** the emission lifetime of perovskite nanocrystals became much shorter from τ_0 = 16.1 ns to τ = 10.0 ns, suggesting the energy transfer to the surface ligand **3**. The energy transfer efficiency (Φ_{ET}) was estimated as $\Phi_{ET} = 1 - \tau/\tau_0 = 0.38$. The further design of inorganic-organic interface would further improve the triplet sensitization efficiency.

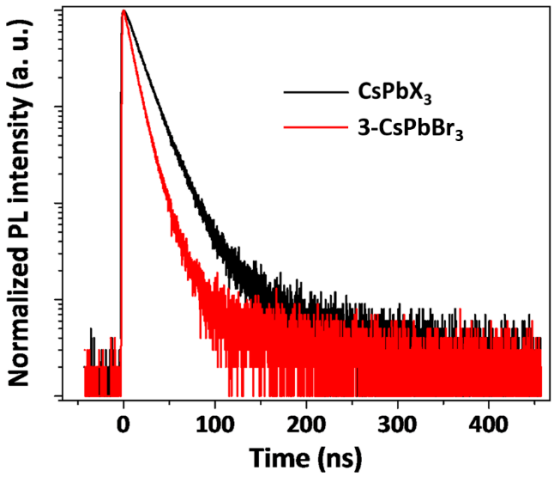

Figure 3-5. Photoluminescence decays of $CsPbX_3$ (black, τ_0 = 16.1 ns, perovskite emission peak at 630 nm) and **3**-$CsPbX_3$ (Red, τ = 10.0 ns, perovskite emission peak at 618 nm) in deaerated toluene (λ_{ex} = 470 nm, λ_{em} = 620 nm).

Under the excitation at 532 nm, the UC emission at 434 nm was clearly observed from a deaerated toluene solution containing **3**-$CsPbX_3$ and 10 mM free DPA (Figure 3-6a). The UC emission was also observed under the excitation at 635 nm (Figure 3-7). For UC measurements, all the sample preparations were done in an Ar-filled glove box (oxygen concentration < 0.1 ppm). To confirm the TTA-based UC mechanism, I measured lifetime and excitation intensity dependence of the UC emission. The UC emission showed millisecond-scale decay profiles which are characteristics to the UC *via* long-lived triplet excited states (Figure 3-8).

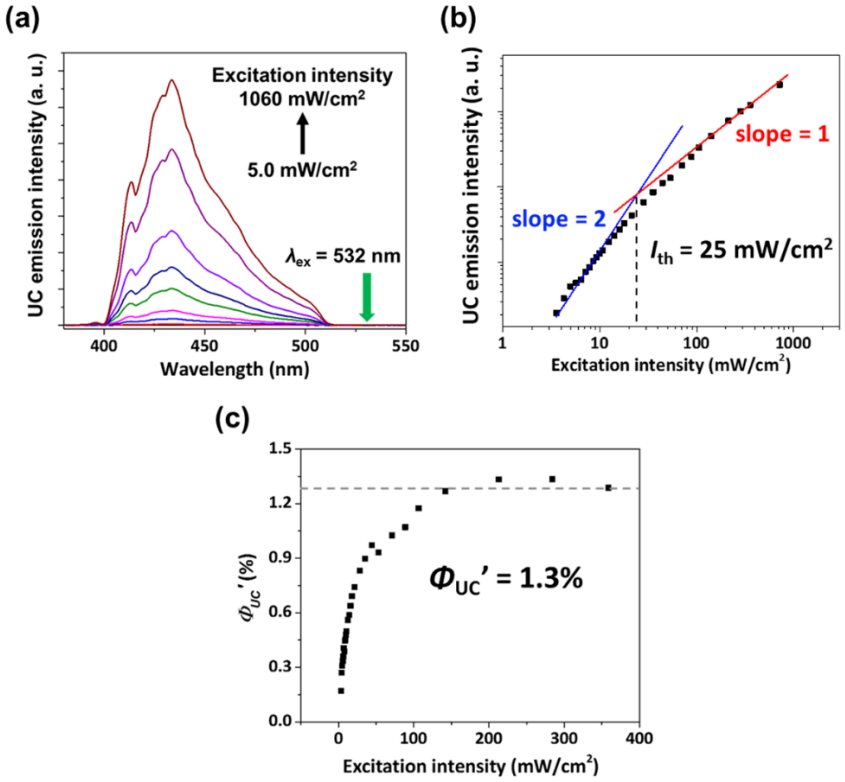

Figure 3-6. (a) UC emission spectra of free DPA and **3**-$CsPbX_3$ in deaerated toluene measured at different excitation intensity using a 532 nm laser. A notch filter (λ = 532 nm) and a short pass filter (λ = 510 nm) were used to remove the scattered incident light. (b) Excitation intensity dependence of UC emission intensity for **3**-$CsPbX_3$ and DPA in deaerated toluene at 430 nm. Blue and red lines show the fitting results with slopes of 2 and 1. The cross-section of these two lines gives the threshold excitation intensity I_{th} = 25 mW/cm^2. (c) Excitation intensity dependence of Φ_{UC}' for **3**-$CsPbX_3$ and DPA in deaerated toluene. In all measurements, the emission peak of involved perovskite nanocrystals was at 618 nm.

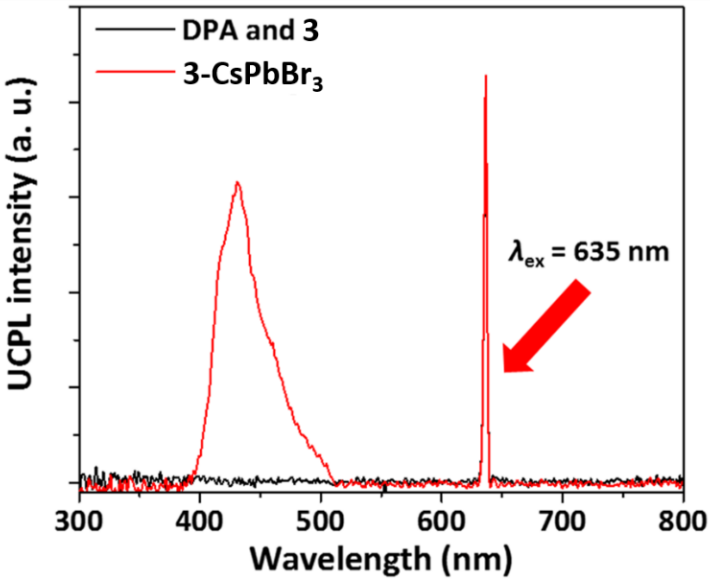

Figure 3-7. UC emission spectrum of **3**-$CsPbX_3$ with 10 mM DPA (red, excitation intensity = 98 W/cm^2, perovskite emission peak at 650 nm), and 10 mM DPA and 0.94 mM **1** in the absence of $CsPbX_3$ (black, excitation intensity = 98 W/cm^2) in deaerated toluene excited by a 635 nm laser. A notch filter (λ = 635 nm) and a short pass filter (λ = 590 nm) were used to remove the scattered incident light.

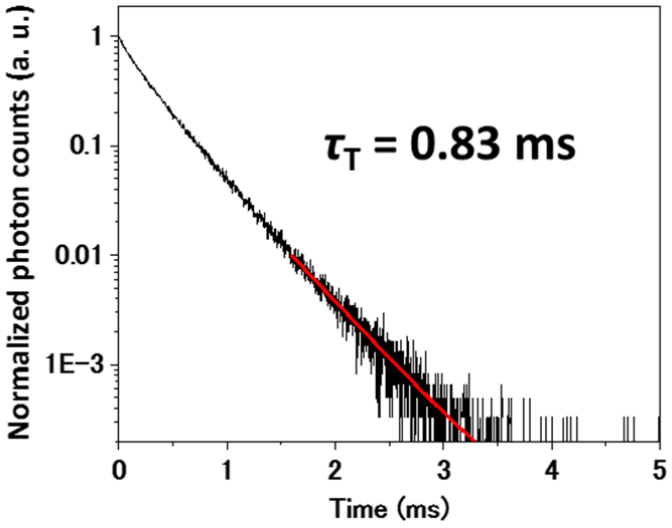

Figure 3-8. UC emission decay at 430 nm of **3**-$CsPbX_3$ in deaerated toluene under pulsed excitation at 531 nm. The red fitting curve was obtained by considering the known relationship of $I_{UC}(t) \propto \exp(-2t/\tau_T)$, where τ_T is acceptor triplet lifetime (0.83 ms).

In general, the TTA-UC emission intensity shows quadratic and linear dependence on the incident light intensity at low and high excitation intensity, respectively.[37-39] At threshold excitation intensity I_{th}, the quadratic-to-linear transition takes place. Above I_{th}, TTA becomes the main deactivation channel for the acceptor triplet.[39] A double logarithmic plot of the UC emission intensity as a function of excitation intensity obtained for the toluene solution of DPA and **3**-$CsPbX_3$ is shown in Figure 3-6b. It showed a slope change from 2 to 1, and the cross-section of these two lines gave the I_{th} value of 25 mW/cm^2. This I_{th} value is comparable to those of efficient TTA-UC systems,[16,23,28,32,38] illustrating the high triplet sensitization ability of the acceptor-modified perovskite nanocrystals.

To confirm the mechanism shown in Figure 3-1, I carried out control experiments in the absence of perovskite nanocrystals or **3**. No UC emission was observed from a mixed solution of **3** and DPA without perovskite nanocrystals (Figure 3-9). This result clearly proves that the triplet excited state of organic acceptors is populated by perovskite nanocrystals. Moreover, UC emission was not detected for the mixture of $CsPbX_3$ and DPA (Figure 3-9) and thus, the surface modification of $CsPbX_3$ by **3** is indispensable. As mentioned before, the triplet energy transfer usually occurs based on the electron-exchange Dexter mechanism which requires effective orbital overlap of the triplet donor and acceptor, typically within the intermolecular distance of 1 nm The absence of UC emission without surface-bound **3** indicates that the triplet energy transfer from $CsPbX_3$ nanocrystals to free DPA molecules is hampered by the long alkyl chains of oleic acid and oleylamine that covered the nanocrystal surface. It is, therefore, apparent that surface-anchored acceptor **3** relays the triplet energy from the $CsPbX_3$ nanocrystals to DPA in the bulk solution, which process is essential to achieve effective TTA-UC.

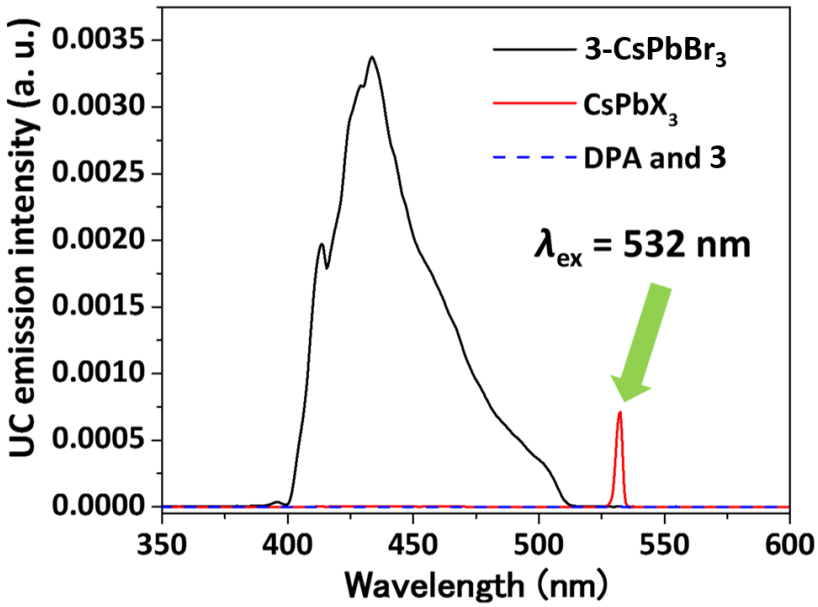

Figure 3-9. UC emission spectrum of **3**-$CsPbX_3$ with 10 mM DPA (black, excitation intensity = 1.1 W/cm^2, perovskite emission peak at 618 nm), $CsPbX_3$ with 10 mM DPA in the absence of **3** (red, excitation intensity = 722 W/cm^2, perovskite emission peak at 630 nm), and 10 mM DPA and 0.94 mM **3** in the absence of $CsPbX_3$ (blue, excitation intensity = 3.9 W/cm^2) in deaerated toluene excited by a 532 nm laser. A notch filter (λ = 532 nm) was used to remove the scattered incident light.

In general, the quantum yield is defined as the ratio of absorbed photons to emitted photons, and thus the maximum yield (Φ_{UC}) of the bimolecular TTA-UC process is 50%. However, many reports multiply this value by 2 to set the maximum efficiency at 100%. To avoid the confusion between these different definitions, the UC efficiency is written as Φ_{UC}' (= $2\Phi_{UC}$) when the maximum efficiency is normalized to be 100%. The Φ_{UC}' of each sample was determined relative to a standard (Rhodamine B) according to the following equation, [24]

$$\Phi_{UC}' = 2\Phi_{std}\left(\frac{A_{std}}{A_{UC}}\right)\left(\frac{F_{UC}}{F_{std}}\right)\left(\frac{I_{std}}{I_{UC}}\right)\left(\frac{\eta_{UC}}{\eta_{std}}\right)^2$$

(Eq. 3-1)

where Φ, A, F, I, and η represent quantum yield, absorbance at the excitation wavelength, integrated photoluminescence spectral profile, excitation intensity, and the refractive index of solvent, respectively. The excitation intensity dependences of Φ_{UC}' were measured for **3**-$CsPbX_3$ and DPA mixed

solutions (Figure 3-6c). With the increase of excitation intensity, the Φ_{UC}' value gradually increased and became saturated, which is common for TTA-UC.[20] The reasonably high Φ_{UC}' values of 1.3% was obtained.

I also studied the effect of the concentration of energy acceptor **3** on the morphology of perovskite nanocrystals and their UC quantum yields (Figure 3-10). The UC quantum yield showed increase from Φ_{UC}' = 0.5% ([**3**] = 0.40 mM) to 1.3% ([**3**] = 0.94 mM), probably due to the higher density of **3** at perovskite nanocrystal surface. Meanwhile, the Φ_{UC}' value dropped to 0.1% at a higher concentration of **3** (4.0 mM). Below the concentration of 0.94 mM, regular cubic nanostructures were maintained. Meanwhile, at an elevated concentration of 4.0 mM, nanocrystals turned into irregular structures as observed in TEM measurements (Figure 3-11). It seems that the binding of excess **3** has lowered the stability of surface passivating monolayers and induced deformation of nanocrystals. These observations indicate the condition for surface modification by **3** needs to be properly determined not to damage the perovskite nanostructure.

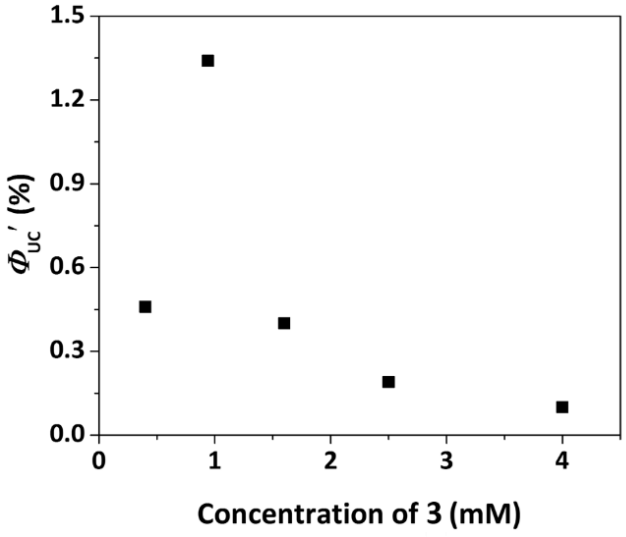

Figure 3-10. Dependence of Φ_{UC}' of **3**-modified perovskite nanocrystals and DPA on the concentration of **3** in deaerated toluene. These samples were excited with 532 nm laser at a sufficiently high intensity (200~1000 mW/cm^2), where the Φ_{UC}' values were saturated. The DPA concentration was fixed at 10 mM for all samples. All samples were treated by 0.64 M LiI ethanol solution.

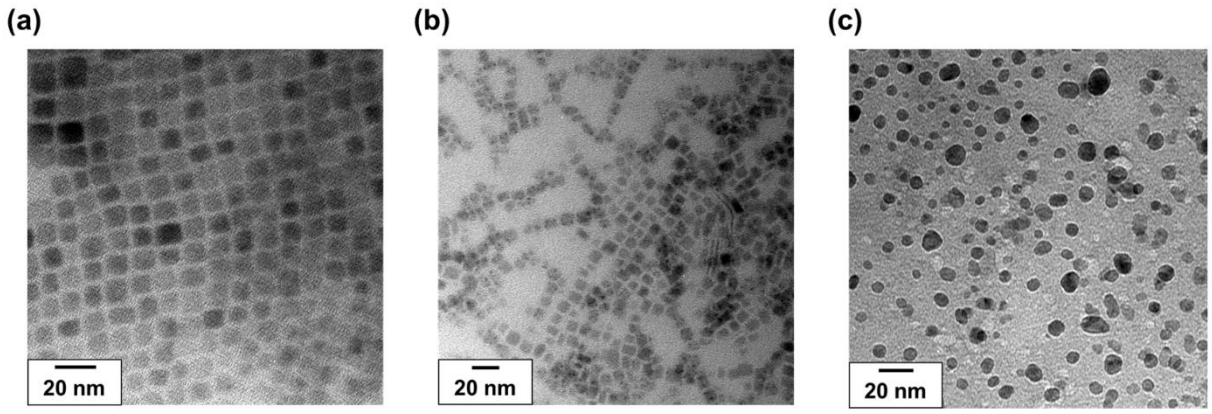

Figure 3-11. TEM images of (a) $CsPbX_3$ (average size = 9.3 ± 1.7 nm), (b) $CsPbX_3$ modified with 0.94 mM **3** (average size = 7.5 ± 1.7 nm), and (c) $CsPbX_3$ modified with 4.0 mM **3** (average size = 7.5 ± 2.2 nm). All samples were treated with 0.64 M LiI ethanol solution.

The effect of perovskite bandgap upon UC efficiency was then investigated by tuning the bandgap of $CsPbX_3$. The saturated Φ_{UC}' values were plotted against the emission wavelength of used perovskite nanocrystals (Figure 3-12).

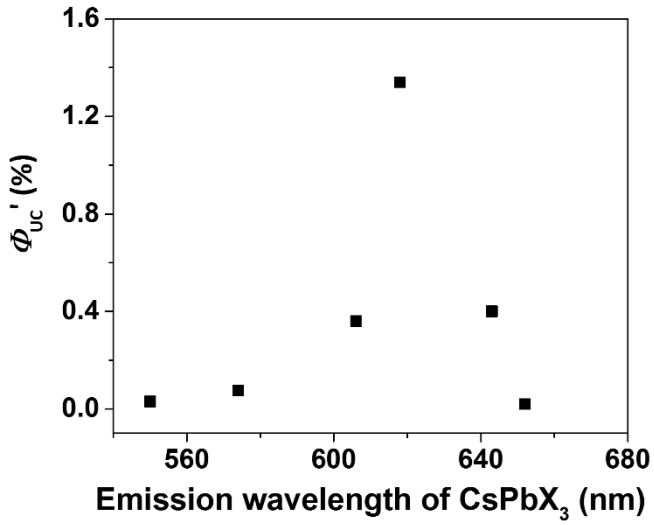

Figure 3-12. Dependence of Φ_{UC}' on the energy bandgap of $CsPbX_3$ in deaerated toluene. These samples were excited with the 532 nm laser at a sufficiently high intensity (200~2000 mW/cm^2), where the Φ_{UC}' values were saturated. **3** and DPA concentrations were fixed at 0.94 mM and 10 mM for all samples.

As the nanocrystal emission wavelength became longer from 550 nm to 620 nm, the Φ_{UC}' value largely increased from 0.03% to 1.3%. On the other hand, further elongation of emission wavelength to 652 nm resulted in a decrease of Φ_{UC}' to 0.02%. To understand this trend, I measured the quantum yield of perovskite emission in the absence of acceptor **3** and DPA (Figure 3-13). As a result, the quantum yield became higher upon elongation of the emission wavelength of perovskite nanocrystals. The improved quantum yield of perovskite nanocrystals by I^- exchange may eventually enhance the triplet sensitization efficiency. In addition, the Φ_{UC}' trend can be associated with the energy level matching between acceptor **3** and perovskite nanocrystals. The energy transfer from perovskite nanocrystals to acceptor **3** would be efficient for the nanocrystal bandgaps close to resonance with the triplet energy level of **3** (ca. 1.77 eV).[40] On the other hand, the smaller $CsPbX_3$ bandgap would result in the smaller driving force of energy transfer to acceptor **3**.[30] It is therefore suggested that the balance between these effects resulted in the observed non-monotonic dependence.

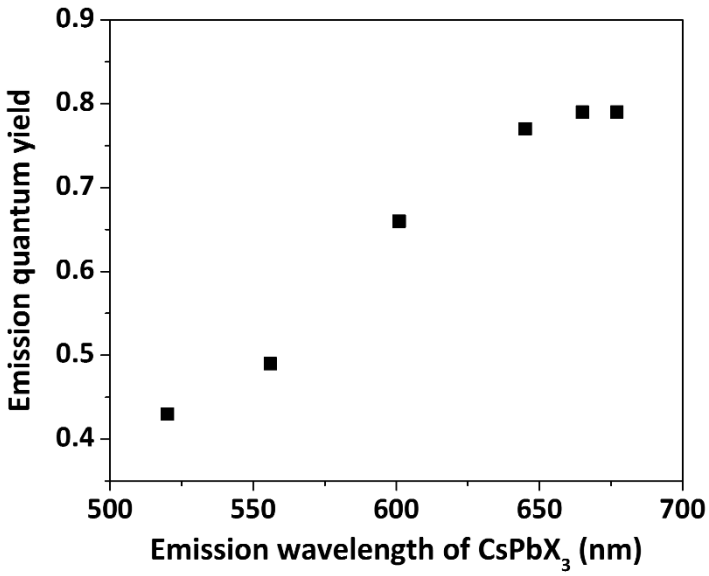

Figure 3-13. Dependence of emission quantum yield of $CsPbX_3$ in deaerated toluene on its emission wavelength.

In conclusion, I showed the triplet sensitization by 3D perovskite nanocrystals for the first time and demonstrated its application in TTA-UC. A series of experiments confirmed the TTA-UC mechanism; the triplet energy transfer from $CsPbX_3$ perovskite nanocrystals to surface-attached acceptor **3**, followed by the triplet energy transfer relay to free DPA and the subsequent TTA event. My initial trial provided the efficient TTA-UC at low excitation intensity, which would be improved by further optimizing the design of inorganic-organic interface structures. The current work initiates the cross-fertilization between 3D perovskite materials and triplet science that would bring a variety of fundamental advances and optical/optoelectronic applications.

3-3 Synthesis

$PbBr_2$, oleic acid, and 48% HBr aqueous solution were purchased from Sigma-Aldrich. Oleylamine, 2-(4-bromophenyl)ethylamine, 10-phenyl-9-anthraceneboronic acid, and 9,10-diphenylanthracene (DPA) were purchased from TCI. Cs_2CO_3 and di-*tert*-butyl dicarbonate were purchased from Wako. LiI was purchased from Kishida.

2-(4-(10-phenylanthracen-9-yl)phenyl)ethan-1-amine (3)

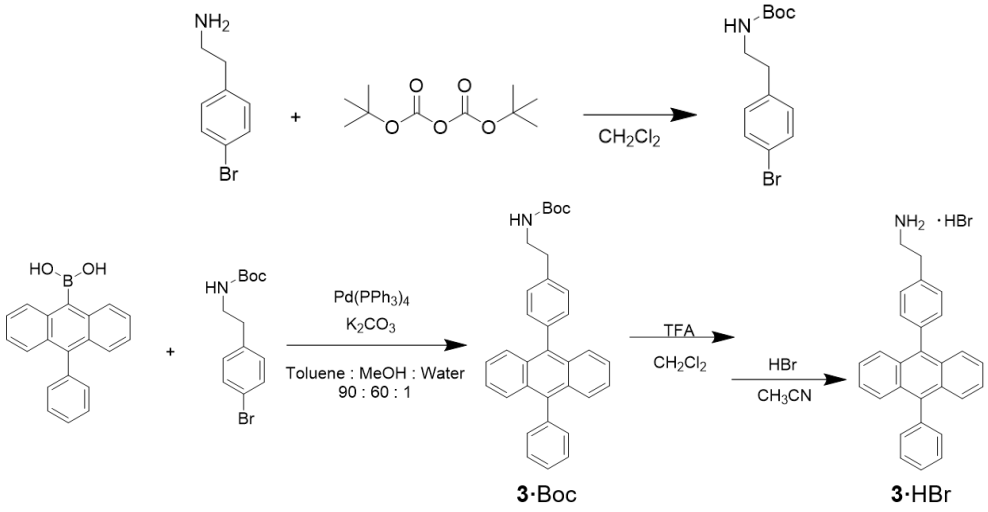

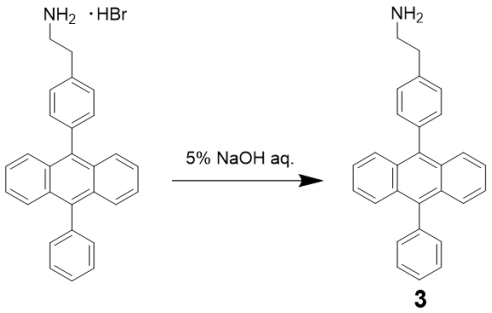

Synthesis of *tert*-butyl(4-bromophenethyl)carbamate.[41] 2-(4-bromophenyl)ethylamine (2.0 g, 10 mmol) and di-*tert*-butyl dicarbonate (2.4 g, 11 mmol) were dissolved in CH_2Cl_2 (100 mL). The mixture was stirred at RT for 3.5 h in N_2 atmosphere. After the reaction, it was washed with a saturated NH_4Cl aqueous solution (100 mL), saturated $NaHCO_3$ aqueous solution (100 mL), and water (100 mL). The organic layer was collected and dried over anhydrous Na_2SO_4 and evaporated under reduced pressure. Since the unreacted material remained, the crude product was again reacted with di-*tert*-butyl dicarbonate (3.9 g, 18 mmol) in CH_2Cl_2 (120 mL) at RT for 11 h in N_2 atmosphere. After the reaction, it was washed with a saturated NH_4Cl aqueous solution (100 mL), saturated $NaHCO_3$ aqueous solution (100 mL), and water (100 mL). The organic layer was collected and dried over anhydrous Na_2SO_4 and evaporated under reduced pressure. The crude product was purified using silica gel column chromatography ($CHCl_3$). After removing $CHCl_3$ under reduced pressure, the colorless solid was obtained. Yield: 2.6 g, 87%. ^{1}H NMR (300 MHz, $CDCl_3$, TMS): δ = 1.43 (s, 9H), 2.73-2.78 (t, 2H), 3.32-3.38 (m, 2H), 4.52 (s, 1H), 7.06-7.08 (d, 2H), 7.41-7.44 (d, 2H).

Synthesis of 3·Boc. *tert*-butyl(4-bromophenethyl)carbamate (600 mg, 2.0 mmol), 10-phenyl-9-anthraceneboronic acid (599 mg, 2.0 mmol), $Pd(PPh_3)_4$ (127 mg, 0.11 mmol), and K_2CO_3 (0.84 g, 6.1 mmol) dissolved in the mixture of toluene (9.5 mL), MeOH (6.3 mL), and water (0.11 mL). The mixture was sealed in a vial tube under N_2, and stirred at 110°C for 3 h in a microwave reactor. After the reaction, the mixture was poured into 50 mL $CHCl_3$ and washed with water (100 mL×3). The organic layer was collected and dried over anhydrous Na_2SO_4 and evaporated under reduced pressure.

The crude product was purified using silica gel column chromatography ($CHCl_3$). After removing $CHCl_3$ under reduced pressure, the colorless solid was obtained. Yield: 0.80 g, 84%. ^{1}H NMR (300 MHz, $CDCl_3$, TMS): δ = 1.49 (s, 9H), 2.96-3.01 (t, 2H), 3.55-3.57 (m, 2H), 4.72 (s, 1H), 7.32-7.72 (m, 17H).

Synthesis of 3·HBr. Under N_2 atmosphere, trifluoroacetic acid (TFA, 6.3 mL) was added to the solution of **3·Boc** (798 mg, 1.7 mmol) in CH_2Cl_2 (40 mL). The mixture was stirred at RT for 4 h. After the reaction, the solvents were removed under reduced pressure. 5% Na_2CO_3 aqueous solution (40 mL) and CH_2Cl_2 (35 mL) were added to the crude product, and it was stirred at RT for 6 h under N_2 atmosphere. The organic layer was collected and dried over anhydrous Na_2SO_4 and evaporated under reduced pressure. The obtained pale yellow solid was dissolved in hot CH_3CN (200 mL), and 48% HBr aqueous solution (0.3 mL) was added. The precipitate was collected and washed with $CHCl_3$ and ethanol. The pale yellow solid was dried under reduced pressure at 60°C. Yield: 449 mg, 58%. ^{1}H NMR (300 MHz, DMSO, TMS): δ = 3.04-3.09 (t, 2H), 3.23-3.28 (t, 2H), 7.39-7.70 (m, 17H), 7.89 (s, 3H). Elemental analysis, calculated for $C_{28}H_{24}NBr$: C, 74.01; H, 5.32; N, 3.08; found: C, 73.86; H, 5.37; N, 3.15.

Synthesis of 3. Under N_2 atmosphere, 5% NaOH aqueous solution (9.5 mL) was added to the solution of **3·HBr** (100 mg, 0.22 mmol) in CH_2Cl_2 (50 mL). The mixture was stirred at RT for 2 h. The organic layer was collected and dried over anhydrous Na_2SO_4 and evaporated under reduced pressure. **3** was obtained as pale yellow solid. Yield: 81 mg, 99%. ^{1}H NMR (300 MHz, DMSO, TMS): δ = 2.81-2.85 (t, 2H), 2.92-2.97 (t, 2H), 7.35-7.69 (m, 17H).

$CsPbBr_3$ nanocrystals

Preparation of Cs-OA solution.[42] Cs_2CO_3 (0.21 g, 0.64 mmol), 1-octadecene (10 mL) and dried oleic acid (OA, 625 μL) were added in a 3-neck flask and degassed at 120 °C for 1 h. Then the mixture

was heated to 150°C under N_2 atmosphere until all Cs_2CO_3 reacted with OA. After the reaction, the solution temperature was maintained at 100°C.

Synthesis of $CsPbBr_3$ NCs.[42] $PbBr_2$ (0.28 g, 0.76 mmol) and 1-octadecene (20 mL) were combined in a 3-neck flask and degassed for 1 h at 120 °C. Dried OA (2 mL) and dried oleylamine (2 mL) were injected at 120 °C under N_2 atmosphere. After $PbBr_2$ was completely dissolved, the temperature was raised to 160 °C. Then 1.6 mL of the Cs-OA solution was injected quickly and 10 s later, the reaction mixture was cooled by the ice-water bath. 20 mL of ethanol was added to the mixture, and the precipitate was collected by centrifugation (3000 rpm, 15 min). In an Ar-filled grove box ($[O_2]<0.1$ ppm), the obtained $CsPbBr_3$ NCs was re-dispersed in toluene (30 mL) and filtered through 0.45 μm PTFE syringe filter.

3-4 Characterizations

^1H NMR spectra were measured on a JEOL JNM-ECX 400 spectrometer. Elemental analysis was conducted at the Elemental Analysis Center, Kyushu University. UV/Vis absorption spectra were recorded on a JASCO V-670 spectrophotometer. Fluorescence spectra were measured by using a PerkinElmer LS 55 fluorescence spectrometer. The absolute quantum yields were measured in an integrating sphere using a Hamamatsu Photonics absolute quantum yield measurement system. Time-resolved photoluminescence lifetime measurements were carried out by using a time-correlated single photon counting lifetime spectroscopy system, HAMAMATSU Quantaurus-Tau C11567–01 (for delayed luminescence lifetime)/C11567–02 (for fluorescence lifetime).

For TTA-UC emission measurements, diode lasers (532 nm, 200 mW, RGB Photonics; 635 nm, 75 mW, RGB Photonics) was used as excitation sources. The laser power was controlled by combining a software (Ltune) and a variable neutral density filter, and measured using a PD300-UV photodiode sensor (OPHIR Photonics). The laser beam was focused on a sample using a lens. The diameter of the laser beam ($1/e^2$) was measured at the sample position using a CCD beam profiler SP620 (OPHIR

Photonics). Typical laser size were 2.8×10^{-4} cm^2 and 5.1×10^{-4} cm^2 for 532 nm and 635 nm lasers, respectively. The emitted light was collimated by an achromatic lens, the excitation light was removed using notch and short-pass filters, and the emitted light was again focused by an achromatic lens to an optical fiber connected to a multichannel detector MCPD-9800 (Otsuka Electronics).

3-5 Reference

1 T. Ishihara, J. Takahashi and T. Goto, *Solid State Commun.*, 1989, **69**, 933-936.

2 J. Calabrese, N. L. Jones, R. L. Harlow, N. Herron, D. L. Thorn and Y. Wang, *J. Am. Chem. Soc.*, 1991, **113**, 2328-2330.

3 D. B. Mitzi, *J. Chem. Soc., Dalton Trans.*, 2001 1-12.

4 O. Selig, A. Sadhanala, C. Muller, R. Lovrincic, Z. Chen, Y. L. A. Rezus, J. M. Frost, T. L. C. Jansen and A. A. Bakulin, *J. Am. Chem. Soc.*, 2017, **139**, 4068-4074.

5 Y. C. Liu, Z. Yang, D. Cui, X. D. Ren, J. K. Sun, X. J. Liu, J. R. Zhang, Q. B. Wei, H. B. Fan, F. Y. Yu, X. Zhang, C. M. Zhao and S. Z. Liu, *Adv. Mater.*, 2015, **27**, 5176-5183.

6 L. Protesescu, S. Yakunin, M. I. Bodnarchuk, F. Bertolotti, N. Masciocchi, A. Guagliardi and M. V. Kovalenko, *J. Am. Chem. Soc.*, 2016, **138**, 14202-14205.

7 Z. K. Tan, R. S. Moghaddam, M. L. Lai, P. Docampo, R. Higler, F. Deschler, M. Price, A. Sadhanala, L. M. Pazos, D. Credgington, F. Hanusch, T. Bein, H. J. Snaith and R. H. Friend, *Nat. Nanotechnol.*, 2014, **9**, 687-692.

8 G. C. Xing, N. Mathews, S. S. Lim, N. Yantara, X. F. Liu, D. Sabba, M. Gratzel, S. Mhaisalkar and T. C. Sum, *Nat. Mater.*, 2014, **13**, 476-480.

9 Y. C. Hsiao, T. Wu, M. X. Li, Q. Liu, W. Qin and B. Hu, *J. Mater. Chem. A*, 2015, **3**, 15372-15385.

10 G. R. Li, Z. K. Tan, D. W. Di, M. L. Lai, L. Jiang, J. H. W. Lim, R. H. Friend and N. C. Greenham, *Nano Lett.*, 2015, **15**, 2640-2644.

11 Z. Xiao, R. A. Kerner, L. Zhao, N. L. Tran, K. M. Lee, T.-W. Koh, G. D. Scholes and B. P. Rand, *Nat. Photon.*, 2017, **11**, 108-115.

12 M. V. Pavliuk, D. L. A. Fernandes, A. M. El-Zohry, M. Abdellah, G. Nedelcu, M. V. Kovalenko and J. Sa, *Adv. Opt. Mater.*, 2016, **4**, 2004-2008.

13 C. Zhang, D. Sun, C. X. Sheng, Y. X. Zhai, K. Mielczarek, A. Zakhidov and Z. V. Vardeny, *Nat. Phys.*, 2015, **11**, 428-435.

14 S. Baluschev, T. Miteva, V. Yakutkin, G. Nelles, A. Yasuda and G. Wegner, *Phys. Rev. Lett.*, 2006, **97**.

15 D. Di, L. Yang, J. M. Richter, L. Meraldi, R. M. Altamimi, A. Y. Alyamani, D. Credgington, K. P. Musselman, J. L. MacManus-Driscoll and R. H. Friend, *Adv. Mater.*, 2017.

16 P. F. Duan, N. Yanai and N. Kimizuka, *J. Am. Chem. Soc.*, 2013, **135**, 19056-19059.

17 P. F. Duan, N. Yanai, H. Nagatomi and N. Kimizuka, *J. Am. Chem. Soc.*, 2015, **137**, 1887-1894.

18 V. Gray, D. Dzebo, M. Abrahamsson, B. Albinsson and K. Moth-Poulsen, *Phys. Chem. Chem. Phys.*, 2014, **16**, 10345-10352.
19 J. H. Kim and J. H. Kim, *J. Am. Chem. Soc.*, 2012, **134**, 17478-17481.
20 A. Monguzzi, R. Tubino, S. Hoseinkhani, M. Campione and F. Meinardi, *Phys. Chem. Chem. Phys.*, 2012, **14**, 4322-4332.
21 T. Ogawa, N. Yanai, A. Monguzzi and N. Kimizuka, *Sci. Rep.*, 2015, **5**, 10882.
22 T. F. Schulze and T. W. Schmidt, *Energy Environ. Sci.*, 2015, **8**, 103-125.
23 Y. C. Simon and C. Weder, *J. Mater. Chem.*, 2012, **22**, 20817-20830.
24 T. N. Singh-Rachford and F. N. Castellano, *Coord. Chem. Rev.*, 2010, **254**, 2560-2573.
25 J. Z. Zhao, S. M. Ji and H. M. Guo, *Rsc Adv.*, 2011, **1**, 937-950.
26 J. Zhou, Q. Liu, W. Feng, Y. Sun and F. Y. Li, *Chem. Rev.*, 2015, **115**, 395-465.
27 S. H. C. Askes, A. Bahreman and S. Bonnet, *Angew. Chem. Int. Ed.*, 2014, **53**, 1029-1033.
28 Z. Y. Huang, X. Li, M. Mahboub, K. M. Hanson, V. M. Nichols, H. Le, M. L. Tang and C. J. Bardeen, *Nano Lett.*, 2015, **15**, 5552-5557.
29 Z. Y. Huang, X. Li, B. D. Yip, J. M. Rubalcava, C. J. Bardeen and M. L. Tang, *Chem. Mater.*, 2015, **27**, 7503-7507.
30 M. Mahboub, Z. Y. Huang and M. L. Tang, *Nano Lett.*, 2016, **16**, 8037-8037.
31 C. Mongin, S. Garakyaraghi, N. Razgoniaeva, M. Zamkov and F. N. Castellano, *Science*, 2016, **351**, 369-372.
32 K. Okumura, K. Mase, N. Yanai and N. Kimizuka, *Chem. -Eur. J.*, 2016, **22**, 7721-7726.
33 M. F. Wu, D. N. Congreve, M. W. B. Wilson, J. Jean, N. Geva, M. Welborn, T. Van Voorhis, V. Bulovic, M. G. Bawendi and M. A. Baldo, *Nat. Photon.*, 2016, **10**, 31-34.
34 G. Nedelcu, L. Protesescu, S. Yakunin, M. I. Bodnarchuk, M. J. Grotevent and M. V. Kovalenko, *Nano Lett.*, 2015, **15**, 5635-5640.
35 L. Protesescu, S. Yakunin, M. I. Bodnarchuk, F. Krieg, R. Caputo, C. H. Hendon, R. X. Yang, A. Walsh and M. V. Kovalenko, *Nano Lett.*, 2015, **15**, 3692-3696.
36 P. Ramasamy, D. H. Lim, B. Kim, S. H. Lee, M. S. Lee and J. S. Lee, *Chem. Commun.*, 2016, **52**, 2067-2070.
37 Y. Y. Cheng, T. Khoury, R. G. C. R. Clady, M. J. Y. Tayebjee, N. J. Ekins-Daukes, M. J. Crossley and T. W. Schmidt, *Phys. Chem. Chem. Phys.*, 2010, **12**, 66-71.
38 A. Haefele, J. Blumhoff, R. S. Khnayzer and F. N. Castellano, *J. Phys. Chem. Lett.*, 2012, **3**, 299-303.
39 A. Monguzzi, R. Tubino and F. Meinardi, *Phys. Rev. B*, 2008, **77**.
40 M. Tabachnyk, B. Ehrler, S. Gelinas, M. L. Bohm, B. J. Walker, K. P. Musselman, N. C. Greenham, R. H. Friend and A. Rao, *Nat. Mater.*, 2014, **13**, 1033-1038.
41 M.-B. S. Kirketerp, T. Ryhding, K. Støchkel, M. B. Nielsen and S. B. Nielsen, *J. Phys. Chem. A*, 2011, **115**, 1222-1227.
42 P. Ramasamy, D. Lim, B. Kim, S. Lee, M. Lee and J. Lee, *Chem. Commun.*, 2016, **52**, 2067-2070.

Chapter 4 Stimuli-Responsive Dual-color Photon Upconversion: S-T absorption sensitizer in soft luminescent cyclophane

4-1 Introduction

ABSTRACT: Reversible emission color switching of triplet-triplet annihilation-based photon upconversion (TTA-UC) was achieved for the first time by employing an Os complex sensitizer with singlet-to-triplet (S-T) absorption and an asymmetric luminescent cyclophane with switchable emission characteristics. The cyclophane contains the 9,10-bis(phenylethynyl)anthracene unit as an emitter and can assemble into two different structures, a stable crystalline phase and a metastable supercooled nematic phase. The two structures exhibit green and yellow fluorescence, respectively and can be accessed by distinct heating/cooling sequences. The hybridization of the cyclophane with an Os complex allowed near-infrared-to-visible TTA-UC. The large anti-Stokes shift was possible by using a sensitizer that displays efficient S-T absorption, instead of relying on the more conventional sequence of singlet-singlet absorption and intersystem crossing. The TTA-UC emission color of the new material could successfully be switched between green and yellow by thermal stimulation, demonstrating the feasibility of tunable upconversion materials

Photon upconversion (UC) processes allow converting lower energy photons to higher energy photons. Among various UC mechanisms, triplet−triplet annihilation-based UC (TTA-UC) is particularly useful, since it allows UC under low excitation power density.[1-13] Recently, the possibility to utilize an external stimulus to control the TTA-UC process has been studied for several advanced applications, such as spatial and temporal high-resolution fluorescence microscopy, multicolor barcoding, and remote control of molecular photo-switching reactions.[14-21] However, successful examples have been limited to ON/OFF switching of UC emission by inhibiting TTA or quenching of the excited states,[14-21] while there have been no reports on UC emission color switching for condensed molecular assemblies. There are two major challenges that have to be overcome to achieve color switching of

TTA-UC in the solid state. Firstly, it must be possible to assemble the luminophores in different molecular assemblies, with inter-luminophore distances that are close enough for triplet energy migration (TEM), and the luminophores should have suitable excited state energy levels for TTA-UC. Secondly, while a significant red-shift of the lower energy state is required to provide a recognizable emission color change, the emission should not overlap with the excitation wavelength of the sensitizer, as otherwise no upconverted emission would occur.

The first challenge can be overcome by utilizing luminescent molecular assembled materials that show a change of the molecular assembled structure in response to an external stimulus such as a temperature change or exposure to mechanical stimuli. As the photophysical properties of molecular materials significantly depend on the molecular assembled structure, external stimuli-induced changes in molecular assembled structures can lead to pronounced alterations of the photoluminescent properties.[22,23] Indeed, many organic or organometallic compounds have been found to show thermally induced photoluminescent color changes in condensed states.[24-31] The second problem can be solved by introducing triplet sensitizers that have strong absorption in the near-infrared (NIR) wavelength region and can sensitize emitter triplets without large energy loss. Some of us have recently shown that triplet sensitizers with a pronounced singlet-to-triplet (S-T) absorption in the NIR range enable larger anti-Stokes shifts than conventional UC sensitizers in which the triplet state is populated by singlet-singlet absorption and subsequent intersystem crossing (ISC).[32-34] From the viewpoint of dual-color TTA-UC, the lower energy loss encountered during the triplet sensitization can compensate the inevitable energy loss arising from switching the luminescence color to a lower wavelength. In addition, taking advantage of good tissue transparency of NIR light in the wavelength range from 700 nm to 900 nm, the dual-color UC emission under NIR excitation is expected to expand the scope of stimuli-responsive luminescent materials to the biological application.[35,36]

In this chapter, I show the first example that stimuli-triggered reversible TTA-UC emission color switching is possible by hybridizing a luminescent cyclophane with an S-T absorption sensitizer (Figure 4-1). Such luminescent cyclophanes represent an attractive platform to attain stimuli-responsive

fluorescence color change,[37-39] as they not only assemble in thermodynamically stable crystalline structures, but can often also be kinetically trapped in at least one metastable state. For example, a pyrene-based asymmetric cyclophane was shown to form a kinetically-trapped, supercooled nematic liquid crystalline phase.[39] The metastable state was accessed by rapid cooling of the nematic phase from 80 °C to ambient. Extending this approach, I synthesized the new asymmetric cyclophane **4** containing the 9,10-bis(phenylethynyl)anthracene (BPEA) moiety. This motif offers excited triplet and singlet energy levels that render it useful as TTA-UC emitter (Figure 4-1b).[40-46] Cyclophane **4** was combined with the S-T absorption sensitizer $Os(bptpy)_2^{2+}$ (Figure 4-1a), having a suitable triplet energy level (1.67 eV) to sensitize the BPEA triplet (1.53 eV).[33,41] Gratifyingly, the rationally designed **4**-$Os(bptpy)_2^{2+}$ hybrid not only displays pronounced TTA-UC under NIR excitation, but the color of the emitted light can be thermally switched between green and yellow (Figure 4-1b, 4-1c).

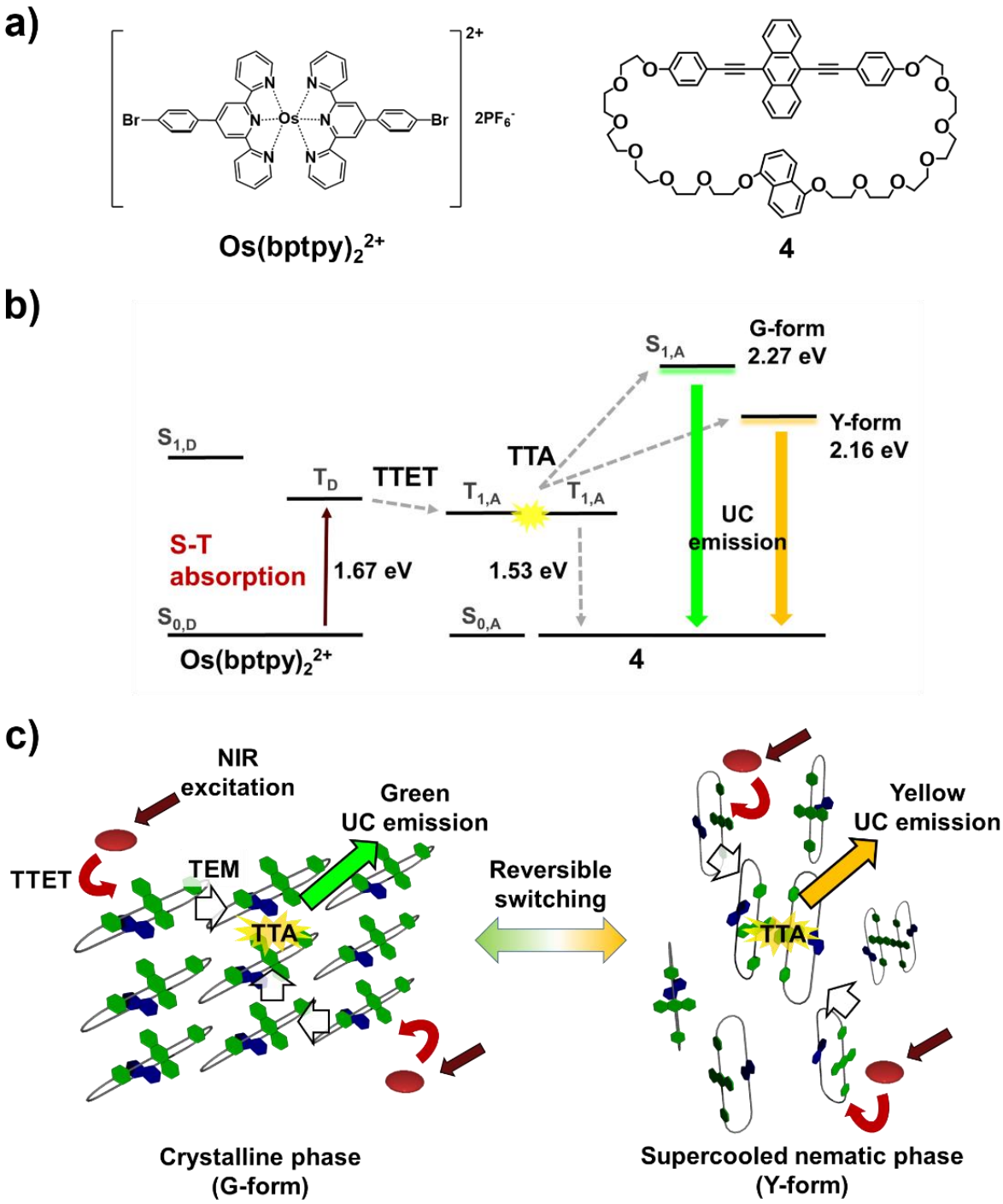

Figure 4-1. (a) Chemical structures of the S-T absorption sensitizer $Os(bptpy)_2^{2+}$ and the asymmetric cyclophane **4**. (b) Energy diagram of the singlet-to-triplet (S–T) absorption-based TTA-UC process involving $Os(bptpy)_2^{2+}$ and the cyclophane **4**. The S-T absorption in the NIR range enables a larger anti-Stokes shift than conventional UC sensitizers in which the triplet state is populated by singlet-singlet absorption and subsequent intersystem crossing. The emitter triplet is populated by triplet-triplet energy transfer (TTET), and leads to the formation of emitter singlet excited states ($S_{1,A}$). The

stimuli-induced change of the $S_{1,A}$ energy level promotes the dual-color TTA-UC emission. (c) Schematic representations of the TTA-UC emission color switching. The UC emission color can be switched between green and yellow depending on the assembled structure of emitter. The S-T absorption of the sensitizer (dark red) under NIR excitation is followed by TTET to emitter cyclophanes. Subsequently, the TEM among densely arranged emitter units results in TTA. Green UC emission is obtained when the emitter is in a crystalline state (G-form), while yellow UC emission is observed in the supercooled nematic LC phase (Y-form).

4-2 Results and Discussion

Differential scanning calorimetry (DSC), X-ray powder diffraction (XRPD), and polarized optical microscope (POM) images reveal that cyclophane **4** shows a nematic LC phase in the temperature range from 119.5°C to 64.8°C and a crystalline phase below (Figure 4-2a-d) on cooling from the isotropic state. A typical schlieren texture, indicative of a nematic LC phase,[47] is observed at 100°C (Figure 4-2d, left). Rapid cooling of the nematic LC phase to room temperature affords a supercooled nematic phase exhibiting yellow photoluminescence (Figure 4-2e, Y-form). The Y-form shows a marble texture characteristic of nematic molecular order. The DSC heating curve of this nematic sample shows an exothermic peak at 45.5°C, which corresponds to a phase transition to the green-emitting crystalline phase (Figure 4-2d, G-form). A transition to the isotropic melt is observed at 127.2°C (Figure 4-2b). The exothermic transition from the Y-form to the G-form confirms that the Y-form is the thermodynamically metastable phase, which is kinetically-trapped by rapid cooling. XRPD measurements at room temperature reveal a significant difference in the molecular order between the Y- and G-forms (Figure 4-2c). A broad, structure-less pattern is observed for the Y-form, indicating that nematic molecular order is retained after rapid cooling from the nematic LC phase. On the other hand, the XRPD spectrum of the G-form shows many sharp peaks that reflect the well-ordered crystalline nature.

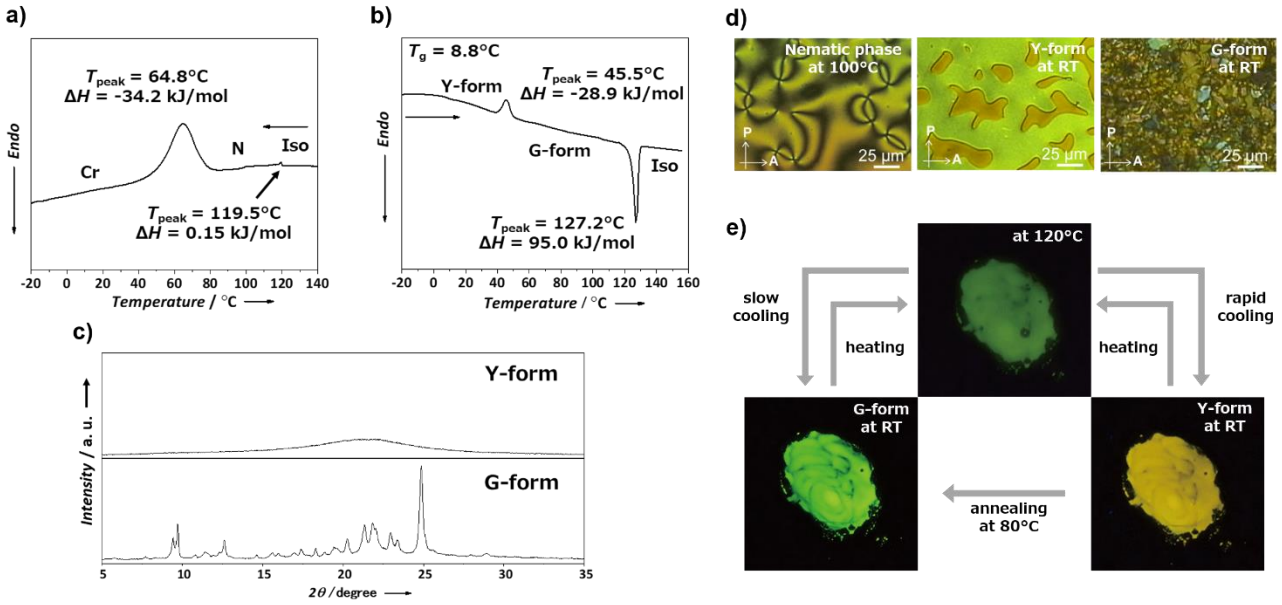

Figure 4-2. (a) DSC cooling trace of **4** in the isotropic phase (cooling rate: 10°C/min, recorded under N_2). (b) DSC heating trace of **4** in the Y-form (heating rate: 10°C/min, recorded under N_2). (c) XRPD patterns of **4** in the supercooled nematic phase (top, Y-form), and in the crystalline phase (bottom, G-form) measured at room temperature. (d) POM images of **4** in the nematic phase at 100°C (left), in the Y-form at room temperature (middle), and in the G-form at room temperature (right). (e) Images summarizing the phase transition behavior of **4**. All images were taken on glass substrates without a cover slide under irradiation with UV light (λ_{ex} = 365 nm)

The absorption spectra of G- and Y-forms show absorption peaks at 500 nm and 486 nm, respectively (Figure 4-3). These peaks are red-shifted compared to that of a chloroform solution of **4** ($\lambda_{abs,max}$ = 474 nm), indicative of inter-chromophore interactions in both condensed states. The fluorescence band of the Y-form is more red-shifted ($\lambda_{em,max}$ = 573 nm) and broadened compared to that of the G-form ($\lambda_{em,max}$ = 546 nm) (Figure 4-4), and the averaged fluorescence lifetime of the Y-form (10.1 ns) is notably longer than that of G-form (3.3 ns) (Figure 4-5). The absolute fluorescence quantum yields were 36% and 25% for the G-form and Y-form, respectively. These observations suggest that BPEA moieties in the Y-form are strongly interacting compare to G-form.[39]

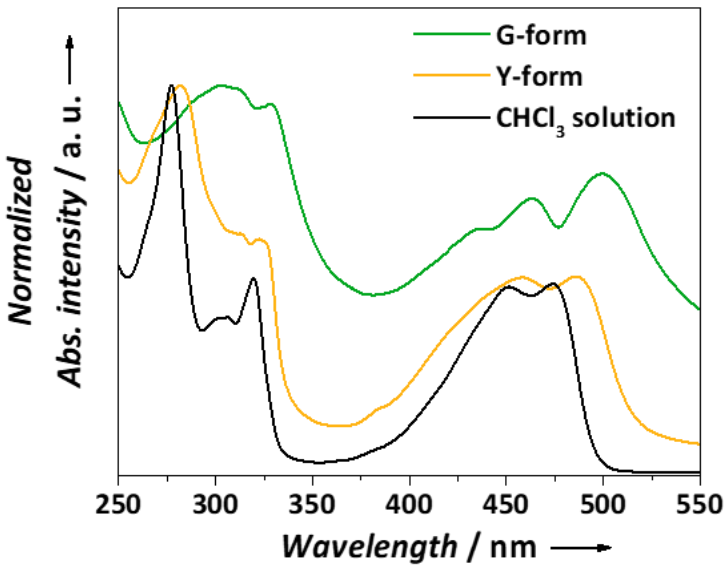

Figure 4-3. Absorption (Abs.) spectra of **4** in the G-form (green), Y-form (yellow), and $CHCl_3$ solution (10 μM, black).

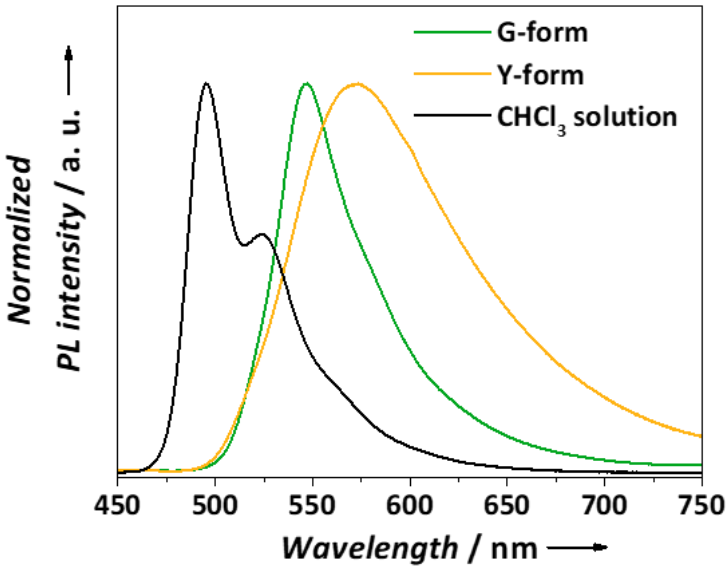

Figure 4-4. Photoluminescence (PL) spectra of **4** in the G-form (green), Y-form (yellow), and $CHCl_3$ solution (10 μM, black).

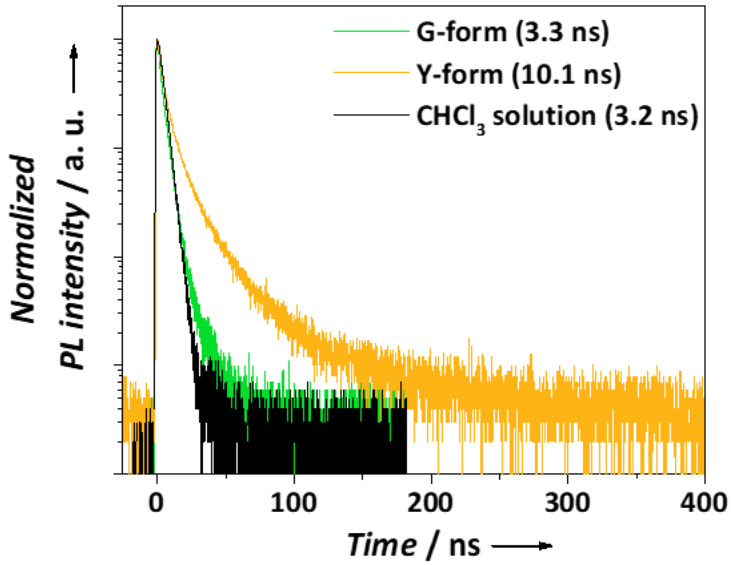

Figure 4-5. Fluorescence decay of **4** in the G-form (green), in the Y-form (yellow), and $CHCl_3$ solution (10 μM, black) under pulsed excitation at 470 nm. The decay of the G-form could be fitted with three components of 1.0 ns (32.1%), 3.6 ns (61.6%) and 12.3 ns (6.3%), and its averaged lifetime was 3.3 ns. The decay of the Y-form could be fitted with three components of 1.5 ns (32.2%), 7.9 ns (47.1%) and 28.2 ns (20.7%), and its averaged lifetime was 10.1 ns. The decay of the $CHCl_3$ solution could be fitted with one component of 3.2 ns.

To enable TTA-UC, **4** was doped with the triplet sensitizer $Os(bptpy)_2^{2+}$, which exhibits S-T absorption in the NIR range (Figure 4-6). The sensitizer $Os(bptpy)_2^{2+}$ and emitter **4** have appropriate singlet/triplet energy levels for TTA-UC, as confirmed by the appearance of TTA-UC emission in de-aerated DMF (Figure 4-7).

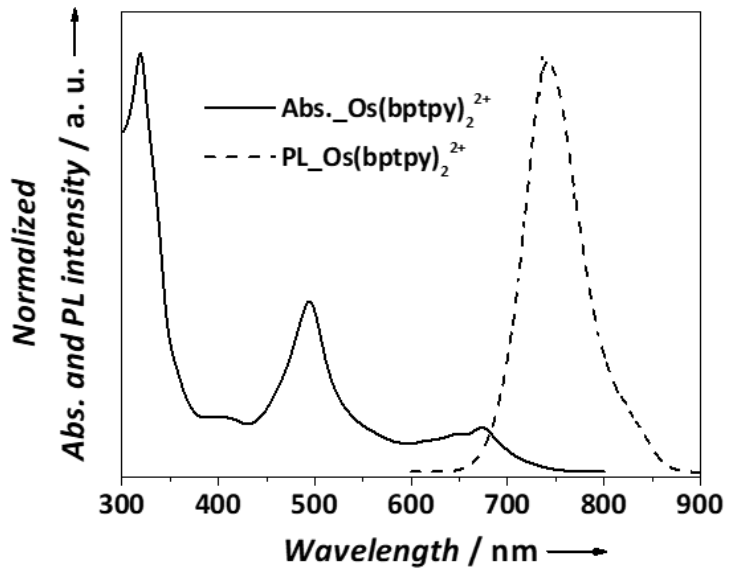

Figure 4-6. Absorption (Abs.) and photoluminescence (PL) spectra of a DMF solution of $Os(bptpy)_2^{2+}$ (100 μM).

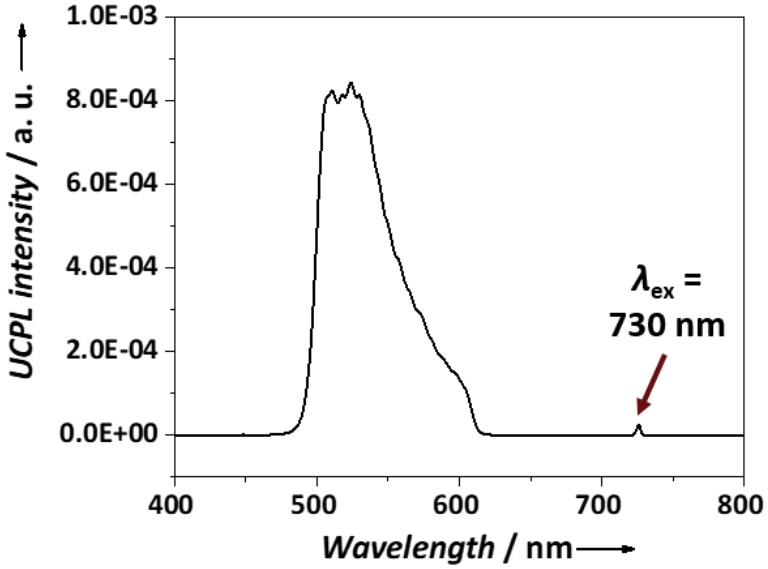

Figure 4-7. UCPL spectrum of a solution of $Os(bptpy)_2^{2+}$ and **4** in deaerated DMF ([$Os(bptpy)_2^{2+}$]/[**4**] = 1 mol%, [**4**] = 2 mM). The spectrum was acquired under excitation with a 730 nm laser (excitation intensity: 390 W/cm^2). Short pass filters (λ = 700 nm and 610 nm) were used to remove the scattered incident light.

The switching of TTA-UC color was examined in the solvent-free conditions. In an Ar-filled glove box ([O_2] < 0.1 ppm), a DMF solution of **4** and $Os(bptpy)_2^{2+}$ ([$Os(bptpy)_2^{2+}$]/[**4**] = 0.5 mol%) was drop-casted onto glass substrates, and samples were heated at 80°C for 1 h to evaporate the solvent. After drying, the samples were annealed at 120°C and sealed by a UV photo-curable resin (The sealing procedure is written in **Characterizations** section). The samples were removed from the glove box, heated to 145°C in an oven, slowly cooled to 80°C, and annealed at this temperature for 1 h before cooling to room temperature to obtain the G-form. Alternatively, samples were heated to 145°C, and rapidly cooled in an ice-bath to obtain the Y-form. Interestingly, both G-form and Y-form showed UC emissions upon excitation with a NIR laser at 730 nm (Figure 4-8a and 4-8b). Moreover, it was possible to change the UC emission color from green to yellow or vice versa, by repeated heating and cooling cycles that followed the two methods, confirming that the switching is reversible.

To prove TTA as the UC mechanism, I confirmed that no UC emission could be observed from neither the G- nor the Y-form of **4** in the absence of $Os(bptpy)_2^{2+}$ (Figure 4-9), confirming the role of this compound as triplet sensitizer. I also measured the UC emission lifetime and excitation intensity dependence of the UC emission. The UC emission displays sub-millisecond-scale decay profiles, characteristic of UC via a long-lived triplet excited state (Figure 4-8c). In the longer timescale region, the annihilation efficiency becomes negligible relative to the spontaneous decay of the triplets, and using the well-known relationship $I_{UC}(t) \propto \exp(-2t/\tau_T)$,[48] the triplet lifetime (τ_T) was estimated to be 550 μs for the G-form and 90 μs for the Y-form. The relation between the UC emission intensity and the incident light intensity is normally characterized by a low and a high excitation intensity regime, in which quadratic and linear dependences are observed,[49-52] with a quadratic-to-linear transition at a threshold excitation intensity I_{th}. Above I_{th}, TTA becomes the main deactivation channel for the acceptor triplet.[49] Double logarithmic plots of the UC emission intensity as a function of the excitation intensity obtained for the G-form and the Y-form are shown in Figure 4-8d. The two plots indeed display slope changes from 2 to 1, and the intersections of the respective functions place the I_{th} values at 240 mW cm^{-2} for the G-form and 2500 mW cm^{-2} for the Y-form.

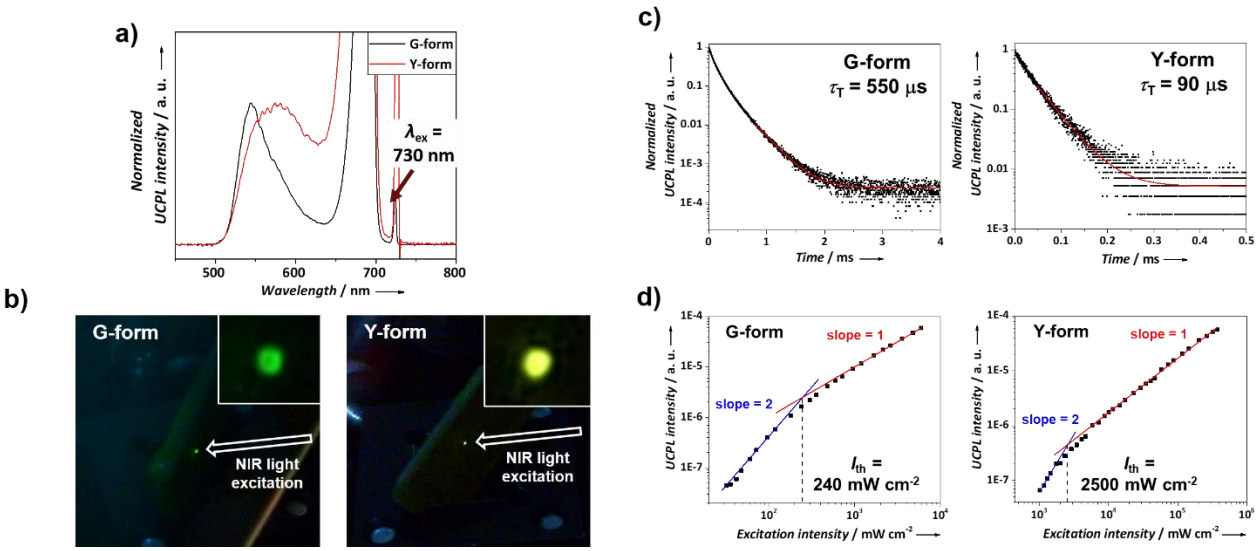

Figure 4-8. (a) UC photoluminescence (PL) spectra of 0.5 mol% $Os(bptpy)_2^{2+}$-doped **4** in the G-form (black) and the Y-form (red) irradiated by a 730 nm NIR laser. The excitation intensities were 6.0 W cm^{-2} for the G-form and 380 W cm^{-2} for the Y-form. A short pass filter (λ = 700 nm) was used to remove scattered incident light. The signals above 640 nm correspond to the tail part of residual excitation light. (b) Photographs of 0.5 mol% $Os(bptpy)_2^{2+}$-doped **4** in the G-form (left) and the Y-form (right) irradiated by a 730 nm NIR laser. A short-pass filter (λ = 610 nm) was used to remove scattered incident light. (c) Plots showing the UC emission decay of 0.5 mol% $Os(bptpy)_2^{2+}$-doped **4** in the G-form (left) and the Y-form (right) under pulsed excitation at 720 nm. The red curve was obtained by fitting the function $I_{UC}(t) \propto \exp(-2t/\tau_T)$ to the data,[48] where τ_T is the acceptor triplet lifetime (550 μs for the G-form, 90 μs for the Y-form). (d) Plots showing the excitation intensity dependence of the UC emission intensity. Blue and red lines show fit with slopes of 2 and 1.

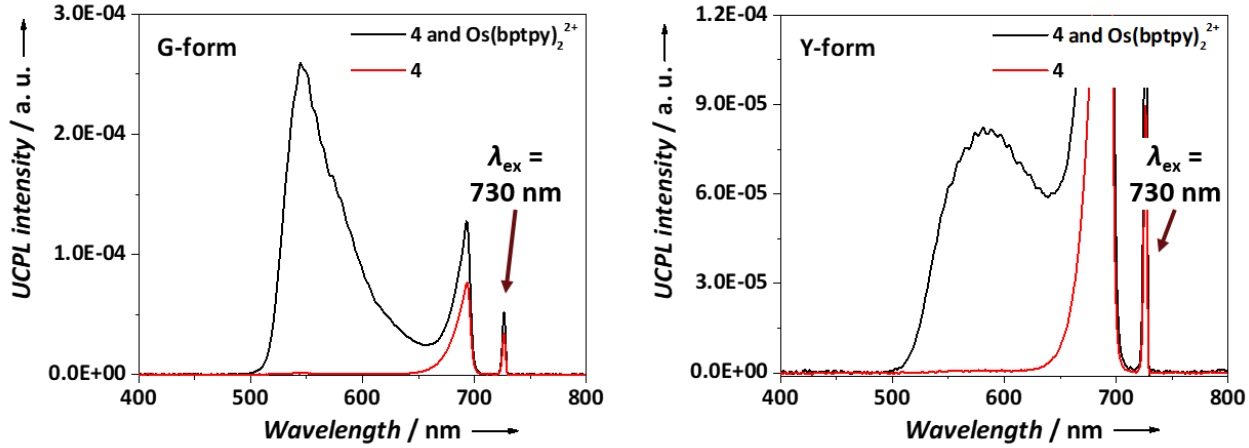

Figure 4-9. UC emission spectra of **4** with/without $Os(bptpy)_2^{2+}$ using the 730 nm laser. (Left) UC emission spectra of **4** in the G-form with 0.5 mol% $Os(bptpy)_2^{2+}$ (black, excitation intensity = 20 W/cm^2) and without $Os(bptpy)_2^{2+}$ (red, excitation intensity = 18 W/cm^2). (Right) UC emission spectra of **4** in the Y-form with 0.5 mol% $Os(bptpy)_2^{2+}$ (black, excitation intensity = 360 W/cm^2) and without $Os(bptpy)_2^{2+}$ (red, excitation intensity = 370 W/cm^2). A short pass filter (λ = 700 nm) was used to remove the scattered incident light.

The shorter triplet lifetime of the Y-form in comparison to the G-form implies the presence of more deactivation sites in the less-ordered Y-form. Since I_{th} is proportional to the inverse of τ_T^2,[52] a lower I_{th} in the G-form than in the Y-form is reasonable. These considerations explain the large difference of the UC quantum yield between the G-form (0.20% at 134 W cm^{-2}) and the Y-form (0.02% at 120 W cm^{-2}). These results indicate that not only the UC emission color but also other UC characteristics can be switched by the transition between the G- and Y-forms. It is worth pointing out that such large differences were not observed in fluorescence lifetime and quantum yield. The excited triplets seem to be more sensitive to defects than the excited singlets. This interesting observation will be more explored in more detail in our future work.

In conclusion, I demonstrated a stimuli-responsive TTA-UC system, whose emission color can be reversibly switched by thermal treatment. The asymmetric structure of cyclophane **4** stabilized a supercooled nematic phase at room temperature, enabling the fluorescence color switching between the

green-emissive crystalline state and yellow-emissive nematic state. Minimizing the energy loss upon the triplet sensitization by exploiting the direct S-T absorption of $Os(bptpy)_2^{2+}$, I successfully achieved TTA-UC emission color switching under NIR light excitation. These results offer a new design guideline of dual-color TTA-UC toward advanced applications in materials science and bio-technology.

4-3 Synthesis

All reagents and solvents were purchased from Aldrich and Tokyo Kasei. Unless otherwise noted, all reactions were carried out under a nitrogen atmosphere. $Os(bptpy)_2^{2+}$ was synthesized by Mr. Yoichi Sasaki according to the reported procedures.[33] Luminescent cyclophane (**4**) was synthesized by Dr. Yoshimitsu Sagara.

Luminescent cyclophane (4)

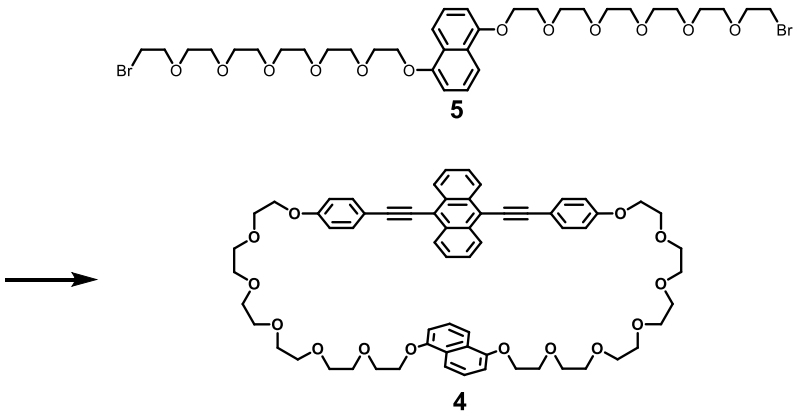

A solution of compound **5** [37,53] (600 mg, 0.737 mmol) and 9,10-bis(4-hydroxyphenylethynyl)anthracene (302 mg, 0.737 mmol) in DMF (20 mL) was dropwise added to a suspension of K_2CO_3 (1.02 g, 7.37 mmol) in DMF (150 mL) at 70 °C over the course of 1 day under vigorous stirring. After further stirring for 24 h at 70 °C, the reaction suspension was cooled and most of the DMF was evaporated in vacuo. The crude product was dissolved in chloroform and washed with saturated aq. NH_4Cl solution (3 × 100 mL) andsaturated aq. NaCl solution. The organic layer was dried over $MgSO_4$, filtered, and the solvent was evaporated. The crude product was purified by flash column chromatography on silica gel (eluent: dichloromethane/acetone = 3:1) and subsequent re-precipitated from a mixture of

dichloromethane and methanol to afford compound **4** (383 mg, 0.360 mmol) as a yellow powder in 49% yield. ^{1}H NMR (400 MHz, $CDCl_3$, TMS): δ = 3.56-3.69 (m, 28H), 3.73-3.77 (m, 8H), 3.89-3.92 (m, 4H), 3.97 (t, J = 4.8 Hz, 4H), 4.25-4.27 (m, 4H), 6.48 (d, J = 8.4 Hz, 2H), 7.04 (d, J = 8.8 Hz, 4H), 7.07 (t, J = 8.0 Hz, 2H), 7.53-7.55 (m, 4H), 7.61 (d, J = 8.8 Hz, 2H), 7.68 (d, J = 8.8 Hz, 4H), 8.60-8.62 (m, 4H). ^{13}C NMR (100 MHz, $CDCl_3$, TMS): δ = 67.54, 67.98, 69.80, 69.89, 70.61, 70.68, 70.70, 70.81, 70.87, 70.89, 71.18, 85.64, 102.67, 105.36, 114.45, 115.34, 115.86, 118.47, 124.98, 126.54, 126.78, 127.32, 131.99, 133.26, 154.15, 159.47. MS (MALDI-TOF): m/z: 1062.62 ($[M]^+$). Elemental analysis (%) calcd. for $C_{64}H_{70}O_{14}$: C 72.30, H 6.64, N 0.00; found: C 72.13, H 6.59, N 0.30.

4-4 Characterizations

^{1}H NMR spectra were measured on a JEOL JNM-ECX 400 spectrometer. Matrix-assisted laser desorption ionization time-of-flight (MALDI-TOF) mass spectra were obtained on an AB SCIEX TOF/TOF 5800. Elemental analysis was carried out with an Exeter Analytical CE440 Elemental Analyzer. The DSC measurements were conducted using a Rigaku Thermo plus EVO DSC8230 with heating/cooling rates of 10 ˚C/min under nitrogen atmosphere. X-ray powder diffraction (XRPD) measurements were carried out with a Rigaku SmartLab. UV-vis absorption spectra were measured with a JASCO V-550 and a JASCO V-670. Fluorescence spectra were measured using a JASCO FP-6500 for **4**, and a PerkinElmer LS 55 fluorescence spectrometer for $Os(bptpy)_2^{2+}$. The solid samples for fluorescence spectra were carefully sandwiched between quartz substrates and were set in the sample position of the spectrometer so that the detector gathered the fluorescence from the surface of the sandwiched solid. Time-resolved photoluminescence lifetime measurements were carried out by using a time-correlated single photon counting lifetime spectroscopy system, HAMAMATSU Quantaurus-Tau C11567–01 (for delayed luminescence lifetime)/C11567–02 (for fluorescence lifetime).

For TTA-UC emission measurements, the samples were sealed by a UV photo-curable resin (MORESCO WB90US). A high-pressure mercury lamp (SEN LIGHTS Corporation HLR100T-2, UV light

intensity: 170 mW/cm^2) was used for curing the resin. After 30 s UV irradiation, the samples were heated at 80°C for 1 h for post-hardening of the resin. The sample sealing was done in an Ar-filled glove box ([O_2] < 0.1 ppm). A diode laser (730 nm, 40 mW, RGB Photonics) was used as excitation source. The laser power was controlled by combining a software (Ltune) and a variable neutral density filter, and measured using a PD300-UV photodiode sensor (OPHIR Photonics). The laser beam was focused on the samples using a lens. The diameter of the laser beam (1/e^2) was measured at the sample position using a CCD beam profiler SP620 (OPHIR Photonics). The typical laser beam size was 6.9×10^{-5} cm^2. The emitted light was collimated by an achromatic lens, the excitation light was removed using a 610 nm and a 700 nm short-pass filter (λ = 610 nm: Asahi Spectra, λ = 700 nm: Edmund Optics), and the emitted light was again focused by an achromatic lens to an optical fiber connected to a multichannel detector MCPD-9800 (Otsuka Electronics). The TTA-UC quantum yield was measured by using an absolute quantum yield measurement system. The sample was held in an integration sphere and excited by the laser excitation source (730 nm, 40 mW, RGB Photonics). The scattered excitation light was removed using a 700 nm short-pass filter and emitted light was monitored with a multichannel detector C10027-01 (Hamamatsu Photonics). The spectrometer was calibrated including the integration sphere and short-pass filter by Hamamatsu Photonics.

4-5 Reference

1 S. Baluschev, T. Miteva, V. Yakutkin, G. Nelles, A. Yasuda and G. Wegner, *Phys. Rev. Lett.*, 2006, **97**, 143903.

2 T. N. Singh-Rachford and F. N. Castellano, *Coord. Chem. Rev.*, 2010, **254**, 2560-2573.

3 J. Zhao, S. Ji and H. Guo, *Rsc Adv.*, 2011, **1**, 937-950.

4 J.-H. Kim and J.-H. Kim, *J. Am. Chem. Soc.*, 2012, **134**, 17478-17481.

5 A. Monguzzi, R. Tubino, S. Hoseinkhani, M. Campione and F. Meinardi, *Phys. Chem. Chem. Phys.*, 2012, **14**, 4322-4332.

6 Y. C. Simon and C. Weder, *J. Mater. Chem.*, 2012, **22**, 20817-20830.

7 K. Börjesson, D. Dzebo, B. Albinsson and K. Moth-Poulsen, *J. Mater. Chem. A*, 2013, **1**, 8521-8524.

8 S. H. C. Askes, A. Bahreman and S. Bonnet, *Angew. Chem. Int. Ed.*, 2014, **53**, 1029-1033.

9 M. Häring, R. Pérez-Ruiz, A. Jacobi von Wangelin and D. D. Díaz, *Chem. Commun.*, 2015, **51**, 16848-

16851.
10 T. F. Schulze and T. W. Schmidt, *Energy Environ. Sci.*, 2015, **8**, 103-125.
11 N. Yanai and N. Kimizuka, *Chem. Commun.*, 2016, **52**, 5354-5370.
12 S. P. Hill and K. Hanson, *J. Am. Chem. Soc.*, 2017, **139**, 10988-10991.
13 Z. Huang and M. L. Tang, *J. Am. Chem. Soc.*, 2017, **139**, 9412-9418.
14 X. Cui, J. Zhao, Y. Zhou, J. Ma and Y. Zhao, *J. Am. Chem. Soc.*, 2014, **136**, 9256-9259.
15 P. Duan, N. Yanai, Y. Kurashige and N. Kimizuka, *Angew. Chem. Int. Ed.*, 2015, **54**, 7544-7549.
16 P. Duan, N. Yanai, H. Nagatomi and N. Kimizuka, *J. Am. Chem. Soc.*, 2015, **137**, 1887-1894.
17 K. Xu, J. Zhao, X. Cui and J. Ma, *J. Phys. Chem. A*, 2015, **119**, 468-481.
18 K. Xu, J. Zhao, D. Escudero, Z. Mahmood and D. Jacquemin, *J. Phys. Chem. C*, 2015, **119**, 23801-23812.
19 G. Massaro, J. Hernando, D. Ruiz-Molina, C. Roscini and L. Latterini, *Chem. Mater.*, 2016, **28**, 738-745.
20 S. H. C. Askes, P. Brodie, G. Bruylants and S. Bonnet, *J. Phys. Chem. B*, 2017, **121**, 780-786.
21 K. Xu, J. Zhao and E. G. Moore, *J. Phys. Chem. C*, 2017, **121**, 22665-22679.
22 Y. Sagara and T. Kato, *Nat. Chem.*, 2009, **1**, 605-610.
23 Y. Sagara, S. Yamane, M. Mitani, C. Weder and T. Kato, *Adv. Mater.*, 2016, **28**, 1073-1095.
24 R. Davis, N. P. Rath and S. Das, *Chem. Commun.*, 2004 74-75.
25 A. Kishimura, T. Yamashita, K. Yamaguchi and T. Aida, *Nat. Mater.*, 2005, **4**, 546-549.
26 T. Mutai, H. Tomoda, T. Ohkawa, Y. Yabe and K. Araki, *Angew. Chem. Int. Ed.*, 2008, **47**, 9522-9524.
27 S. Yamane, Y. Sagara and T. Kato, *Chem. Commun.*, 2009 3597-3599.
28 Y. Zhao, H. Gao, Y. Fan, T. Zhou, Z. Su, Y. Liu and Y. Wang, *Adv. Mater.*, 2009, **21**, 3165-3169.
29 S. Yagai, S. Okamura, Y. Nakano, M. Yamauchi, K. Kishikawa, T. Karatsu, A. Kitamura, A. Ueno, D. Kuzuhara, H. Yamada, T. Seki and H. Ito, *Nat. Commun.*, 2014, **5**, 4013.
30 Y. Sagara, A. Lavrenova, A. Crochet, Y. C. Simon, K. M. Fromm and C. Weder, *Chem. Eur. J.*, 2016, **22**, 4374-4378.
31 Y. Sagara, K. Kubo, T. Nakamura, N. Tamaoki and C. Weder, *Chem. Mater.*, 2017, **29**, 1273-1278.
32 S. Amemori, Y. Sasaki, N. Yanai and N. Kimizuka, *J. Am. Chem. Soc.*, 2016, **138**, 8702-8705.
33 Y. Sasaki, S. Amemori, H. Kouno, N. Yanai and N. Kimizuka, *J. Mater. Chem. C*, 2017, **5**, 5063-5067.
34 N. Yanai and N. Kimizuka, *Acc. Chem. Res.*, 2017, **50**, 2487-2495.
35 S. He, K. Krippes, S. Ritz, Z. Chen, A. Best, H.-J. Butt, V. Mailänder and S. Wu, *Chem. Commun.*, 2015, **51**, 431-434.
36 J. Zhou, Q. Liu, W. Feng, Y. Sun and F. Li, *Chem. Rev.*, 2015, **115**, 395-465.
37 Y. Sagara, Y. C. Simon, N. Tamaoki and C. Weder, *Chem. Commun.*, 2016, **52**, 5694-5697.
38 Y. Sagara, C. Weder and N. Tamaoki, *Rsc Adv.*, 2016, **6**, 80408-80414.
39 Y. Sagara, C. Weder and N. Tamaoki, *Chem. Mater.*, 2017, **29**, 6145-6152.
40 S. Baluschev, V. Yakutkin, T. Miteva, G. Wegner, T. Roberts, G. Nelles, A. Yasuda, S. Chernov, S. Aleshchenkov and A. Cheprakov, *New J. Phys.*, 2008, **10**, 013007.
41 A. Monguzzi, R. Tubino and F. Meinardi, *J. Phys. Chem. A*, 2009, **113**, 1171-1174.

42 J.-H. Kim, F. Deng, F. N. Castellano and J.-H. Kim, *ACS Photonics*, 2014, **1**, 382-388.

43 C. Mongin, J. H. Golden and F. N. Castellano, *ACS Appl. Mater. Interfaces*, 2016, **8**, 24038-24048.

44 V. Gray, A. Dreos, P. Erhart, B. Albinsson, K. Moth-Poulsen and M. Abrahamsson, *Phys. Chem. Chem. Phys.*, 2017, **19**, 10931-10939.

45 R. Vadrucci, A. Monguzzi, F. Saenz, B. D. Wilts, Y. C. Simon and C. Weder, *Adv. Mater.*, 2017, **29**, 1702992.

46 F. Zhong and J. Zhao, *Dyes Pigm.*, 2017, **136**, 909-918.

47 W. Song, I. A. Kinloch and A. H. Windle, *Science*, 2003, **302**, 1363.

48 M. Pope and C. E. Swenberg. *Electronic Processes in Organic Crystals and Polymers*; Oxford University Press: New York, 1999.

49 A. Monguzzi, R. Tubino and F. Meinardi, *Phys. Rev. B*, 2008, **77**, 155122.

50 Y. Y. Cheng, T. Khoury, R. G. C. R. Clady, M. J. Y. Tayebjee, N. J. Ekins-Daukes, M. J. Crossley and T. W. Schmidt, *Phys. Chem. Chem. Phys.*, 2010, **12**, 66-71.

51 A. Haefele, J. Blumhoff, R. S. Khnayzer and F. N. Castellano, *J. Phys. Chem. Lett.*, 2012, **3**, 299-303.

52 A. Monguzzi, F. Bianchi, A. Bianchi, M. Mauri, R. Simonutti, R. Ruffo, R. Tubino and F. Meinardi, *Adv. Energy Mater.*, 2013, **3**, 680-686.

53 S. G. Ramkumar and S. Ramakrishnan, *Macromolecules*, 2010, **43**, 2307-2312.

Chapter 5　Conclusions

In this dissertation, I described TTA-UC in condensed systems with the aim to solve the major three issues: (1) low triplet diffusion, (2) phase separation of donor and acceptor, and (3) red-shifting of acceptor emission (Figure 5).

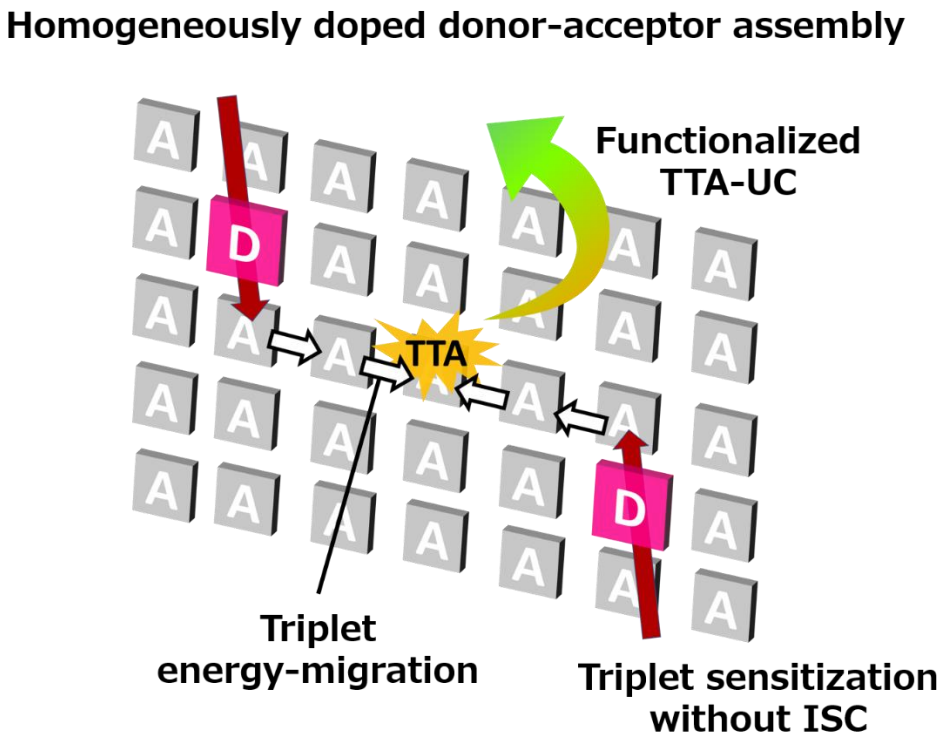

Figure 5. Overview of TTA-UC in the condensed system on this dissertation.

In **Chapter 2**, the strategy to solve the problems of phase separation of donors and acceptors and triplet energy migration efficiency was described. The structural flexibility and the orientation of the columnar liquid crystal acceptor **1** allowed homogeneous doping with the donor and energy-migration for TTA. Furthermore, systematic control over the liquid crystalline structure by mixing **2** gave efficient energy migration, and critical effect of the structural order upon the performance of TTA-UC was unveiled. However, the anti-Stokes shift in this system was relatively small because of inter-molecular interaction between the acceptor molecules.

Therefore, I focus on the solution to the decrease in anti-Stokes shifts in **Chapter 3**. I employed 3D cesium lead halide perovskite nanocrystals as a new inorganic triplet sensitizer. The optical

properties of perovskite nanocrystals could be tuned by facile halide exchange reactions, which made triplet sensitization possible with various excitation wavelengths. Moreover, perovskite nanocrystals could sensitize the triplet state of acceptor **3** without energy loss during ISC, it showed TTA-UC emission with the large anti-Stokes shift. Although there is the problem with the stability of perovskite nanocrystals, this study will promote a variety of fundamental advances to not only TTA-UC studies but also perovskite research fields.

New function of TTA-UC is discussed in **Chapter 4**. By solving the intrinsic problems of condensed systems, I successfully obtained a stimuli-responsive dual-color TTA-UC. This function is specific to condensed systems, and the result clearly exhibited the availability of TTA-UC in condensed systems.

This research, which solved intrinsic problems of TTA-UC in the condensed systems, is expected to be the guideline for the further development of TTA-UC.

Acknowledgments

The study in this thesis has been carried out under the direction of Professor Nobuo Kimizuka during April 2012 – March 2018 at the Department of Chemistry and Biochemistry, Graduate School of Engineering, Kyushu University.

The author would like to express his sincerest gratitude to Professor Nobuo Kimizuka for his great guidance, precious suggestion, and warm encouragement throughout this work.

The author is greatly indebted to Associate Professor Nobuhiro Yanai for his helpful suggestion, continuous encouragement, and valuable discussion.

The author wishes to express his gratitude to Associate Professor Shigenori Fujikawa for his precious suggestion and support. The author is greatly indebted to Associate Professor Teppei Yamada for his valuable advice and warm encouragement. The author wishes to express his gratitude to Assistant Professor Masa-aki Morikawa for his valuable support and warm encouragement. The author would like to thank Technical Staff Kazumi Matsuno, Azusa Suematsu, Chihoko Fukakusa, and Ryo Maeda for their warm encouragements and supports.

The author sincerely appreciates Professor Takuma Yasuda and Professor Yoshiko Miura for reviewing this thesis.

The author expresses great gratitude to Associate Professor Yuki Kurashige (Kyoto University), Assistant Professor Angelo Monguzzi (Dipartimento di Scienza dei Materiali, Università Milano-Bicocca), Assistant Professor Go Watanabe (Kitasato University), Assistant Professor Yoshimitsu Sagara (Hokkaido University), and Professor Christoph Weder (University of Fribourg) for their helpful suggestion and valuable discussion.

The author would like to express the deep appreciation to Mr. Yoichi Sasaki, Mr. Masanori Hosoyamada, and Mr. Keisuke Okumura for their experimental help.

The authors wish to thank Assistant Professor Joseph Ka Ho Hui for comments on earlier version of this dissertation.

The author wishes to express his gratitude to Assistant Professor Hiroaki Iguchi (Tohoku University), Assistant Professor Shogo Amemori (Kanazawa University), Mr. Kenta Takemasu, Dr. Keita Ishiba, Dr. Kouta Masutani, Dr. Deepak Asthana, Dr. Rakesh Kumar Gupta, Dr. Pankaj Bharmoria, Dr. Biplab Joarder, Mr. Hisanori Nagatomi, Mr. Taku Ogawa, Mr. Daisuke Kichise, Mr. Yuya Nagao, Mr. Masaya Matsuki, Mr. Shota Hisamitsu, Mr. Taro Wakiyama, Ms. Rina Yoshida, Mr. Yimin Liang, Mr. Tsubasa Kashino, Mr. Hironori Kouno, Mr. Kanji Shiraishi, Mr. Ryosuke Yamamoto, Mr. Keisuke Kanakogi, Mr. Yuta Kubo, Mr. Tomoya Shimono, Ms. Mariko Kozue, Mr. Shinya Uchino, Mr. Hirotaka Ohara, Ms. Hanyu Yang, Mr. Toshiki Eguchi, Mr. Yuki Nagai, Ms. Nao Hirakawa, Mr. Saiya Fujiwara, Mr. Junji Miyano, Mr. Yusuke Kawashima, Ms. Fan Gao, Ms. Risa Okeda, Ms. Mika Kinoshita, Mr. Takashi Kobayashi, Mr. Tetsuro Kobayashi, Mr. Keisuke Hayashi, Ms. Rena Haruki for warm supports and discussion.

Finally, the author wishes to offer special thanks to his parents Tetsuo Mase and Naomi Mase for constant financial supports and warm encouragement.

Kazuma Mase

Department of Chemistry and Biochemistry

Graduate School of Engineering, Kyushu University

March 2018